Vector Bosons and Jets in Proton Collisions

Paolo Azzurri

INFN Pisa, Largo B. Pontecorvo 3, 56127 Pisa, Italy

Marek Schönherr

Institute for Particle Physics Phenomenology, Durham University, Durham, DH1 3LE, United Kingdom

Alessandro Tricoli

Brookhaven National Laboratory, Upton, New York 11973, U.S.A.

(Dated: December 29, 2020)

Events with vector bosons produced in association with jets have been extensively studied at hadron colliders and provide high-accuracy tests of the Standard Model. A good understanding of these processes is of paramount importance for precision Higgs physics, as well as for searches for new physics. In particular, associated production of γ, W or Z bosons with light-flavor and heavy-flavor jets is a powerful tool for testing perturbative QCD calculations, Monte Carlo event generators, and can also constrain the parametrizations used to describe the parton content of the proton. Furthermore, events with a W or Z boson produced with two well-separated jets can be used to distinguish between electroweak and strong production mechanisms, and to set limits on contributions of physics beyond the Standard Model. This review summarises the historical theoretical developments and the state-of-the-art in the modeling of vector-boson-plus-jet physics, while focusing on experimental results by LHC collaborations in Run-1 and Run-2, and including comparisons with recent measurements at the TEVATRON.

CONTENTS

I. INTRODUCTION

Vector boson production in association with hadronic jets is one of the most important classes of processes that can be measured at hadron colliders. While the vector bosons, i.e. photons, Z, and W bosons, are the carriers of electroweak interactions, associated hadronic jets stem from the presence of strong interactions, as a result of the process of fragmentation and hadronization of energetic partons (quarks and gluons). Figure 1 shows a proton collision event recorded by the CMS experiment with a Z boson produced in association with two jets. The two jets were identified to be likely originating from charm quarks. Each jet is a spray of hadronic particles collimated in the general direction of the initial parton, carrying the bulk of its total energy and transverse momentum.

Therefore the study of V+jets ($V = \gamma, W, Z$)

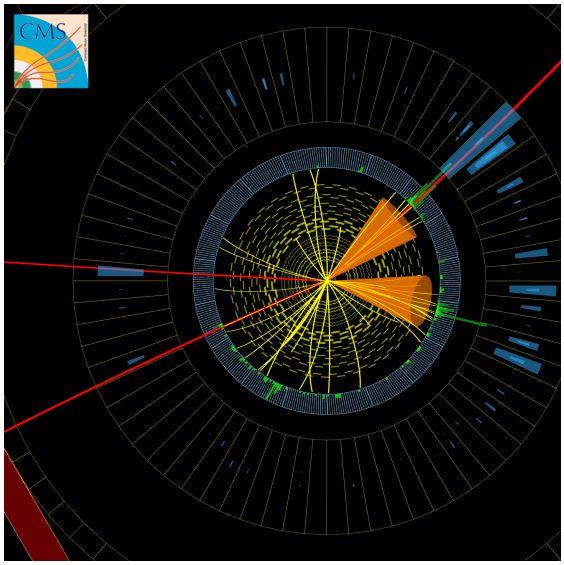

Figure 1 A vector boson plus jets event recorded by the CMS experiment in proton collisions at 13 TeV center-of-mass energy. The two solid lines on the left correspond to two reconstructed muons from the decay of a Z boson. The two cones on the right contain two collimated sprays of particles reconstructed as hadronic jets. The internal composition of the jets indicate that both are likely to have originated from charm quarks, and one of them contains a muon from a displaced hadronic decay. Figure taken from (CMS Collaboration, 2019a).

events constitutes an ideal probe for testing quantum chromodynamics (QCD) and electroweak (EW) interactions as well as a major source of backgrounds to searches for new physics. Measurements of $V+$jets also validate the adequacy of the approximations used in theoretical calculations and models used for background estimates in precision measurements. For example, the modeling of $V+$jets has a significant impact on studies of the Higgs boson and top-quark sectors of the Standard Model (SM), or in searches for physics beyond the Standard Model. Thanks to their large cross sections, the colorless nature of the γ, W and Z bosons as carriers of electromagnetic and weak forces respectively, and their high sample purities, accurate studies of $V+$ jets are of paramount importance for the success of a hadron collider physics program.

More specifically, a precise understanding of $\gamma+$ jet production and its modeling plays an important role in new physics searches, as $\gamma+$ jets constitute a background, for example, to the production of high-mass resonances in the search for excited quarks in quark-compositeness models or quantum black holes in models of extra spatial dimensions. Similarly, reliable $W/Z+$jet calculations are important to correctly model the SM backgrounds in many searches of new particles in processes producing a single or two charged leptons[1] with associated multi-jets, as they occur for example in supersymmetric theories.

Vector boson production processes in association with jets containing heavy-flavor hadrons play important roles in several measurements at hadron colliders. From them, the dynamics of the underlying heavy-flavor quark processes can be inferred. In particular, they can give access to the heavy-flavor content of the proton, which is a limiting factor in several analyses at the Large Hadron Collider (LHC). In addition, a detailed understanding of heavy-flavor quark dynamics in these processes was of paramount importance to the recent observation of the Higgs boson decay into a b-quark pair (ATLAS Collaboration, 2018f; CMS Collaboration, 2018f), and is vital for many new physics searches.

In the last 30 years many measurements of $V+$ jet event properties have been carried out starting from UA1 and UA2 experiments (Appel *et al.*, 1986; Arnison *et al.*, 1983a,b,c, 1984a,b; Bagnaia *et al.*, 1983, 1984; Banner *et al.*, 1983) at the Sp$\bar{\text{p}}$S. Extensive measurements of such processes by the CDF and the DØ collaborations at the TEVATRON have prompted significant development in the understanding of the underlying QCD dynamics, including new techniques for calculating high-precision theoretical predictions as well as non-perturbative modeling in Monte Carlo (MC) event generators. TEVATRON data provided an important stepping-stone for $V+$ jet analyses at the LHC, despite the large difference in center-of-mass energies between the two colliders. The measurements carried out by the LHC collaborations, ATLAS, CMS and LHCb, in the LHC Run-1 and Run-2 have motivated further developments in the theoretical description of such processes both in the QCD and the EW sectors. The wide range of center-of-mass energies, from 1.96 TeV in $p\bar{p}$ collisions at the TEVATRON to 7, 8 and 13 TeV in pp collisions at the LHC, allows to explore QCD dynamics in different energy regimes over a broad range of energy scales. The ranges of $V+$jet cross sections at the LHC, compared to inclusive vector boson production and other SM processes, are shown in Figure 2.

The underlying physics for the production of $V+$ jet processes at the LHC cannot be con-

[1] In the following sections 'charged lepton' refers to an electron or a muon, unless explicitly stated, since $W/Z+$ jet measurements have primarily focused on electronic and muonic decay channels of the W and Z bosons.

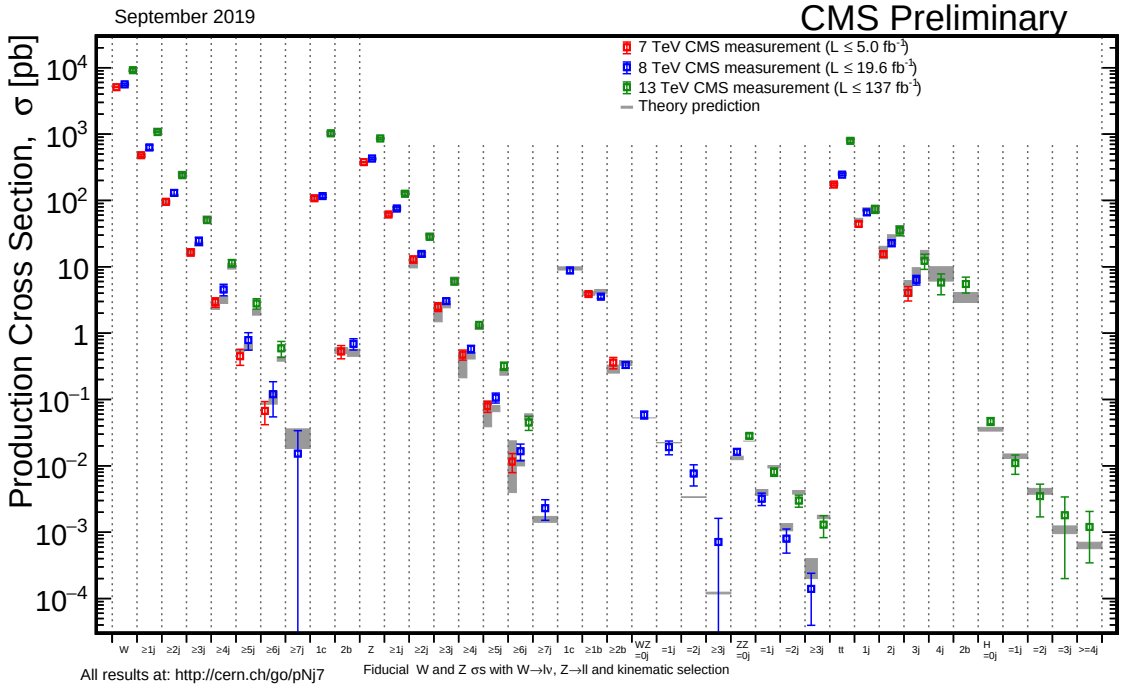

Figure 2 Summary of production cross sections for processes with a W or a Z boson produced in association with light or heavy-flavor jets studied at different center of mass energies at the LHC, and their cross sections compared to other SM processes. Figure taken from (CMS Collaboration, 2020f).

sidered as a simple rescaling of scattering processes at the TEVATRON. The different beam types and center-of-mass energies between the two colliders lead to a different relative importance of the various underlying production mechanisms and their associated phenomenology. More specifically, the LHC reaches far larger energy scales Q than the TEVATRON thanks to the higher beam energies, while it can simultaneously probe a lower Bjorken-x range. The inclusive production of a W boson at the LHC is dominated by events with a Bjorken-x in the range $10^{-4} - 10^{-1}$ and $Q^2 \approx M_W^2$, while the exclusive production of a W boson and at least one jet is shifted to larger values of x, with the majority of the events in the x range of $10^{-2} - 3 \cdot 10^{-1}$ and larger Q^2 values.

As a consequence the two colliders are sensitive to particulars of the parameterizations of the parton densities inside the proton and their collision events are subject to different production mechanisms. For instance, at the TEVATRON, V + jet processes have a significant valence-quark contribution from $q\bar{q}$ interactions, where the quark (q) is originating from the colliding proton and the anti-quark ($\bar{q}$) from the colliding anti-proton. On the other hand, at the LHC there are significant gluon (g) and sea-quark contributions, including $\bar{q}g$, qg and gg interactions. For example, the Z+ 2 jet production, i.e. $qg \to Z + qg$ process, contributes around 75% at the LHC, while only around 25% at the TEVATRON. At the LHC the relative fraction of sub-processes initiated by $qq/q\bar{q}/\bar{q}\bar{q}$, $gq/g\bar{q}$, and gg interactions varies with the number of associated jet production in the final state. In W + jet processes the fraction of $qq/q\bar{q}/\bar{q}\bar{q}$ ($gq/g\bar{q}$) sub-processes increases (decreases) from 18 (82)% with 1 jet to 21 (73)%, 23 (70)% and 25 (67)% with 2, 3 and 4 jets, respectively, while for gg sub-processes it increases from 0% with 1 jet to 6%, 7% and 8% with 2, 3 and 4 jets, cf. (Kom and Stirling, 2010).

As a result of the LHC sensitivity to large contributions of sea-quark and gluon densities, V + jet cross sections are far larger at the LHC than at the TEVATRON. For example the W+ 4-jet cross section at the LHC is 500 times larger than that at the TEVATRON with similar kinematic selection, while the inclusive $Z + b$ cross section at the LHC is 50 times larger than that at the TEVATRON (Campbell *et al.*, 2004).

This article reviews the evolution of the theoretical developments in the description of V + jets physics for the TEVATRON and the LHC, focusing on the recent achievements for the LHC Run-1 and Run-2. An overview of experimental analysis techniques to identify V+jet events and reconstruct their kinematics will be given together with a selection of measurements at different center-of-mass energies. The review

of experimental results of $W/Z+$jets will focus on the leptonic decays of the W and Z bosons. The comparisons between experimental measurements and cutting-edge theoretical predictions will be highlighted. This review starts with the discussion of the production of vector bosons in association with light-flavor jets in Section II, which is followed by the presentation of the EW production of vector bosons in Sections III and the associated production of a vector boson and heavy-flavor jets, i.e., $V+b$ or c jets, in Section IV. Each of these sections starts with the discussion of the theoretical predictions for the different $V+$jet production modes, specifically highlighting the most recent developments on higher-order calculations and MC event generators, then proceeds with the discussion of the experimental results and their comparison with the theory. In this review the authors do not attempt to accomplish the arduous task of exhaustively presenting all available measurements, but they have striven to highlight selected examples of measurements that give specific insight into $V+$jet production dynamics. The numerous measurements of $V+$jets make it also difficult to select a representative set of results, therefore the authors have chosen to provide a balanced representation of the different types of measurements and by the different experiments at the TEVATRON and the LHC. Section V illustrates some examples of analyses and interpretations of experimental $V+$jet results, for example for tuning of MC generators, constraining the proton parton densities and for setting limits on anomalous contributions to SM interactions. The article concludes in Section VI with a summary and an outlook for $V+$jet analyses at future LHC runs and future colliders.

II. ASSOCIATED PRODUCTION OF A VECTOR BOSON AND LIGHT-FLAVOR JETS

A. Theoretical predictions

The production of a single vector boson, γ, W or Z, is the class of processes with the largest cross sections among the electroweak processes at hadron colliders. While the massive vector bosons, W and Z, can be produced by simple quark-anti-quark annihilation without additional final-state partons at leading order (LO), photons, as the massless gauge boson of QED, are only measurable when they have finite transverse momentum and therefore always need at least one parton to recoil against.

To set the stage, the Feynman diagrams of the dominant leading and next-to-leading order (NLO), in both the strong and electroweak couplings α_s and α, production processes of inclusive massive gauge bosons are detailed in Fig. 3. A substantial fraction of all events with single massive vector bosons are accompanied by additional hadronic jet activity. These processes are of specific interest due to their clean signature and the relative precision with which they can be calculated in the Standard Model. Representative leading order Feynman diagrams are shown in Fig. 4.

Single photon production, on the other hand, is always accompanied by hadronic recoil, as discussed above. Figure 5 shows representative diagrams of photon production in association with jets.

1. Higher order computations

The effort to increase the available accuracy of the theory predictions[2] for inclusive W and Z boson production processes started early. While the first results beyond leading order accuracy date back forty years (Altarelli *et al.*, 1979), the current standard sees the inclusive cross sections determined at next-to-next-to-leading order (NNLO) in QCD with NLO EW corrections, i.e., NNLO QCD + NLO EW (Anastasiou *et al.*, 2004; Catani *et al.*, 2009; Gavin *et al.*, 2011; Hamberg *et al.*, 1991; Li and Petriello, 2012; Melnikov and Petriello, 2006a,b). The NNLO QCD-EW mixed contributions of $\mathcal{O}(\alpha_s\alpha)$ are known in the pole approximation (Dittmaier *et al.*, 2014), which is valid in the region where the invariant mass of the charged lepton pair is close to the respective gauge boson's mass. Figure 6 displays on its left hand side such a state-of-the-art calculation for the inclusive transverse momentum of the positively-charged lepton in the inclusive production of a charged-lepton pair, showing the relatively large corrections received through the higher-order QCD corrections with respect to the leading order calculation.

Another key inclusive experimental observable is the transverse momentum distribution of the vector boson itself. Its description, however, depends on an accurate description of its recoil. It thus vanishes identically at leading order and only starts at $\mathcal{O}(\alpha_s)$ or $\mathcal{O}(\alpha)$, respectively. Its precise description is further

[2] Theoretical uncertainties are typically estimated by varying all unphysical scales of the calculation, e.g., the renormalization and factorization scale, etc. The resulting quoted error estimate has, however, no statistical interpretation.

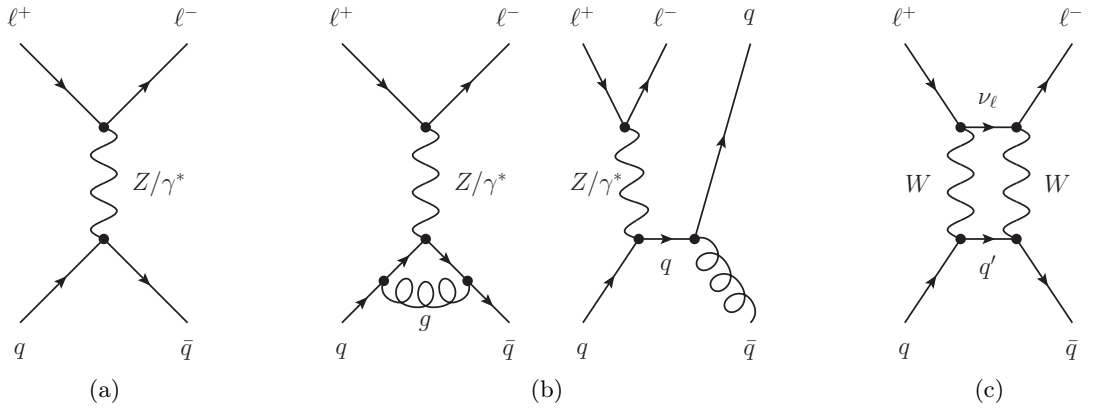

Figure 3 Representative Feynman diagrams for the production of a pair of charged leptons at LO (a) and representative contributions at NLO QCD (b) and NLO EW (c).

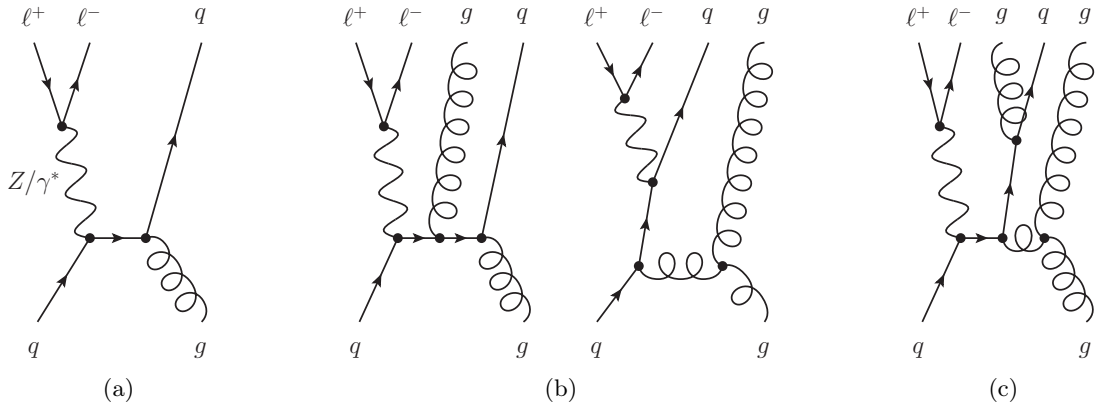

Figure 4 Representative Feynman diagrams for the production of a pair of charged leptons in association with one jet (a), two jets (b), and three jets (c) at LO.

complicated by large logarithms in the small-transverse-momentum region, as a result of an infrared divergence at $p_{\mathrm{T}} = 0$, which spoil the convergence of the perturbative expansion in the coupling parameters. As the same logarithms reappear order-by-order, however, they can be resummed, and the respective results will be detailed in Sec. II.A.2. In the medium- to large-transverse-momentum region, a fixed-order expansion is sufficient to achieve percent-level accuracy. While the QCD two-loop amplitudes have been available for some time (Garland *et al.*, 2002a,b; Moch *et al.*, 2002), the inception of novel subtraction formalisms (Boughezal *et al.*, 2015a; Catani *et al.*, 2019; Catani and Grazzini, 2007; Currie *et al.*, 2013; Gaunt *et al.*, 2015; Gehrmann-De Ridder *et al.*, 2005; Kosower, 1998) along with the computational frameworks that are able to deal with the complexity of the infrared structure of such a calculation were only recently available. They paved the way for precise NNLO QCD calculations for this kinematic region (Boughezal *et al.*, 2016a, 2015b, 2016b,c; Campbell *et al.*, 2017b; Gauld *et al.*, 2017; Gehrmann-De Ridder *et al.*, 2016a,b, 2018, 2019, 2016c), as is detailed in the right hand side of Fig. 6.

At the same time, the electroweak corrections for both the vector boson transverse momentum and vector-boson-plus-jet production in general are also known (Actis *et al.*, 2013; Denner *et al.*, 2011, 2013, 2015; Hollik *et al.*, 2015; Kallweit *et al.*, 2015a, 2016, 2015b; Kühn *et al.*, 2005a,b, 2007, 2008; Lindert *et al.*, 2017). In their combination with the higher-order QCD corrections typically two schemes are followed. They can be combined additively, corresponding to a strict next-to-leading order expansion, commonly denoted as NLO QCD+EW. Or they can be combined multiplicatively, referred to as NLO QCD×EW, which assumes a factorization of both effects and is especially suited if the typical scales of both processes are well separated. The difference is formally of higher order and can be used to estimate the potential size of the mixed QCD−EW NNLO corrections.

Conversely, the inclusive photon production cross section, as it is always accompanied by

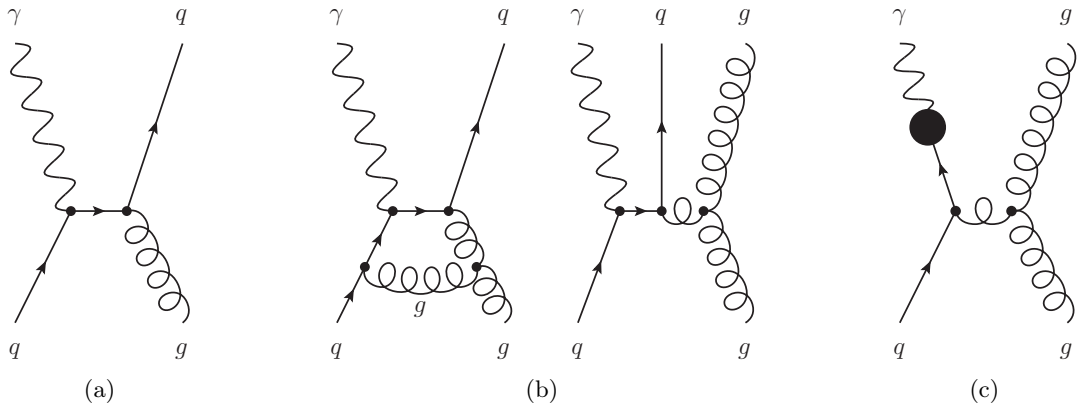

Figure 5 Representative Feynman diagrams for the production of a photon at LO (a), representative contributions at NLO QCD (b) and photon production from quark fragmentation (c) that enters at the same order.

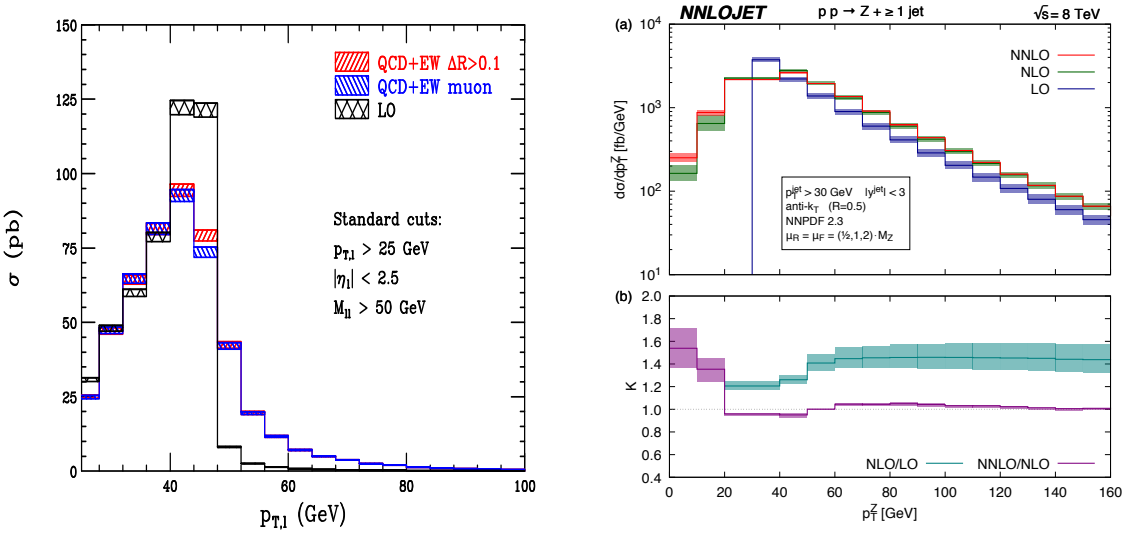

Figure 6 Charged lepton transverse momentum in the inclusive production of two charged leptons at NNLO QCD plus NLO EW (left), figure taken from (Li and Petriello, 2012). Transverse momentum of two charged leptons in the production of two charged leptons in association with at least one jet at LO, NLO and NNLO QCD (right), figure taken from (Gehrmann-De Ridder *et al.*, 2016b).

hadronic activity, starts at $\mathcal{O}(\alpha_s\alpha)$ at the Born level and is thus of the same level of complexity as $W/Z+1$jet production. Hence, all pieces of the calculation at NNLO accuracy in the strong coupling have only been computed recently (Campbell *et al.*, 2017a,b; Chen *et al.*, 2020) while the NLO EW corrections have been known for a slightly longer period (Kallweit *et al.*, 2015b; Kühn *et al.*, 2006; Lindert *et al.*, 2017).

In addition, due to their nature as massless gauge bosons, photons can be produced both promptly by the hard interaction and emerge from a fragmentation process, cf. Fig. 5. Thus, unless the photon is identified using the smooth cone isolation procedure (Frixione, 1998), which completely removes the fragmentation component by construction, such additional fragmentation processes have to be considered starting at the next-to-leading order (Aurenche *et al.*, 2006; Glück *et al.*, 1994). It remains to be noted that the smooth cone isolation cannot be adopted by the experiments due to finite detector resolution, while the standard cone isolation, that is typically used experimentally, necessitates the use of fragmentation functions in theory calculations. Thus, for all calculations using the smooth cone isolation the correspondence of its parameters to approximately match the experimentally used ones needs to be confirmed. Mixed schemes, e.g., a smooth/standard cone hybrid (Siegert, 2017) can be used to mediate such differences.

The transverse momentum distribution of a Z boson decaying into neutrino pairs is of particular interest to new physics searches at the

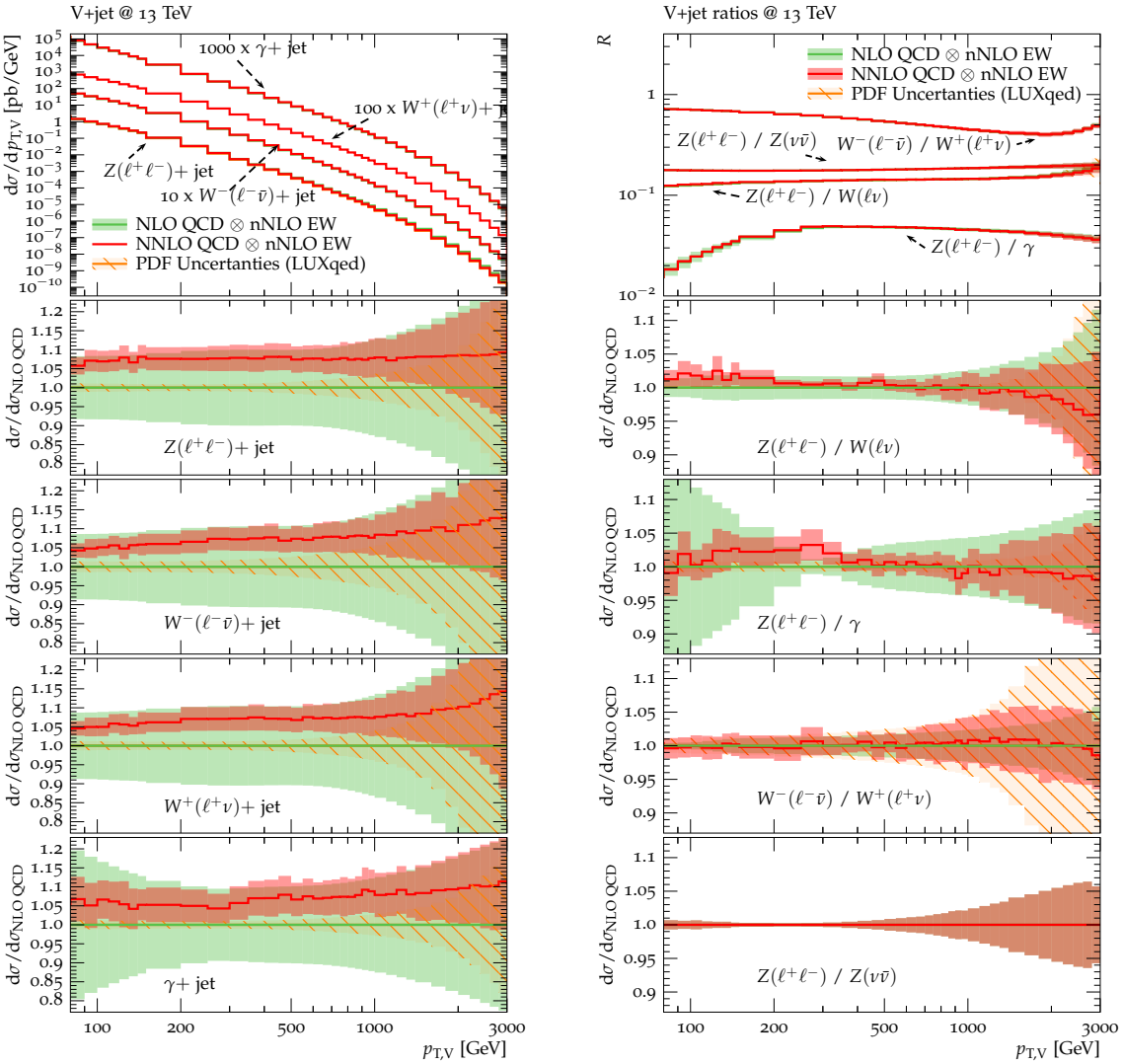

Figure 7 Transverse momentum of the reconstructed vector boson (left, from top to bottom Z, W^-, W^+ and γ) in inclusive vector boson production at NLO and NNLO QCD plus nNLO EW, figure taken from (Lindert *et al.*, 2017). Pairwise ratios of the differential cross section in the transverse momentum of the reconstructed vector bosons in inclusive vector boson production at NLO and NNLO QCD plus nNLO EW (right), figure taken from (Lindert *et al.*, 2017).

LHC, e.g., as a background to searches for Dark Matter, as it has a similar topology and features particles that are invisible to the LHC detectors. Due to this very fact, however, measuring this Standard Model background independently proves to be challenging. Typically it is indirectly inferred by measuring the transverse momentum of a leptonically decaying Z or W boson or a photon instead, relying on theory predictions to estimate to the sought after $Z \to \nu\bar{\nu}$ distribution. The needed ratios of production cross sections of the different processes can now be predicted with high precision (Bern *et al.*, 2011; Bizoń *et al.*, 2019; Campbell *et al.*, 2017b; Gehrmann-De Ridder *et al.*, 2018; Lindert *et al.*, 2017), thanks to the recently available NNLO QCD plus NLO EW accurate predictions, as discussed above, and an understanding of the correlations across processes. Figure 7 details the predictions for these ratios, which are found to have percent-level accuracy for vector boson transverse momenta up to around 1 TeV, growing to 5-10% in the regions beyond.

Finally, also vector boson production in association with multiple jets is of interest. Not only are such final states frequently measured at the LHC, they also often constitute backgrounds to searches for particular new physics models. With the adoption of the anti-k_t jet definition (Cacciari *et al.*, 2008), a sequential recombination algorithm of the longitudinally-invariant-k_t family (Catani *et al.*, 1993; Dokshitzer *et al.*, 1997; Ellis and Soper, 1993), by

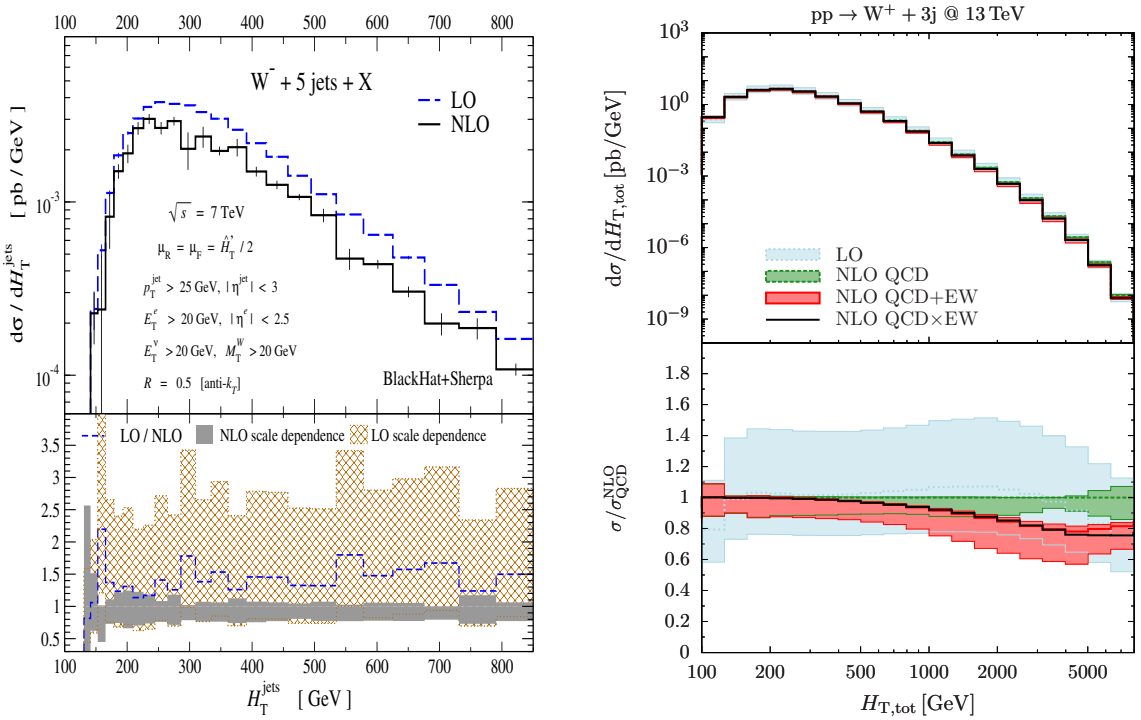

Figure 8 Scalar sum of jet transverse momenta in single charged lepton production in association with missing transverse momentum and at least five jets at LO and NLO QCD (left), figure taken from (Bern *et al.*, 2013). Scalar sum of jet transverse momenta in single charged lepton production in association with missing transverse momentum and at least three jets at LO and NLO QCD plus NLO EW (right), figure taken from (Kallweit *et al.*, 2015a).

the LHC experiments as their default jet definition, longstanding issues around the compromised infrared safety of the TEVATRON era jet algorithms (Blazey *et al.*, 2000) were resolved. This allows for high-precision higher-order calculations to be made for the precise observable that is measured.

The NLO QCD predictions are available for W plus up to five jets (Berger *et al.*, 2011, 2009; Bern *et al.*, 2013; Campbell and Ellis, 2002; Ellis *et al.*, 2009) and Z plus up to four jets (Berger *et al.*, 2010; Campbell and Ellis, 2002; Ita *et al.*, 2012), and approximate NNLO corrections, dubbed n̄NLO, can be calculated through the LOOPSIM method (Maître and Sapeta, 2013; Rubin *et al.*, 2010). At the same time, NLO EW corrections are known for fully off-shell production only up to two jets (Denner *et al.*, 2015; Kallweit *et al.*, 2016), and in the on-shell approximation for up to three jets (Chiesa *et al.*, 2016; Kallweit *et al.*, 2015a). The effect of these corrections are detailed in Fig. 8. Processes with up to nine jets can, however, be calculated at LO accuracy (Höche *et al.*, 2019b).

2. Resummation calculations

Fixed-order calculations fail to yield reliable cross-section predictions in phase space regions where large, typically logarithmic, terms appear at every order of the perturbative expansion. Consequently, a truncation of the perturbative series fails to converge quickly enough after the first, second or third order. To render a truncation after any finite number of orders meaningful, a resummation of the terms spoiling the convergence is mandated. As the functional form of these convergence-impairing terms is dependent of the phase space region probed by the respective observable, all resummation formulations are observable specific. In the literature, several approaches to identify and resum the relevant logarithms have been formulated, cf. (Bacchetta *et al.*, 2020; Balazs and Yuan, 1997; Becher and Neubert, 2011; Bermudez Martinez *et al.*, 2019; Bizoń *et al.*, 2018; Bozzi *et al.*, 2011; Catani *et al.*, 2014; Collins *et al.*, 1985; Coradeschi and Cridge, 2019; Ebert and Tackmann, 2017; Ladinsky and Yuan, 1994; Mantry and Petriello, 2011; Monni *et al.*, 2016). This is in particular relevant for electroweak precision measurements like the W mass, or for probing so-called intrinsic transverse momentum of the partons inside the pro-

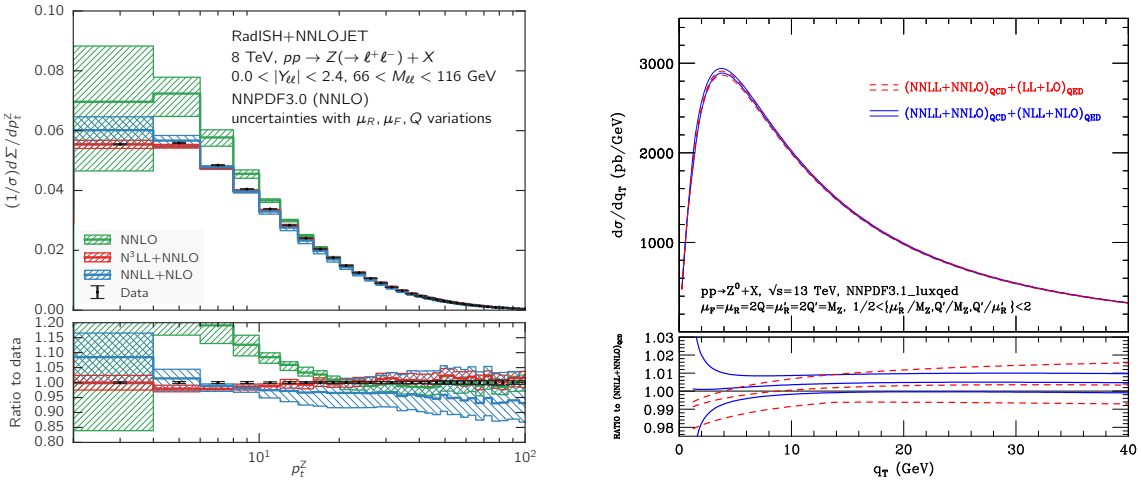

Figure 9 Transverse momentum of the charged lepton pair in the inclusive production of two charged leptons at NNLO, NNLL+NLO and N^{3}LL+NNLO QCD (left), showing the QCD scale uncertainties, figure taken from (Bizoń *et al.*, 2018). Transverse momentum of the charged lepton pair in the inclusive production of two charged leptons at NNLL+NNLO QCD plus LL+LO and NLL+NLO QED (right), showing the QED-related uncertainties only, figure taken from (Cieri *et al.*, 2018).

ton.

For the production of vector bosons in association with light-flavor jets, the transverse momentum of the vector boson is of particular interest. In this observable, resummation is required to accurately describe the small-p_T region, whereas the large-p_T region suffers no such effects and is most accurately described by fixed-order perturbation theory. Thus, to achieve the best predictions for the spectrum, the resummed calculation at small p_T has to be matched to the fixed-order calculation at large p_T. Several solutions, fitting the various resummation procedures, are available. Figure 9 displays two examples. On the left hand side, the state-of-the-art next-to-next-to-next-to leading logarithmic (N^{3}LL) resummation matched to NNLO fixed-order prediction in QCD is shown (Bizoń *et al.*, 2018). The effect of resumming large logarithms in the expansion of the cross-section in the strong coupling, α_s, as well as including the large logarithms appearing in the simultaneous expansion in the electroweak coupling, α, is shown on the right hand side of Fig. 9 (Cieri *et al.*, 2018; de Florian *et al.*, 2018). Although the effects are somewhat small in this case, they are needed for a meaningful interpretation of the high-precision data to be taken in the future LHC runs.

Other resummed calculations are available for related observables, e.g., the ϕ^*-distribution (Banfi *et al.*, 2011b) that can be measured with superior experimental precision (Banfi *et al.*, 2011a; Vesterinen and Wyatt, 2009), or the jet veto efficiency (Banfi *et al.*, 2012; Stewart *et al.*, 2011; Tackmann *et al.*, 2012).

3. Monte Carlo event generators

The previously-discussed high-precision calculations suffer from one important shortcoming: they are parton-level calculation and do not fully account for parton evolution or non-perturbative effects. Thus, to arrive at either particle-level[3] predictions that can be directly compared to detector-corrected experimental data, or at simulated detector readouts to derive the detector corrections in the first place, these high-precision calculations need to be interfaced to parton-shower calculations, multiparton interaction and hadronisation models, as well as hadron decays. This is implemented in so-called Monte Carlo event generators, for example HERWIG (Bellm *et al.*, 2016), PYTHIA (Sjöstrand *et al.*, 2015), and SHERPA (Bothmann *et al.*, 2019). They can produce fully differential calculations, i.e., results that explicitly provide the flavor and four momentum of every particle that is produced in a high-energy collision. This allows the predictions to be projected onto arbitrary observables a posteriori.

Within the Monte Carlo event generators, the parton showers (PS) provide a fully-differential resummation of the parton splitting process in terms of their respective evolution variable, albeit at a lower theoretical accu-

[3] Particles with a lifetime of $c\tau > 10$ mm are considered stable by the typical collider experiments. The stage of event evolution where all remaining particles are stable on this scale is referred to as particle-level.

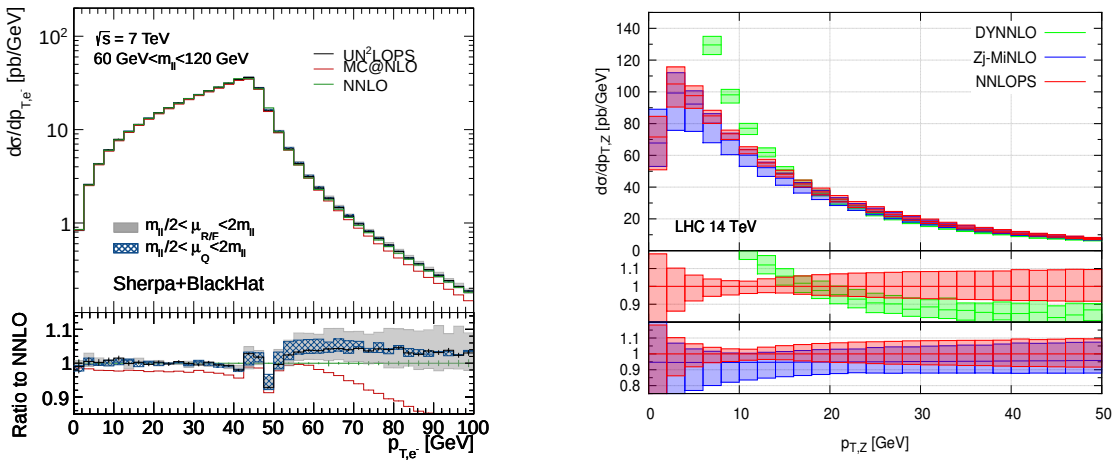

Figure 10 Lepton transverse momentum in the inclusive production of a charged lepton pair calculated at NNLO QCD accuracy matched to the parton shower using the UN^{2}LOPS method as implemented in SHERPA, compared to MC@NLO and NNLO calculations (left), figure taken from (Höche *et al.*, 2015). Reconstructed Z boson transverse momentum in the production of a charged lepton pair calculated at NNLO QCD accuracy matched to the parton shower using the MINLO method as implemented in POWHEG interfaced to PYTHIA8, compared to DYNNLO and NNLOPS calculations (right), figure taken from (Karlberg *et al.*, 2014).

racy, as compared to the inclusive observable-specific resummations discussed in the previous section. They are matched to fixed-order expressions for the hard scattering at the leading, next-to-leading and next-to-next-to-leading orders to improve the precision of the calculation outside the strongly hierarchical regime. While the matching to LO matrix elements is trivial, there exist two general variants of matching strategies for the combination with next-to-leading order matrix elements, POWHEG (Frixione *et al.*, 2007; Höche *et al.*, 2011a; Nason, 2004) and MC@NLO (Alwall *et al.*, 2014; Frixione and Webber, 2002; Höche *et al.*, 2012). Both are formulated in a generic way and, especially the MC@NLO method, can be applied in an automated way to arbitrary processes. These methods have been applied to inclusive vector boson production (Alioli *et al.*, 2008; Frixione and Webber, 2004; Hamilton *et al.*, 2008; Höche *et al.*, 2011a) as well as vector boson production in association with up to three jets (Alioli *et al.*, 2011; Campbell *et al.*, 2013; Frederix *et al.*, 2012; Höche *et al.*, 2012, 2013b; Ježo *et al.*, 2016; Re, 2012; Siegert, 2017). In addition, at least in the POWHEG approach for the inclusive Drell-Yan production, also next-to-leading order electroweak corrections have been matched to co-evolving QCD+QED parton showers (Barzè *et al.*, 2012, 2013; Bernaciak and Wackeroth, 2012; Mück and Oymanns, 2017). They constitute the state-of-the-art tools to calculate the Standard Model predictions for electroweak precision measurements, such as the W mass, the angular coefficients and charged-lepton asymmetry in lepton-pair production.

The current logarithmic accuracy of parton showers, however, only allows them to be matched to matrix elements at NNLO accuracy with the most trivial color structure. Thus, results are only available for inclusive W and Z boson production, but not for their production in association with a jet. Here, again, two different schemes exist: for NNLOPS matched calculations, MINLO (Hamilton *et al.*, 2013, 2012) simulations reweighted to inclusive NNLO distributions (Karlberg *et al.*, 2014; Monni *et al.*, 2020), and q_T-slicing combined with MC@NLO predictions in the UN^{2}LOPS scheme (Höche *et al.*, 2015). Figure 10 details the results of both approaches, including their uncertainties, and compares them to the fixed-order results of the same accuracy. In both approaches, the advantages of combining the resummation properties of the parton shower with the fixed-order matrix element become apparent throughout the respective spectrum. The otherwise unphysical description of the low transverse momentum region of the weak boson is now described in a reliable way. For prompt photon production, as it is always accompanied by a jet at leading order, no NNLOPS description is available.

Beyond the description of a fixed multiplicity at the highest possible accuracy, the inclusive production of a vector boson with any number of jets is of prime interest to the ex-

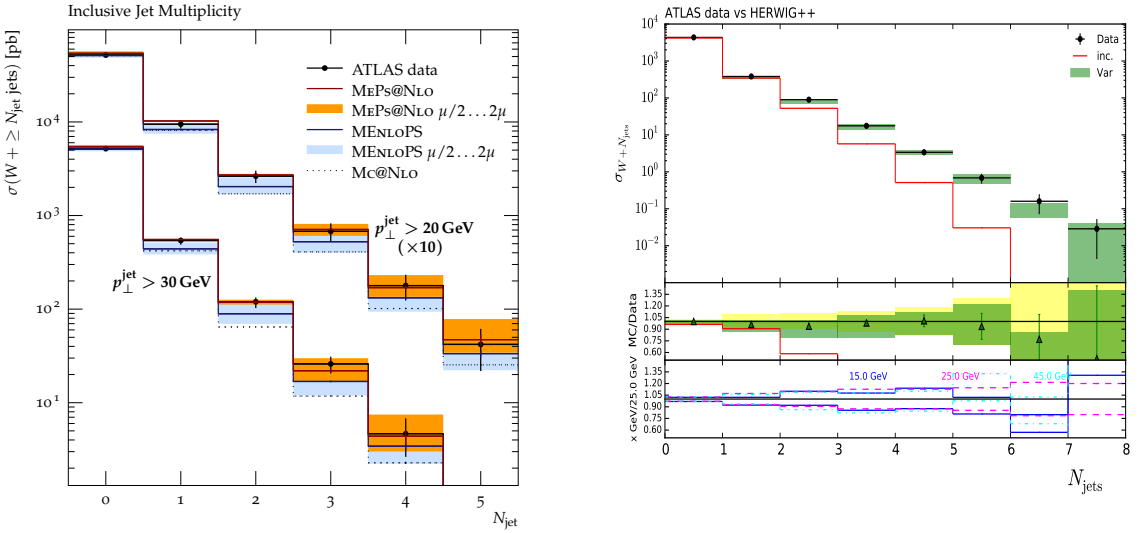

Figure 11 Inclusive jet multiplicity in the production of a charged lepton and a neutrino in association with jets using the MEPS@NLO method and merging up to two jets at NLO and four jets at LO accuracy as implemented in SHERPA, compared to MENLOPS predictions and ATLAS data (left), figure taken from (Höche *et al.*, 2013a). Exclusive jet multiplicity in the production of a charged lepton and a neutrino in association with jets using the FXFX method and merging up to two jets at NLO accuracy as implemented in MADGRAPH5_aMC@NLO and HERWIG++ (right), figure taken from (Frederix *et al.*, 2016).

periments. Thus, multijet-merged calculations aim to combine the advantages of both the high-precision descriptions of hard and wide-angle radiation through fixed-order matrix elements with the excellent description of the soft-collinear intrajet dynamics offered by the parton shower. Prescriptions to merge multiple LO-accurate parton shower (LOPS) calculations of successive jet multiplicities into inclusive calculations were derived about twenty years ago. They can be grouped in the CKKW-like methods (Catani *et al.*, 2001; Hamilton and Nason, 2010; Hamilton *et al.*, 2009; Höche *et al.*, 2011b, 2009; Lavesson and Lönnblad, 2008b; Lönnblad, 2002; Lönnblad and Prestel, 2012, 2013b) on the one hand side, and the MLM-like approaches (Alwall *et al.*, 2008; Mangano *et al.*, 2002) on the other.

The CKKW-like approaches split the emission phase-space of a lower-order process into a matrix element region and a parton-shower region using the merging scale Q_{cut} as a separator. While the soft and collinear phase space is populated by the parton shower acting on lower-multiplicity matrix-elements, radiation into the matrix element region is vetoed. This veto, as it is determined by the parton-shower emission probability, now provides the correct Sudakov weight for the higher-multiplicity matrix element to correctly include the respective resummation properties in this region.

Conversely, the MLM-like prescriptions attach an unconstrained parton shower to the matrix element configuration of each individual jet multiplicity, letting it run its course without any awareness of the merging scale which was used to define the matrix element region initially. Only at this point of the generation, jets are reconstructed using a given jet algorithm and matched, both in direction and transverse momentum, to their counterparts in the originating matrix element. If non-matching jets are found in either configuration the event is discarded, in this way providing the needed Sudakov weights. Although both methods yield comparable results (Alwall *et al.*, 2008), it should be noted that a formal proof of the mathematical correctness only exists for the CKKW-like approaches (Höche *et al.*, 2009).

These methods have then subsequently been promoted to merging NLOPS-matched calculations, both in the CKKW-like approach, see Refs. (Gehrmann *et al.*, 2013; Höche *et al.*, 2014, 2013a; Lavesson and Lönnblad, 2008a) for the MEPS@NLO variant, Refs. (Bellm *et al.*, 2018; Lönnblad and Prestel, 2013a; Plätzer, 2013) for the UNLOPS variant, and Refs. (Alioli *et al.*, 2015) for the GENEVA variant, as well as in the MLM-like prescription (Frederix and Frixione, 2012) (FXFX). In the former, possibilities to complement the NLOPS-accurate prescriptions of the lowest few multiplicities with LOPS-accurate higher multiplicities have been formulated (Gehrmann *et al.*, 2013; Hamilton and Nason, 2010; Höche *et al.*, 2014, 2011b). Figure 11 displays the results of these state-of-the art computations compared to data taken by the ATLAS experiment at the LHC at 7 TeV. When

contrasted, the NLO-accurate predictions prove to be superior in both their central values and their uncertainties.

As discussed in Section II.A.1, electroweak corrections are not only important for precision measurements but also in observables probing regions of large momentum transfers. So far, however, no solution to incorporate the exact NLO electroweak corrections in the TeV regime has been formulated. Nonetheless, there exist two methods to incorporate the dominant electroweak correction in this region in an approximate way. The first method (Chiesa *et al.*, 2013) supplements the leading order matrix elements used in a LO-accurate multi-jet merged prediction with multiplicative EW Sudakov form factors (Denner and Pozzorini, 2001a,b). Conversely, the second method (Kallweit *et al.*, 2016) completes the NLO QCD components of NLO-accurate multi-jet merged calculations with exact NLO EW virtual corrections and approximate NLO EW real emission corrections integrated over the single-emission phase space. The latter can, where needed, be supplemented with subleading LO corrections to account for further relevant contributions. Results for both methods are shown in Fig. 12, and the general feature of a logarithmic suppression of the production cross section, the so-called EW Sudakov correction, can be observed, e.g., reaching several tens of percent for the transverse momentum of the vector boson.

Electroweak effects also become relevant through the radiation of either massive weak bosons (Christiansen and Sjöstrand, 2014; Krauss *et al.*, 2014) (again, mostly relevant for TeV scale objects), or photon bremsstrahlung (Barberio *et al.*, 1991; Bloch and Nordsieck, 1937; Hamilton and Richardson, 2006; Schönherr and Krauss, 2008; Seymour, 1992; Yennie *et al.*, 1961). The latter mainly affects observables that depend on the charged lepton kinematics, ranging from a few percent on charged-lepton p_{T}-spectra to $\mathcal{O}(1)$ effects on invariant mass distributions below resonance peaks or threshold-induced shoulders. In particular, since QED is an infrared-free theory, various different charged-lepton definitions can be and are used in measurements at various colliders: bare charged-leptons take the final-state charged-lepton at face value, and dressed charged-leptons recombine all photonic energy in a cone of size ΔR with the bare charged-lepton. While the bare charged-lepton definition demands a charged-lepton mass carried through at least some parts of the calculation (Dittmaier *et al.*, 2008), the dressed charged-lepton definition is suitable also for calculations with massless leptons through its insensitivity to collinear radiation. The historic and occasionally still used Born charged-lepton definition relies on event record documentation entries[4] and is not infrared safe at any higher order. It thus should be abandoned, for precision measurements in particular. Figure 13 details the corrections effected through photon bremsstrahlung where the dominant effect originates in the changes of the charged-lepton transverse momentum and invariant mass distributions, which influence the efficiency of the kinematic selection.

Besides providing a fully exclusive event description at parton level, event generators comprise tools to calculate non-perturbative effects like multi-parton interactions (Bähr *et al.*, 2008b; Butterworth *et al.*, 1996; Corke and Sjostrand, 2010; Gieseke *et al.*, 2017; Sjöstrand and Skands, 2004; Sjöstrand and van Zijl, 1987), parton-to-hadron transition (Andersson *et al.*, 1983; Field and Feynman, 1977; Field and Wolfram, 1983; Webber, 1984; Winter *et al.*, 2004) and hadron decays to arrive at a fully differential event description at particle level. Since methods to calculate these effects on timescales of $\mathcal{O}(1\,\text{CPU-s})$ per event are currently not available, phenomenological models with tunable, a priori unknown, parameters are used. These parameters, believed to be universal, have to be determined by a finite set of measurements in dedicated phase space regions, to be used in all other calculations. The size of these non-perturbative corrections is typically estimated using HERWIG and PYTHIA, and Fig. 14 shows an example of these corrections for an ATLAS Z + jet study at the LHC. These corrections are usually applied on partonic calculations, e.g., fixed-order NNLO QCD calculations described in Sec. II.A.1, to be compared to data.

B. Experimental results

The extensive program for measurements of V + jet processes at the TEVATRON has provided a critical incentive for the development of sophisticated higher-order calculations and

[4] In event generators, before NLO EW parton-shower matched calculations were available and, in fact, in most cases it is still the case now, the charged-lepton kinematics are generated first at LO accuracy, before dressing the interaction by photon radiation. The Born charged-lepton definition then relates the physical bare, or dressed charged-lepton, to its Born-level counterpart by using the recorded technical details of how the above calculation was carried out.

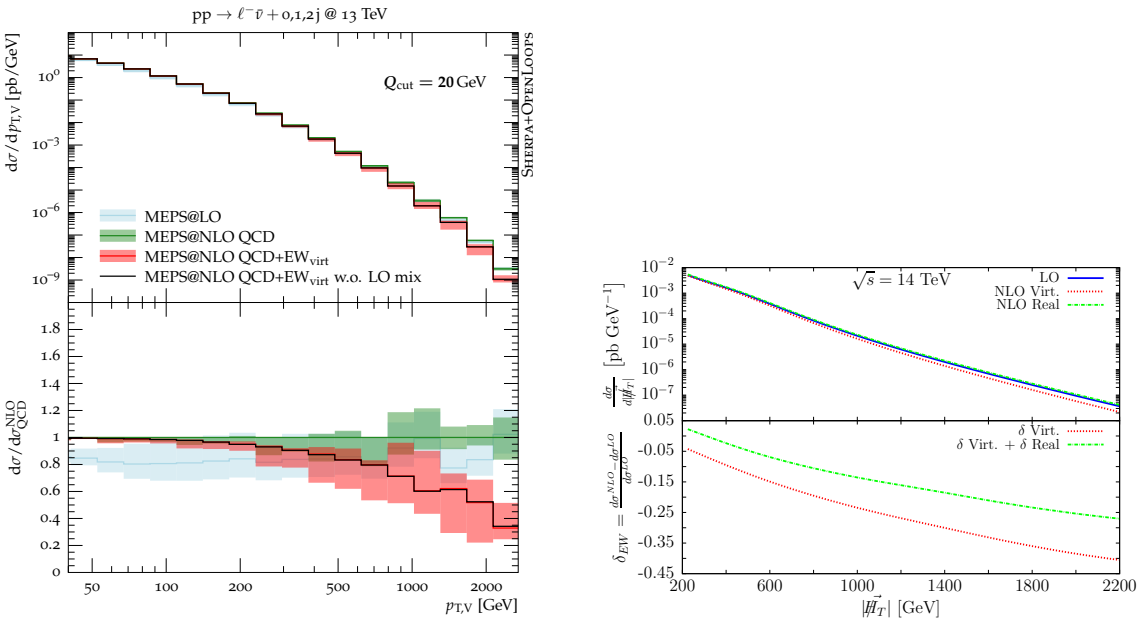

Figure 12 Reconstructed W boson transverse momentum in the production of a charged lepton and a neutrino in association with jets calculated using the MEPS@NLO method including approximate electroweak corrections as implemented in SHERPA (left), figure taken from (Kallweit *et al.*, 2016). Missing transverse momentum in neutrino-pair production in association with jets at leading order in QCD including EW corrections in the Sudakov approximation as implemented in ALPGEN and HERWIG (right), figure taken from (Chiesa *et al.*, 2013).

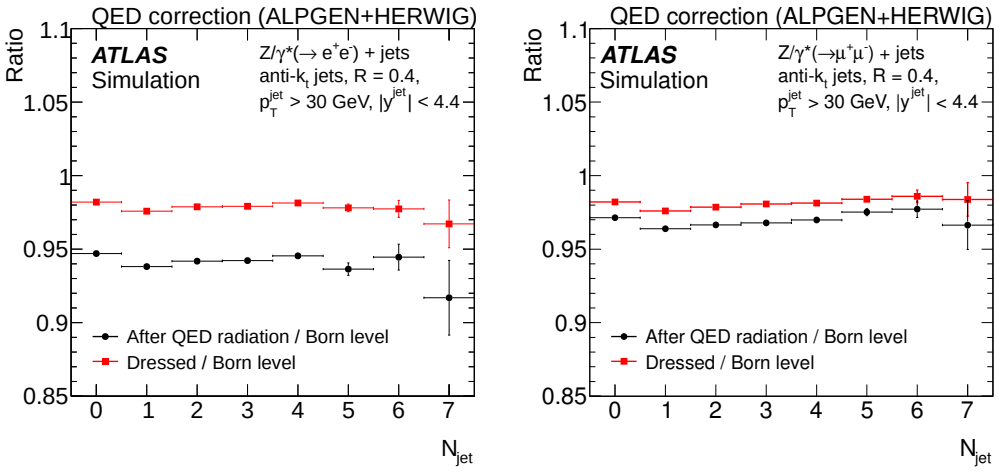

Figure 13 QED final state correction factors from Born-level to the infrared-safe bare and dressed charged lepton definitions as calculated using PHOTOS (Davidson *et al.*, 2016) for electrons (left) and muons (right) as a function of the number of accompanying jets. Figure taken from (ATLAS Collaboration, 2013e).

MC generators. In the first years of the LHC data-taking, LHC experiments benefited from the availability of accurate calculations and MC generators tuned to TEVATRON data, however the production of V + jet events at the LHC is not a simple rescaling of TEVATRON scattering, therefore a new program for extensive measurements of V + jet processes was setup early on in the LHC physics program and V + jet papers were among the first published by the LHC collaborations (ATLAS Collaboration, 2011b,c; CMS Collaboration, 2011b, 2012a). While the first LHC measurements of V + jet processes established SM measurements and assessed the validity of theoretical predictions at the LHC energy scales, later measurements considerably improved the experimental precision, reaching the percent level, and were thus able to expose data-prediction discrepancies and shortcomings in calculations. Such precision measurements highlighted the need for the development of more precise higher-order calculations in QCD

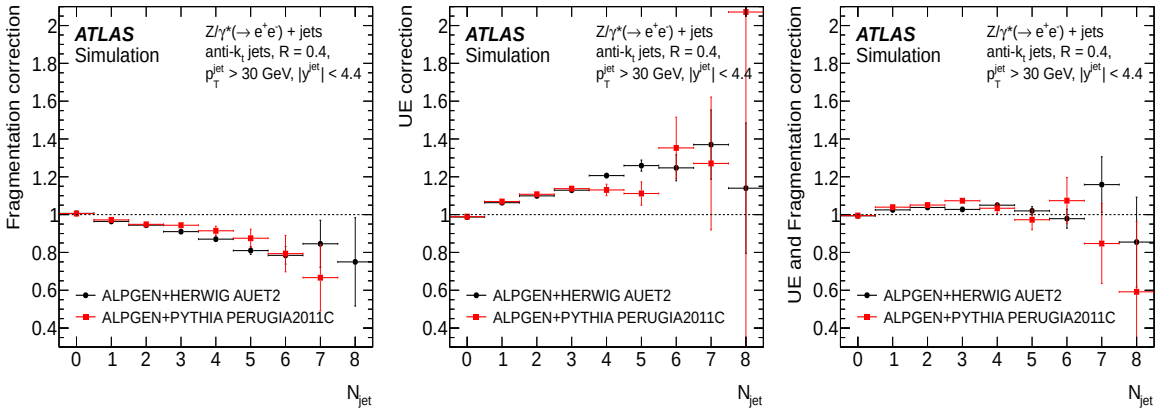

Figure 14 Non-perturbative correction factors as calculated using HERWIG and PYTHIA for the ATLAS Z + jet measurement in the electron-pair decay channel as a function of the number of accompanying jets: fragmentation (left), underlying event (middle) and the result of the two (right). Figure taken from (ATLAS Collaboration, 2013e).

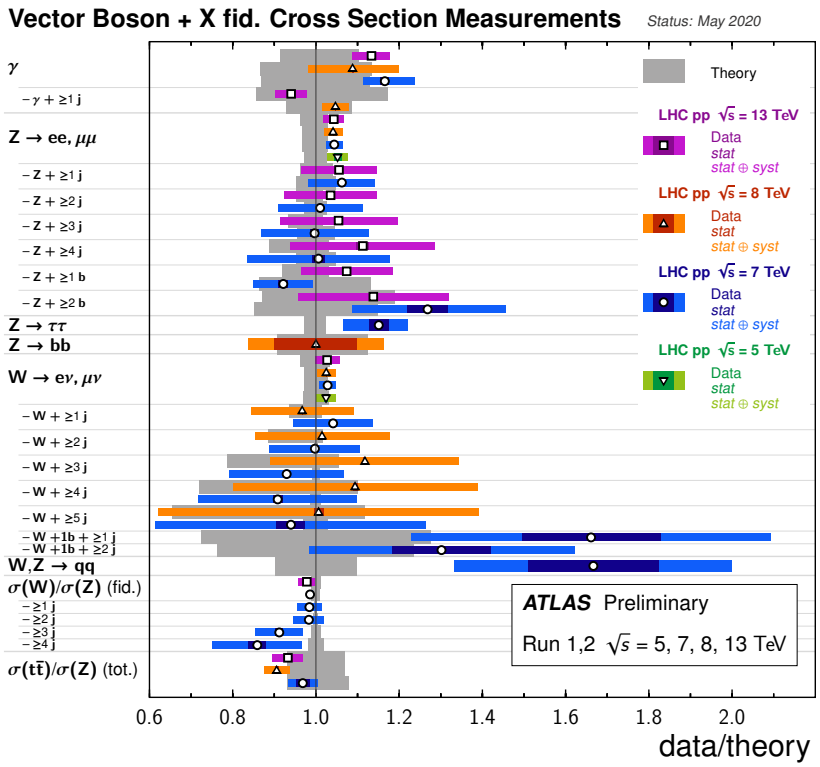

Figure 15 Summary of ratios of vector boson +X cross section measurements and predictions at 5, 7, 8 and 13 TeV center-of-mass energies in pp collisions at the LHC. Figure taken from (ATLAS Collaboration, 2019f).

and electroweak physics at the LHC, as detailed in Sec. II.A.

With the high precision achieved by LHC experiments the accurate definitions of the quantities that are experimentally measured is of great importance, as they must be theoretically sound, i.e., independent of the order of the theoretical approximation used, they must be related to fundamental physical quantities rather than parameters in theoretical models and as close as possible to experimental definitions to minimize model-dependent extrapolations. These general guidelines allow for accurate comparison of experimental results with theoretical predictions and ensure that results can be compared with future predictions without prior knowledge of the experimental apparatus or possibly dated theoretical models.

In this spirit, V + jets measurements at the TEVATRON and the LHC are primarily reported in fiducial phase spaces. Cross section measurements for W/Z + jet processes at the LHC are reported with decay charged leptons defined at "dressed-level", and corrections to a Born-level definition are often provided (see Sec.II.A.3). The cross sections measured in different decay channels of the W or Z bosons can be combined when the charged leptons are defined at Born level, however channel combination with charged leptons defined at dressed level is also done with a per-mille accuracy, i.e., below the experimental precision of the measurements. For a discussion of phase space and particle definitions at the LHC see Ref (ATLAS Collaboration, 2015c). For the measurements of the γ + jet production cross sections, isolation requirements are imposed on the photon to improve the identification at detector-level and to suppress the contribution of photons from the fragmentation of quarks and gluons at particle level (see Sec. II.A).

Experimental measurements include absolute or normalized differential cross sections in a fiducial phase space. The differential cross sections are measured as a function of several observables, i.e., event-based observables (jet multiplicity N_{jets}, boson transverse momentum p_{T}, H_{T} that is the scalar sum of the p_{T} of clustered jets, event-shapes etc.), and jet-based observables (n^{th}-jet p_{T} or rapidity y). Measurements also include angular correlations between final-state objects (jet-jet, lepton-jet, Z-jet or γ-jet etc.), for example the azimuthal difference $\Delta\phi$, the rapidity difference Δy, $\Delta R = \sqrt{\Delta\phi^2 + \Delta\eta^2}$, or the invariant mass of the two leading jets m_{jj}.

Particle-level measurements are finally compared to theoretical predictions from MC simulations or to fixed-order calculations. While MC simulations provide particle-level final states, fixed-order calculations (e.g., by BLACKHAT (Berger *et al.*, 2010, 2011, 2009, 2008; Bern *et al.*, 2013; Ita *et al.*, 2012), MCFM (Campbell and Ellis, 2010) or JETPHOX (Aurenche *et al.*, 2006; Catani *et al.*, 2002)) are at parton level and are often corrected for non-perturbative effects, such as underlying event and hadronisations ($3-4\%$ corrections), as discussed in Sec. II.A.3. Uncertainties in fixed-order NLO calculations in perturbative QCD (pQCD) due to missing higher-order terms are (conventionally) estimated by variations of the scales (renormalization and factorization), and are typically found in the $4-20\%$ range. These are followed by uncertainties on parton densities in the $1-4\%$ range, and on α_s in the $1-3\%$ range.

Figure 15 shows the breadth of V + jet measurements at different center-of-mass energies at the LHC and gives an overview of the level of agreement between measurements and state-of-the-art theoretical predictions. It is impressive to see such a level of agreement overall, however in the most precise experimental measurements, e.g., the ratios of W + jets and Z + jets, discrepancies are visible. These discrepancies become more significant, up to two standard deviations or greater, in some regions of phase space in differential cross section measurements. These measurements and comparisons with theoretical predictions will be presented in greater detail in following sections.

1. Experimental event reconstruction

In experimental analyses, V + jet events are reconstructed by identifying particles, such as photons, leptons, and clusters of particles such as jets, and applying selection requirements to purify the data samples. After background subtraction and corrections for the detector efficiency and resolution (*unfolding*), the production cross sections are measured inclusively or differentially in a fiducial phase space at particle level that is defined as close as possible to the detector-level kinematic selection. The unfolding of experimental results is an important part of the process of extraction of experimental measurements as it allows for the direct comparison with theoretical predictions with no prior knowledge of the detector layout, efficiency or resolution.

a. Particle reconstruction: photons, electrons, muons, missing transverse momentum and jets

The selection of photons is based on energy clusters reconstructed in the electromagnetic calorimeter, and depending on the number of matching tracks in the tracker they can be classified as unconverted or converted photons. Photons are reconstructed within the tracker acceptance, typically of $|\eta| < 1.0$ at the TEVATRON and $|\eta| < 2.37 - 2.5$ in the ATLAS and CMS detectors at the LHC. See (ATLAS Collaboration, 2019a; CMS Collaboration, 2015g) and references therein for a representative selection of recent articles on photon reconstruction, calibration and identification strategies and performance at ATLAS and CMS. Since the reconstruction of the photon momentum relies on measurements of energy deposits in cells in the calorimeter system, the transverse

momentum of the photon is often reported as transverse energy ($E_{\rm T}$). Measurements of prompt-photon production require isolation of photons to avoid the large contribution from neutral-hadron decays into photons. While a smooth cone isolation criterion (see Sec. II.A) is used for photon isolation in theoretical calculations, experimentally a cone-base isolation technique is used as most suitable for finite-granularity detectors: the photon is required to be isolated based on the amount of transverse energy in a cone of typical size $\Delta R = 0.4$ around the photon.

An electron is reconstructed as a charged-particle track geometrically associated with energy clusters in the electromagnetic calorimeter, while a muon is identified as a track segment in the muon system consistent with a track in the inner tracker, and can be associated with a minimum ionization signature in the calorimeters. Both electrons and muons are reconstructed within the inner tracker acceptance and are required to be isolated to further suppress background from misidentified objects, such as hadrons, or semi-leptonic heavy-flavor decays. The isolation requirements are tuned so that the electron or muon isolation efficiencies are high for signal, typically greater than 90%. The reader is referred to the following articles and references therein for details on electron and muon reconstruction, calibration, and identification as well as their performance at the LHC (Aaij *et al.*, 2019; ATLAS Collaboration, 2016e, 2019a; CMS Collaboration, 2015f, 2020d; LHCb Collaboration, 2015a, 2019c). Small correction factors, typically within 1% are applied to correct differences in the photon, muon and electron efficiencies between data and simulation.

Jets are clustered from energy deposits in the calorimeters in the ATLAS detector (ATLAS Collaboration, 2016g, 2020b) and from particle candidates reconstructed by a particle flow algorithm in the CMS detector (CMS Collaboration, 2017b,h, 2020e). Different jet algorithms are used at the TEVATRON and the LHC. At the TEVATRON, iterative cone algorithms, e.g., MidPoint, with split-merge prescriptions to resolve cases of overlapping stable cones, are used with a typical cone radius of $R = 0.4 - 0.7$. The experiments at the LHC migrated to the anti-k_t infra-red and collinear-safe jet algorithm, that also produces cone-shaped clustered jets. Jets are calibrated based on the jet $p_{\rm T}$ response in MC simulations, and pileup (the particle production from multiple interactions per bunch crossing) contribution to the jet energy is subtracted on an event-by-event basis in the calibration process using data-driven techniques. In situ measurements of the momentum balance in dijet, γ + jet, Z + jet, and multi-jet events are used to correct for any residual difference in jet energy scale between data and simulation.

In W + jet analyses with the W decaying leptonically, the event selection purity can be improved by imposing a requirement on the presence of missing transverse momentum in the event since the neutrino escapes direct detection. The missing transverse momentum is calculated as the negative vectorial sum of the transverse momenta of final-state particles. In the CMS experiment particles are reconstructed by a particle flow algorithm and are used as inputs to the computation of the missing transverse momentum, while in the ATLAS experiment the selected final state particles, e.g., electrons, muons, photons and jets, are used together with soft particles that are not associated with any other selected object, i.e., low-energy deposits in the calorimeter or low-momentum tracks associated with the primary vertex (ATLAS Collaboration, 2018g; CMS Collaboration, 2019e; LHCb Collaboration, 2015a).

b. Event reconstruction: photon+jets

Events with a photon and jets reconstructed in the final states are recorded using highly efficient (close to 100% efficiency) single-photon triggers, see Refs. (ATLAS Collaboration, 2020e; CMS Collaboration, 2017j) and references therein for a representative selection of articles on photon trigger architecture and performance at the LHC. Despite the application of the tight identification and isolation requirements on the photon, a non-negligible background originating from hadrons misidentified as photons contaminates the selected sample. The signal purity is typically higher for photon reconstructed centrally in the detector, increases as the photon $E_{\rm T}$ or jet $p_{\rm T}$ increase, and can reach values in the 70—90% range at high photon $E_{\rm T}$. The background is subtracted using data-driven methods based on signal-suppressed control regions. The photon reconstruction and selection efficiencies depend on the photon $E_{\rm T}$ and η and are in the approximate range of 70—100%. They decrease with the increasing number of jets in the event, primarily due to the photon isolation requirement.

Photons are selected in a broad range of minimum $E_{\rm T}$ requirements, approximately 20 – 200 GeV, similarly, the minimum jet $p_{\rm T}$ requirement varies and ranges between about 15 GeV

and 100 GeV.

The γ + jet cross section measurements are dominated by experimental systematic uncertainties, such as photon calibration and identification, and jet energy scale, at the level of few percent over a broad range of jet or photon transverse momenta. Only around the TeV energy scales, statistical uncertainty in data becomes the leading contribution at the LHC.

c. Event reconstruction: W/Z + jets

Events with a W or Z boson provide clean experimental signatures in the leptonic decay channels that can be triggered by single high-p_{T} electron or muon, or low-p_{T} dilepton (electron and muon) triggers (Aaij *et al.*, 2019; ATLAS Collaboration, 2020e; CMS Collaboration, 2017j; LHCb Collaboration, 2019a). The two leptonic channels with one (in W events) or two (in Z events) electrons or muons provide useful cross-checks of the results and can provide additional information to constrain experimental uncertainties in the combination of the cross sections. In addition to requirements on the charged lepton and jet transverse momenta and (pseudo-)rapidity acceptance, in W + jet events further requirements on the missing transverse momentum or on the transverse invariant mass are applied, while for Z + jet event reconstruction a requirement on the dilepton invariant mass is imposed in a window around the nominal Z boson mass. Typical selection requirements for W/Z + jet events include electrons or muons with a minimum p_{T} in the range 20–30 GeV within the tracker acceptance, jets with distance parameter in the range $R = 0.4$–0.7 with p_{T} requirement in the range 20–50 GeV and in rapidity ranges that vary from about 2 to 5 units, with a minimal separation between the lepton and jets of ΔR(lepton,jet) $>$ 0.4–0.7. At the LHCb experiment the weak boson decay charged leptons are reconstructed in the forward pseudo-rapidity region, in the range $2.0 < \eta < 4.5$, while jets are reconstructed in the pseudo-rapidity range $2.2 < \eta_{\mathrm{jet}} < 4.2$. W + jet and Z + jet events have different levels of background contamination. While for both processes at high jet multiplicity the background from $t\bar{t}$ production is dominant, W + jet events have a larger background contribution from multi-jet production in which hadronic particles are misidentified as an electron or a muon. The multi-jet background is estimated using data-driven techniques and contributes to $\approx 5 - 15\%$ of the W + jet data samples. The background from $t\bar{t}$ events contributes to about 0% (1 jet), 20% (Z + 6 jets) and 80% (W + 6 jets) and is estimated by MC or with data-driven techniques, and can be suppressed by a b-jet veto. Figure 16 shows the jet multiplicity distributions and the levels of background contamination in W + jet and Z + jet events in the muon decay channels in the CMS

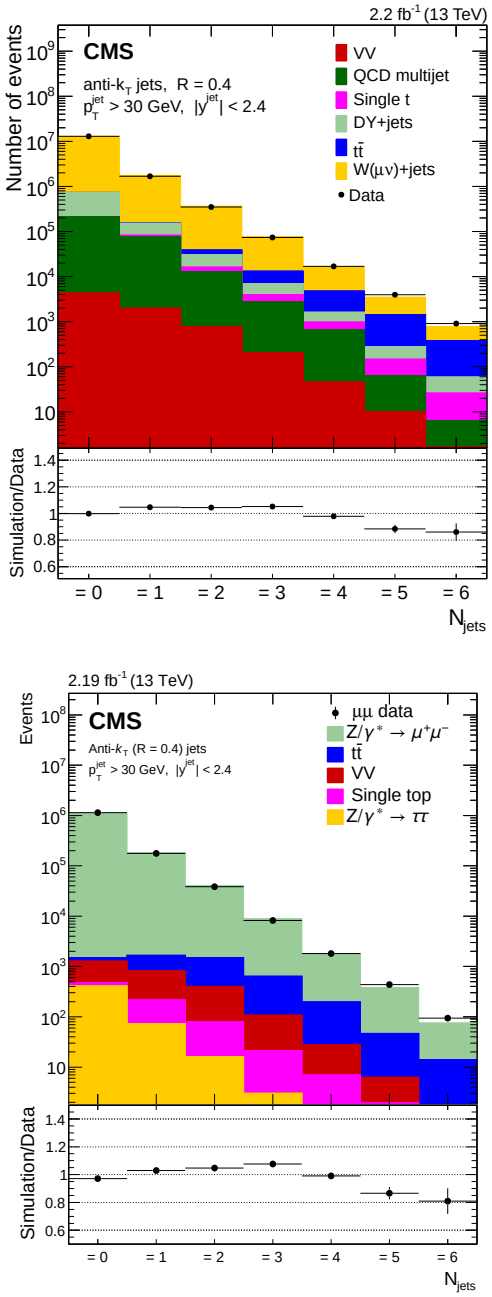

Figure 16 Reconstructed data, simulated signal and background events in the jet multiplicity distributions in pp collisions at 13 TeV center-of-mass energy at the LHC for W + jet events in the muon decay channel of the W boson (top), figure taken from (CMS Collaboration, 2017c), and for Z + jet events in the muon decay channel of the Z boson (bottom), figure taken from (CMS Collaboration, 2018d).

N_{jets}	$\frac{d\sigma}{dN_{\text{jets}}}$ [pb]	Tot. unc [%]	Stat [%]	JES [%]	JER [%]	Eff [%]	Lumi [%]	Bkg [%]	Pileup [%]	Unf model [%]	Unf stat [%]
=0	652	3.0	0.091	1.1	0.046	1.5	2.3	<0.01	0.22	—	0.026
=1	97.9	5.1	0.27	4.3	0.18	1.5	2.3	0.012	0.30	—	0.10
=2	22.2	7.3	0.63	6.7	0.20	1.6	2.3	0.026	0.43	—	0.26
=3	4.68	10	1.4	9.9	0.39	1.7	2.3	0.13	0.29	—	0.54
=4	1.01	11	3.5	10	0.24	1.7	2.3	0.43	0.56	—	1.4
=5	0.275	14	5.0	12	0.081	2.0	2.3	1.2	0.29	—	2.2
=6	0.045	24	15	17	0.36	1.8	2.4	3.5	1.7	—	6.6

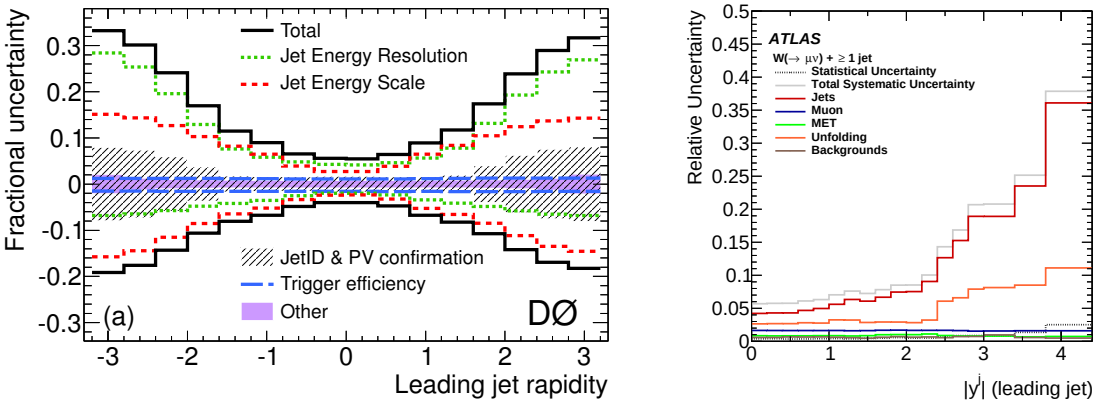

Figure 17 Cross section in exclusive jet multiplicity in Z+jets with 13 TeV pp collisions at the LHC for the combination of both decay channels and breakdown of uncertainties (top table), table taken from (CMS Collaboration, 2018d). Fractional experimental uncertainties in $W+1$ jet analyses in 1.96 TeV $p\bar{p}$ collisions at the TEVATRON (bottom-left plot), figure taken from (DØ Collaboration, 2013d), and in 7 TeV pp collisions at the LHC (bottom-right plot) as a function of the leading jet rapidity, figure taken from (ATLAS Collaboration, 2015b).

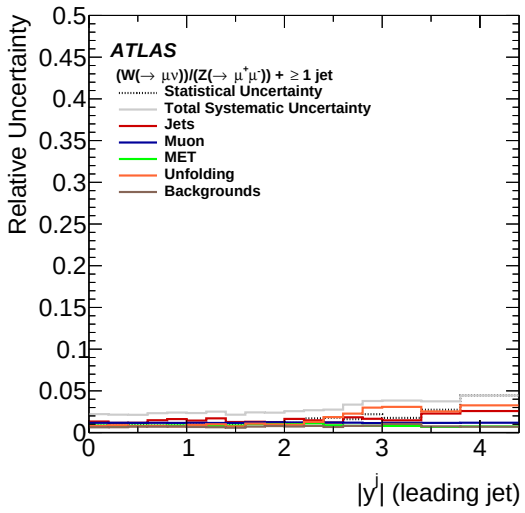

Figure 18 Relative experimental uncertainties on the inclusive ratio $W+1$ jet to $Z+1$ jet cross section as a function of the leading jet rapidity in 7 TeV pp collisions at the LHC. Figure taken from (ATLAS Collaboration, 2014a).

detector.

Experimental uncertainties are dominated at low jet p_{T} or low N_{jets} by systematics associated to the energy scale and resolution of the jets. At high jet p_{T} or high N_{jets}, unfolding and statistical uncertainties become important. At high N_{jets} the uncertainties on the backgrounds dominate in W + jet analyses. Figure 17 shows the level of experimental uncertainties in the Z + jet production cross section measurement as a function of the jet multiplicity, and the level of jet energy calibration uncertainty in $W+\geq$ 1 jet events as a function of the leading jet rapidity. The levels of experimental uncertainties in W/Z + jets are similar in analyses at 7, 8 and 13 TeV center-of mass energies at the LHC and comparable with TEVATRON experiments.

Measurements of ratios of differential cross sections allow for partial cancellations of uncertainties (both experimental and theoretical), for example in the ratio of W + jet to Z + jet differential cross sections, known as R_{jets}. The comparison of the experimental uncertainties in Fig. 17 (bottom-right) for W + jets and in Fig. 18 shows that in R_{jets} the experimental systematics, and especially those associated to jets, cancel from about 40% to about 5% at high jet rapidity. This large cancellation of uncertainties allows for an accurate test of SM predictions at the percent level in a wide region of phase space.

Measurements of V + light-jet production cross sections as functions of the jet multiplicity, jet transverse momenta and the jet rates are carried out at hadron colliders, as they provide benchmarks for the understanding of the underlying QCD dynamics and its modeling in MC generators. This sections starts with the presentation of the measurements of the associated production of jets and a photon, and concludes with the discussion of those of the associated productions of jets and a massive vector boson, i.e., W or Z.

a. Photon+jets cross section measurements

The processes of γ + jet production have the largest cross sections of all V + jet processes and they approach the W/Z + jet cross sections at high photon transverse momentum, i.e., in the regime where weak boson mass effects play a lesser role. Figure 19 presents the triple differential cross-section as a function of the photon transverse momentum, and the γ and jet pseudo-rapidities, at the TEVATRON in $p\bar{p}$ collisions at 1.96 TeV center-of-mass energy and at the LHC in pp collisions at 7 TeV center-of-mass energy. The DØ measurement is carried out in two regions of the jet rapidity and in event configurations in which the jet and photon have either the same or opposite signs in rapidity, while the CMS analysis is in two regions of the jet pseudo-rapidity and in four regions of the photon pseudo-rapidity. In both cases the measurements span several orders of magnitude in the production cross sections. The predictions include the NLO pQCD calculation implemented in JETPHOX and, in the CMS analysis, the tree-level matrix elements with up to 3 parton-jets matched to parton showering in the SHERPA generator. The predictions are overall consistent with data but unable to describe the cross section variations across the entire measured range of phase space. TEVATRON results are an important benchmark for theoretical calculations and have served as a stepping stone for more accurate modeling of such processes for the LHC. However, despite this progress in theoretical predictions, some data-theory discrepancies are observed at the LHC in specific kinematic regions of γ + jets. For example, in regions with large photon η and p_{T} in γ + 1-jet events, the ratios between data and NLO pQCD predictions by JETPHOX and SHERPA are in the range of 50% to 70% (CMS Collaboration, 2014e), and in the photon p_{T} region

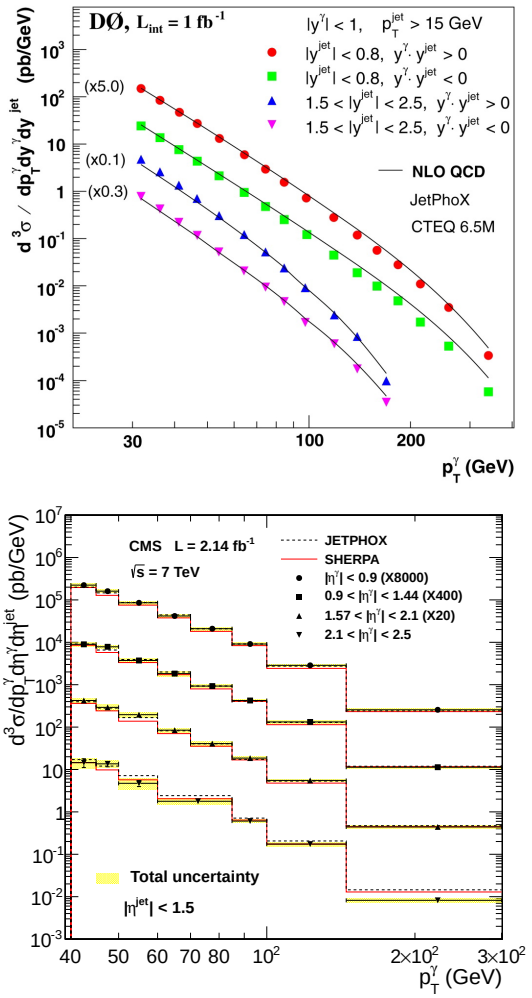

Figure 19 Triple differential cross sections as a function of p_{T}^{γ} in four photon rapidity intervals in $p\bar{p}$ collisions at 1.96 TeV center-of-mass energy at the TEVATRON, figure taken from (DØ Collaboration, 2008b) (top), and in four different ranges of η^{γ} for $p_{\mathrm{T}}^{\mathrm{jet}} > 30$ GeV and $|\eta^{\mathrm{jet}}| < 1.5$ in pp collisions with 7 TeV center-of-mass energy at the LHC (bottom), figure taken from (CMS Collaboration, 2014e). The measured cross sections are compared with the NLO pQCD calculation by JETPHOX and with the LO MC SHERPA simulation (bottom).

greater than 750 GeV in γ + 2-jet events (ATLAS Collaboration, 2017b) the discrepancy between data and the NLO calculation reaches about 2σ.

In addition to testing QCD calculations and MC predictions, the measurements of photon + jet production can be used to constrain the parton density functions (PDFs). The results in Fig. 20 are shown as an example of ratios between theory and LHC data for the measurement of the differential cross section for γ + jet production as a function of the photon E_{T}. The measurement is carried out in two photon and two jet rapidity regions, while the figure shows

the results in the forward photon and forward jet bin. The measurement shows good agreement between LHC data and NLO predictions in pQCD from JETPHOX. As Fig. 20 (top) shows, the experimental and theoretical uncertainties are comparable, and the theoretical jet scale uncertainty dominates the theoretical uncertainties in the NLO pQCD approximation. Figure 20 (bottom) shows the NLO prediction by JETPHOX using various NLO PDF sets. Although the differences between the studied PDF sets are small and subleading with respect to the scale uncertainty estimated in the NLO pQCD approximation, new calculations at higher orders in QCD with smaller scale uncertainties, i.e., next-to-next-to-leading order, are available (Campbell *et al.*, 2017a,b; Chen *et al.*, 2020) and motivate the use of such measurements at the LHC to improve the gluon and other PDFs (Campbell *et al.*, 2018), especially in the kinematic regions where the experimental uncertainties are smaller or comparable to theoretical uncertainties, e.g., in low to middle range in photon E_{T}.

For other inclusive photon and photon + light-jet measurements carried out at the TEVATRON and at the LHC the reader is referred to the analyses reported in Refs. (ATLAS Collaboration, 2011a,b, 2012g, 2013a, 2014d, 2016c, 2017d, 2019c,d, 2020c; CMS Collaboration, 2011a,b, 2013f, 2019d; DØ Collaboration, 2010a, 2011b).

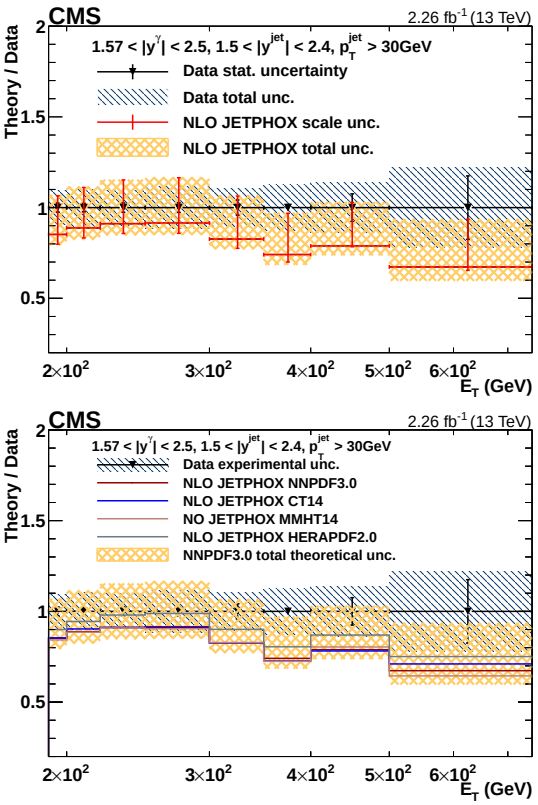

Figure 20 Ratios of NLO (JETPHOX) predictions to data as a function of the photon transverse energy in γ+jet events in the forward photon and jet rapidity regions in pp collisions at the LHC with 13 TeV center-of-mass energy. The plot on the top shows the contribution of the scale uncertainty to the total theoretical uncertainty in the NLO JETPHOX calculation, compared to the experimental uncertainties. The plot on the bottom shows NLO JETPHOX calculation with various NLO PDF sets, compared to the experimental uncertainties. Figures taken from (CMS Collaboration, 2019c).

b. W/Z + jets cross sections measurements

A typical measurement of W/Z + jet processes is the production cross section (multiplied by the leptonic branching ratio) as a function of jet multiplicity, as shown in Fig. 21 for Z + jet production. Such a measurement is important to assess the accuracy of SM predictions that are used to estimate the W/Z + jet yield in searches of new physics signatures.

The production of W/Z + jets is a multi-scale process and various observables can be used to define the scale of the process, depending on the kinematic configuration. A common variable used to set the scale in W/Z + jet processes is H_{T}, which is also used to discriminate new physics from SM background, for example in supersymmetry searches. This variable has, however, different definitions: in ATLAS is defined as the scalar sum of the transverse momenta of leptons (including neutrinos) and jets in the event, while in CMS as the scalar p_{T} sum of the jets only. Figure 22 shows two examples of the differential cross section for $W + \geq 1$ jet production as a function of H_{T} by the CMS and ATLAS experiments. The measurements in Figures 21 and 22 show excellent agreement with theoretical predictions over 4 orders of magnitude in cross-section. The multitude of models that are compared to data show the variety of theoretical approaches that can be validated with such measurements. These results show that MC simulations with multi-parton calculations in the matrix element matched to the parton shower are in agreement with the data up to very high jet multiplicity and in a broad range in energy scale. The high experimental precision also exposes discrepancies between measurements and predictions. In Figure 22 (right) discrepancies with pQCD NLO calculations (BLACKHAT) are visible at large H_{T} values, when the jets are measured in a broad rapidity region ($|y^{\mathrm{jet}}| < 4.4$). The accuracy of the calculation improves when higher-order

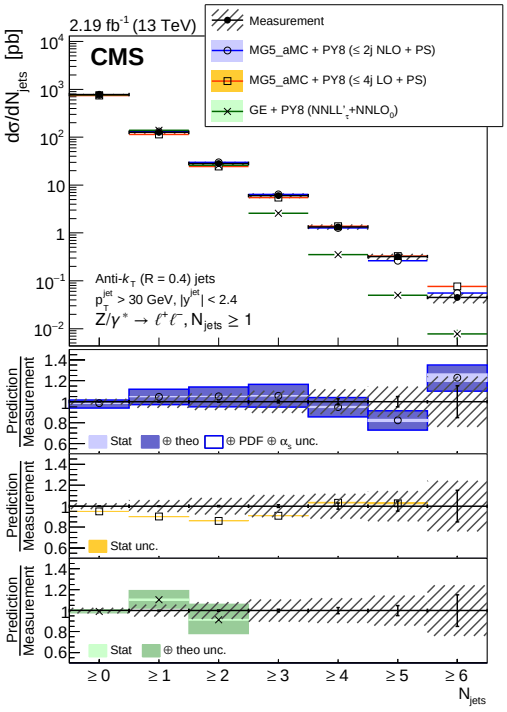

Figure 21 Cross section as a function of the inclusive jet multiplicity for Z + jet events at 13 TeV center-of-mass energy in pp collisions at the LHC. Figure taken from (CMS Collaboration, 2018d).

pQCD corrections are included, i.e., in N_{jetti} NNLO (Boughezal *et al.*, 2015b; Gehrmann-De Ridder *et al.*, 2016b) or with the *exclusive sum* approach (Alcaraz Maestre *et al.*, 2012) in BLACKHAT (Berger *et al.*, 2010, 2011; Bern *et al.*, 2013) in which NLO information from higher multiplicity processes are included to the standard fixed-order prediction, cf. Sec. II.A.

The large statistics of W/Z + jet events allows to carry out double differential measurements, similarly to what is typically done in inclusive jet or γ + jet measurements, see two examples in Refs. (ATLAS Collaboration, 2019b; CMS Collaboration, 2017e) by the ATLAS and CMS experiments. Figure 23 shows an example of a double differential cross section as a function of the leading jet p_{T} and rapidity that is performed in a broad region of phase space up to jet $p_{\text{T}} = 500$ GeV and $|y| = 4.7$. Such measurements are expected to provide valuable input to the understanding of parton density functions in addition to QCD dynamics. However, in several regions of phase space the precision of experimental results is higher than current prediction-to-prediction differences, and discrepancies between data and theoretical predictions can be up to 40% i.e., larger than the effects from PDFs, and thus the potential PDF sensitivity of the data cannot be exploited. The MC simulation that includes NLO QCD corrections provides a more accurate normalization and better modeling of the shapes of the distributions than LO QCD predictions. Similar conclusions can be reached from several other results on Z+jet and W+jet processes: the inclusion of higher-order QCD corrections in fixed-order calculations and in MC simulations generally provides predictions that more accurately describe the data and are also more precise. Figures 24 and 25 show examples of such an effect. Better agreement with data and smaller uncertainties are found in predictions that include higher-order corrections, such as in the NLO MADGRAPH5_aMC@NLO MC prediction with respect to the LO MADGRAPH, the n̄NLO approximation with LOOPSIM + MCFM (Rubin *et al.*, 2010) and the NNLO N_{jetti} calculation, for the distribution of the leading jet p_{T} at the TEVATRON, up to 400 GeV, and at the LHC, up to 1 TeV. Such an effect is corroborated by other studies, such as those in Refs. (ATLAS Collaboration, 2019b; CMS Collaboration, 2017c, 2018d), where data are compared to NNLO predictions. These experimental results also show that such processes can test theoretical calculations in a broad region of phase space with great precision, i.e., with an uncertainty as low as few percent in the $W+ \geq 1$ jet events.

The jet multiplicity in W/Z + jet events is correlated to the energy scale of the process. Figure 26 shows the correlation between the average jet multiplicity ($\langle N_{\text{jet}} \rangle$) and H_{T} in W+jet and Z + jet events at the TEVATRON and at the LHC, and a similar correlation is demonstrated between $\langle N_{\text{jet}} \rangle$ and the Z boson p_{T} in Z + jets events in Fig. 27. At $H_{\text{T}} \approx 300$ GeV in W events or $p_{\text{T}}^{Z} \approx 300$ GeV in Z events the average jet multiplicity is about 2, while at $H_{\text{T}} = 1000$ GeV the average jet multiplicity reaches 3. In the TEVATRON study in Figure 26 (left) a fixed-order NLO calculation is used to computed the mean number of jets in an inclusive W + n-jet sample by using the following prescription to improve the description beyond the NLO approximation: $\langle N_{\text{jets}} \rangle = n + (d\sigma_{n+1}^{\text{NLO}} + d\sigma_{n+2}^{\text{LO}})/d\sigma^{\text{NLO}}$ (Alcaraz Maestre *et al.*, 2012). Such a calculation describes well this effect while the MC simulations underestimate the effect of the correlation. At the LHC a good agreement between data and simulation is found.

Multi-differential cross section measurements of the vector boson production allow detailed studies of QCD dynamics. In the absence of QED corrections, the five-dimensional differential cross-section $\mathrm{d}\sigma/(\mathrm{d}p_{\text{T}}^{Z}\,\mathrm{d}y^{Z}\,\mathrm{d}m^{Z}\,\mathrm{d}\cos\theta\,\mathrm{d}\phi)$ that describes the kinematics of the two lep-

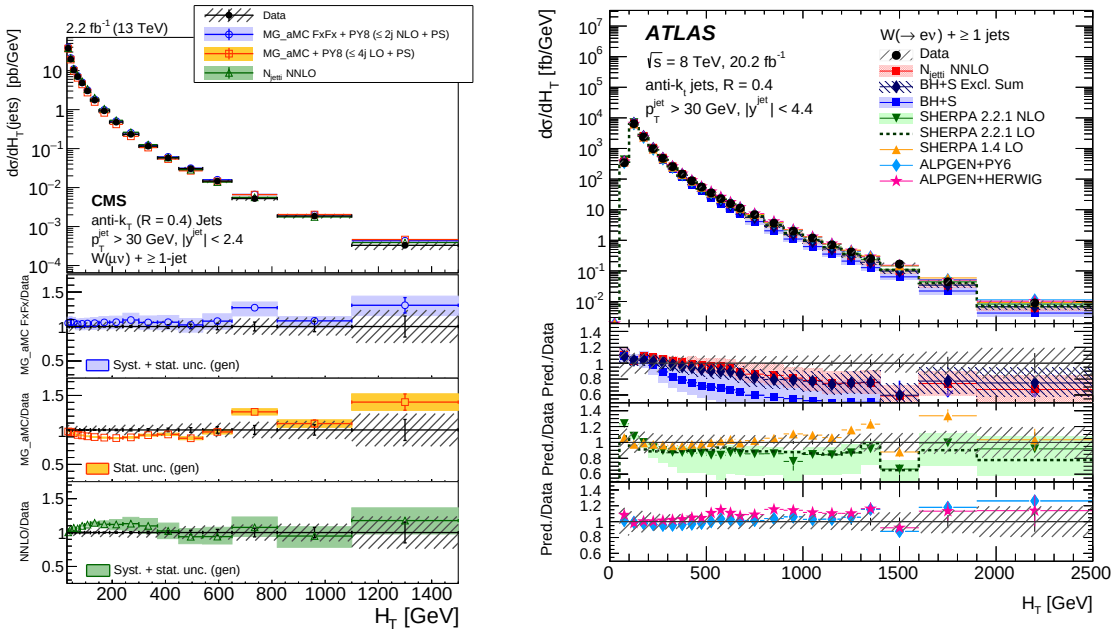

Figure 22 Differential cross section for the production of a W boson with at least one jet as a function of H_{T} at 13 TeV (left), figure taken from (CMS Collaboration, 2017c), and at 8 TeV (right), figure taken from (ATLAS Collaboration, 2018a), in pp collisions at the LHC.

tons from the Z boson decay can be decomposed into a sum of nine harmonic polynomials $P_i(\cos\theta, \phi)$ and eight dimensionless angular coefficients $A_i = A_i(p_{\mathrm{T}}^Z, y^Z, m^Z)$ $(i = 0..7)$, which represent the ratios of helicity cross-sections with respect to the unpolarised one (σ^{U+L}) (Mirkes, 1992; Mirkes and Ohnemus, 1994) [5],

$$
\begin{aligned}
&\mathrm{d}\sigma/(\mathrm{d}p_{\mathrm{T}}^Z\,\mathrm{d}y^Z\,\mathrm{d}m^Z\,\mathrm{d}\cos\theta\,\mathrm{d}\phi) \\
&= 3\,\mathrm{d}\sigma^{U+L}/(16\pi\,\mathrm{d}p_{\mathrm{T}}^Z\,\mathrm{d}y^Z\,\mathrm{d}m^Z) \\
&\quad\times\Big\{(1+\cos^2\theta) + \tfrac{1}{2}\,A_0\,(1-3\cos^2\theta) \\
&\qquad + A_1 \sin 2\theta\cos\phi + \tfrac{1}{2}\,A_2\,\sin^2\theta\cos 2\phi \\
&\qquad + A_3 \sin\theta\cos\phi + A_4\cos\theta \\
&\qquad + A_5\sin^2\theta\sin 2\phi + A_6\sin 2\theta\sin\phi \\
&\qquad + A_7\sin\theta\sin\phi\Big\}\ .
\end{aligned}
$$

In this formulation the dependence on the QCD dynamics from the Z boson production mechanism, i.e., p_{T}^Z, y^Z, and m^Z, is entirely provided by the A_i coefficients and σ^{U+L}. It is clear, however, that in order to access all eight coefficients, the full dependence on θ and ϕ has to be analyzed. In particular, for Z production at LO in QCD, i.e., $\mathcal{O}(\alpha_{\mathrm{s}}^0)$, only A_4 is non-zero, while at NLO, i.e., $\mathcal{O}(\alpha_{\mathrm{s}})$, also the A_{0-3} receive non-zero contributions due to the spin-1 nature of the additional gluon. The final coefficients, A_{5-7}, receive contributions starting at NNLO QCD, i.e., $\mathcal{O}(\alpha_{\mathrm{s}}^2)$, arising through the effective ggZ interaction (Hagiwara *et al.*, 1992), and are thus comparatively small.

The CDF collaboration at the TEVATRON carried out a measurement of some of the A_i angular coefficients in $p\bar{p}$ collision data at a center-of-mass energy of 1.96 TeV (CDF Collaboration, 2011), and the average value of the A_4 coefficient was used to indirectly measure the weak mixing angle $\sin^2\theta_W$ (CDF Collaboration, 2013a). The ATLAS and CMS collaborations at the LHC measured the angular coefficients for W boson polarization at 7 TeV (ATLAS Collaboration, 2012e; CMS Collaboration, 2011c), and more recently for the Z boson at 8 TeV (ATLAS Collaboration, 2016b; CMS Collaboration, 2015a). From the Z boson angular coefficient A_4 measured at the LHC, the $\sin^2\theta_W$ parameter is also extracted (ATLAS Collaboration, 2018d). Other measurements of $\sin^2\theta_W$ at the LHC are included in Refs. (ATLAS Collaboration, 2015a; CMS Collaboration, 2011d, 2018e; LHCb Collaboration, 2015b), and a legacy combination of TEVATRON measurements can be found in Ref. (CDF and D0 Collaborations, 2018) (see references therein for individual TEVATRON measurements). As illustrated in Fig. 27, for high values of the Z

[5] In the presence of QED corrections, the expansion in terms of sperical harmonics does not terminate after $l = 2$, but instead turns into an infinite sum.

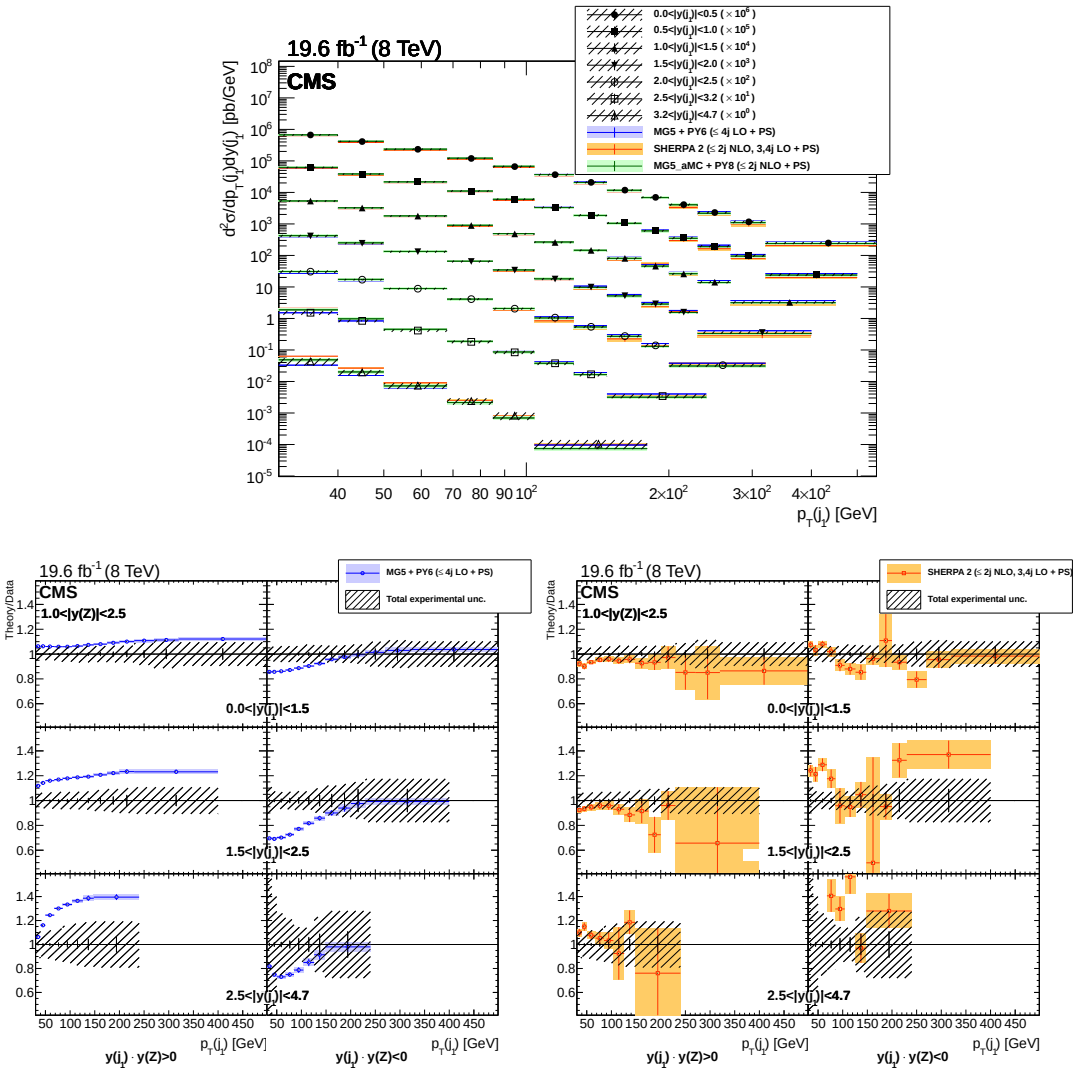

Figure 23 Differential cross section (top) and theory-to-data ratio (bottom) for Z + jet production as a function of the leading jet transverse momentum and rapidity in 8 TeV pp collisions at the LHC. Figures taken from (CMS Collaboration, 2017f).

boson p_{T} the measurements become sensitive to the production of the Z boson in association with jets. Although NLO and NNLO are in general agreement with the A_i distributions as functions of the Z boson p_{T} in data, the A_2 coefficient, which is among the most sensitive coefficients to higher-order corrections, increases less steeply in the data than in the calculations as the Z boson p_{T} increases, see Fig. 28. The difference between A_0 and A_2 coefficients, i.e., $A_0 - A_2$, is particularly interesting since it is zero if calculated at NLO in pQCD, the so-called Lam-Tung relation (Lam and Tung, 1978, 1980), and becomes positive at NNLO in pQCD. As Fig. 29 (top) shows, the measured values of $A_0 - A_2$ increase for increasing values of p_{T}^Z, up to about 0.15, while significant deviations are observed in the comparison with MC predictions that include NLO pQCD calculations matched to the parton shower. While ATLAS and CMS experimental measurements are consistent, the CMS measurement is not sufficiently precise to show significant disagreement between data and predictions. These measurements prompted a dedicated study (Gauld *et al.*, 2017) of the A_i coefficients in Z boson events that calculated $\mathcal{O}(\alpha_{\mathrm{s}}^3)$ pQCD corrections and their uncertainties on $A_0 - A_2$. As seen in Fig. 29 (bottom), the $\mathcal{O}(\alpha_{\mathrm{s}}^3)$ corrections are large and lead to a significant improvement in the agreement with the data, however a tendency of underestimating the data is visible at high Z boson p_{T}. It must be noticed that in Fig. 29 (bottom), differently from the results shown in Fig. 28 and Fig. 29 (top), the $\mathcal{O}(\alpha_{\mathrm{s}}^2)$ and $\mathcal{O}(\alpha_{\mathrm{s}}^3)$ calculations are denoted as NLO and NNLO, respetively.

The studies of QCD scaling properties are

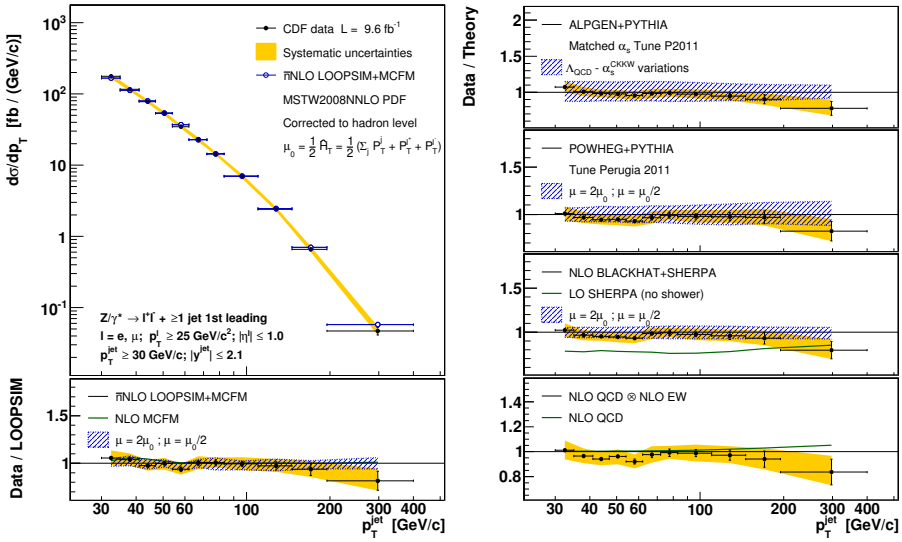

Figure 24 Differential cross section and data-to-theory ratios as a function of the leading-jet p_{T} for $Z+ \geq 1$ jet events in 1.96 TeV $p\bar{p}$ collisions at the TEVATRON. Figure taken from (CDF Collaboration, 2015).

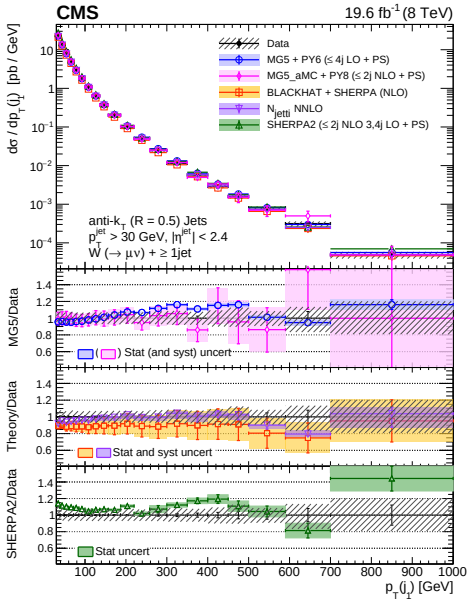

Figure 25 Differential cross section as a function of the leading-jet p_{T} in $W+ \geq 1$ jet events with 8 TeV pp collisions at the LHC, figure taken from (CMS Collaboration, 2017e).

useful for a better understanding of QCD dynamics and in analyses that employ jet vetoes to separate signal processes from W/Z + jets backgrounds (Berends *et al.*, 1989; Gerwick *et al.*, 2012). Figure 30 from Ref. (ATLAS Collaboration, 2013e) reports a study of two different types of scaling in Z + jets in the exclusive jet multiplicity ratios $R_{(n+1)/n} = N_{Z+(n+1)}/N_{Z+n}$. When a symmetric selection of the jet transverse momenta is applied, i.e., $p_{\mathrm{T}} > 30$ GeV for all jets, the so-called "Staircase scaling" is seen, whereas when an asymmetric selection of the jet transverse momenta is applied, i.e., p_{T}(leading) > 150 GeV and $p_{\mathrm{T}} > 30$ GeV for all other jets, a falling distribution is seen, i.e., the so-called "Poisson scaling". The scaling properties measured in data are well reproduced by the theory. The staircase scaling is a property of non-abelian theories with $R_{(n+1)/n} = R = e^{-b}$, as $\sigma_n = \sigma_0 e^{-bn}$, and occurs in events with democratic jet selection and no major scale separations. The first bin of the distribution in Fig. 30 (top), i.e., $R_{1/0}$, is suppressed by PDF effects by about 60%. The Poisson scaling (already known from final-state-radiation QED at e^+e^- colliders) occurs in events that feature large differences between the scale Q of the process and the radiation cut-off scale Q_0. For $Q \gg Q_0$ each emission is independent from the previous one (the primary emission is typically off the hard parton leg), while for $Q \approx Q_0$ the emissions are correlated (for secondary emissions from secondary quark lines). In this configuration the ratio $R_{(n+1)/n} = \langle n \rangle / n + 1$ follows a Poissonian distribution with $P_n = \frac{1}{n!} \langle n \rangle^n e^{-\langle n \rangle}$ and occurs in abelian theories too. Asymptotically for large N_{jets} the staircase approximation dominates as can be seen in Fig. 30 (bottom).

For other cross section measurements of W/Z + jet processes at the TEVATRON Run-2 and at the LHC, the reader is referred to the publications in Refs. (ATLAS Collaboration, 2011c, 2012f,h, 2017h, 2019b; CDF Collaboration, 2008b,c; CMS Collaboration, 2012a, 2015c,e, 2017c, 2018d; DØ Collabora-

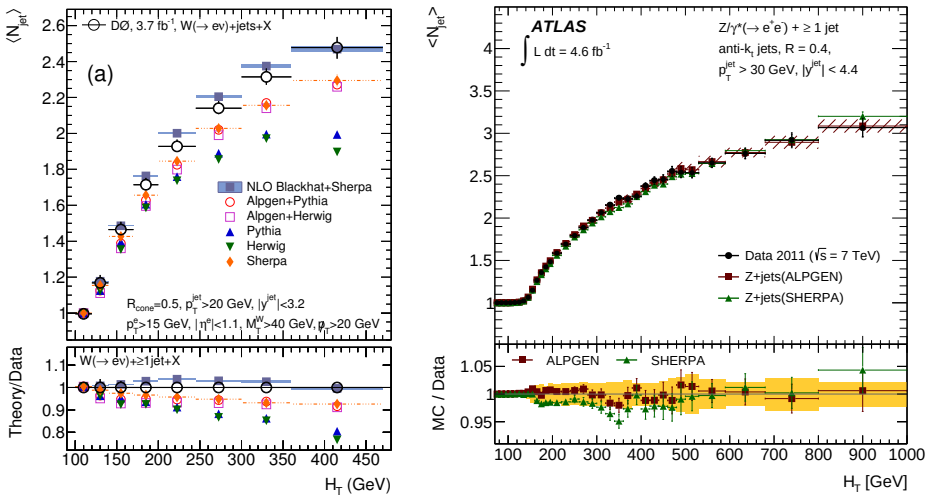

Figure 26 Average number of jets $\langle N_{\text{jet}} \rangle$ as a function of H_{T} in W + jet events in 1.96 TeV $p\bar{p}$ collisions at the TEVATRON (left), figure taken from (DØ Collaboration, 2013d), and in Z + jet events with 7 TeV pp collisions at the LHC (right), figure taken from (ATLAS Collaboration, 2013e).

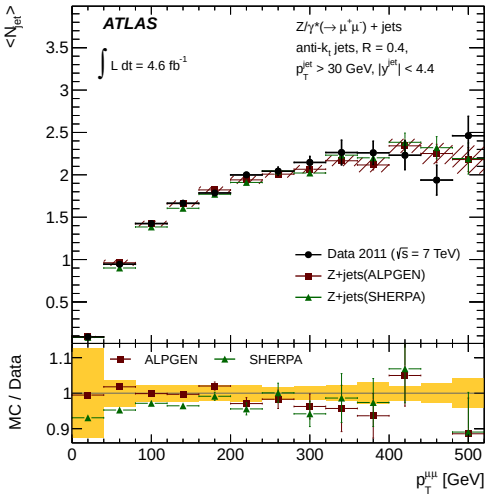

Figure 27 Average number of jets $\langle N_{\text{jet}} \rangle$ as a function of the Z boson p_{T} in Z + jet events with 7 TeV pp collisions at the LHC, figure taken from (ATLAS Collaboration, 2013e).

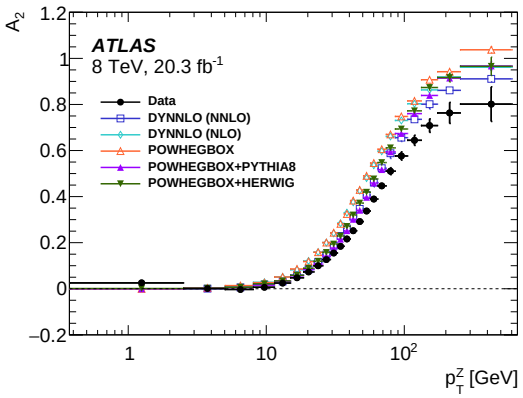

Figure 28 Distribution of the angular coefficient A_2 as a function of p_{T}^Z, integrated over y^Z, in data, measured in 8 TeV pp collisions at the LHC, compared to the predictions at NLO, i.e., $\mathcal{O}(\alpha_{\text{s}})$, and NNLO, i.e., $\mathcal{O}(\alpha_{\text{s}}^2)$, in pQCD, as well as to those from NLO calculations with two different parton-shower models. Figure taken from (ATLAS Collaboration, 2016b).

tion, 2008a, 2009b, 2011c; LHCb Collaboration, 2016, 2019b).

3. Event properties

The measurements of angular distributions provide important tests of the modeling of QCD in the theory, as these measurements are sensitive to the parton emission at small and large angles. Hard emissions at large angles are typically calculated by matrix elements, while unresolved soft or collinear radiation is typically modeled in MC generators by the parton shower. Measurements of the angular ($\Delta\phi(\text{j}_1,\text{j}_2)$) or rapidity ($\Delta y(\text{j}_1,\text{j}_2)$) separation between the two associated leading jets or their invariant mass (m_{jj}) distribution are important for studies of vector boson fusion or scattering to disentangle the electroweak from the QCD production mechanisms, see Sec. III. Figures 31 and 32 show selected measurements of $\Delta y(\text{j}_1,\text{j}_2)$ and m_{jj} at the TEVATRON and at the LHC, respectively, in events with a W boson produced in association with at least two jets selected in a broad kinematic region, i.e., jet $p_{\text{T}} > 30(20)$ GeV and $|y| < 4.4(3.2)$ at the LHC (TEVATRON). The fixed-order NLO calculation (BLACKHAT) is in good agreement with data on $\Delta y(\text{j}_1,\text{j}_2)$,

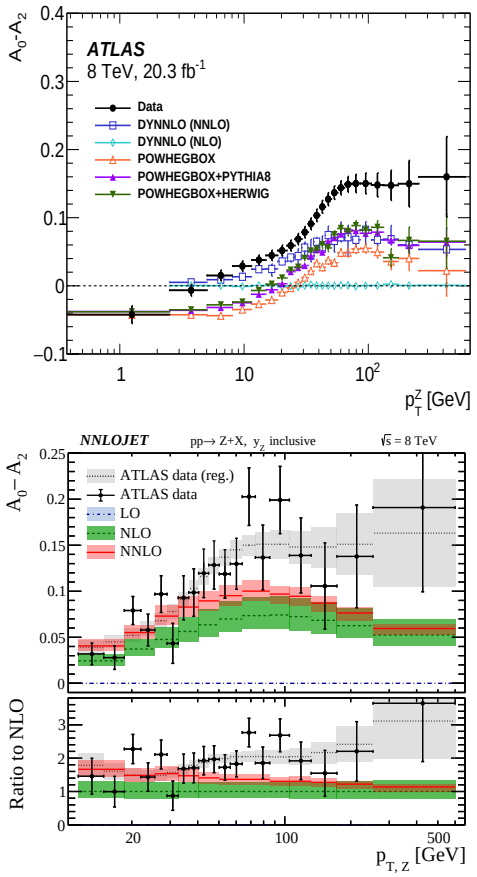

Figure 29 Distribution of the angular coefficient $A_0 - A_2$ as a function of p_{T}^Z, integrated over y^Z, in data, measured in 8 TeV pp collisions at the LHC, compared to the predictions at NLO, i.e., $\mathcal{O}(\alpha_{\mathrm{s}})$, and NNLO, i.e., $\mathcal{O}(\alpha_{\mathrm{s}}^2)$, in pQCD, as well as to those from NLO calculations with two different parton-shower models (top), figure taken from (ATLAS Collaboration, 2016b). Theoretical predictions with associated uncertainties at $\mathcal{O}(\alpha_{\mathrm{s}})$ (denoted here as LO), $\mathcal{O}(\alpha_{\mathrm{s}}^2)$ (denoted here as NLO), and $\mathcal{O}(\alpha_{\mathrm{s}}^3)$ (denoted here as NNLO) are compared to data (bottom), figure taken from (Gauld *et al.*, 2017).

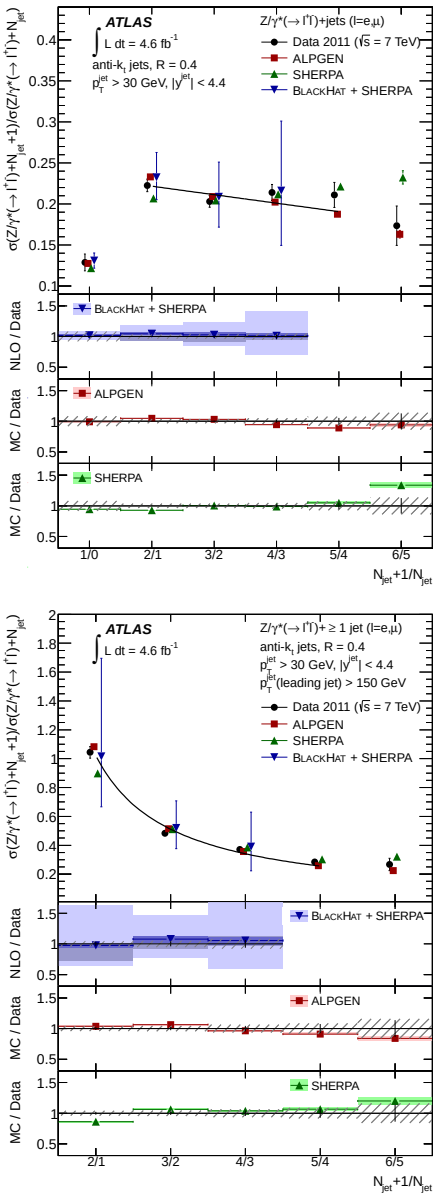

Figure 30 Ratio of Z + jet cross sections for successive exclusive jet multiplicities, N_{jet}, in events selected with symmetric jet selection, i.e., $p_{\mathrm{T}} > 30$ GeV for all jets in the event (top) and in events with at least one jet with $p_{\mathrm{T}} > 150$ GeV (bottom), with 7 TeV pp collisions at the LHC. The figures include comparisons with fixed-order calculation, MC simulations as well as a linear fit (top) and a Poisson fit (bottom) to the data. Figures taken from (ATLAS Collaboration, 2013e).

especially at the LHC. A similar level of discrepancy is seen at the TEVATRON and at the LHC for SHERPA, while ALPGEN and HEJ (based on BFKL-like resummation) MC generators are in better agreement with the data. The fixed-order NLO calculation (BLACKHAT) is in good agreement with the data in the m_{jj} distribution in the range accessible by the TEVATRON, i.e., up to about 300 GeV. The LHC measurement of the m_{jj} distribution extends to 2 TeV, and the fixed-order NLO calculation is compared to LHC data up to 1 TeV, showing good agreement up to approximately 500 GeV. The HEJ simulation is in agreement with data over the whole m_{jj} range at the TEVATRON and at the LHC, but its associated uncertainties are large. Significant discrepancies in the high m_{jj} region at the LHC are visible in LO and NLO multi-leg MC predictions in the SHERPA and MEPS@NLO calculations. In such a kinematic region important contributions are expected from the modeling of the beam remnant, underlying event, multi-parton interactions and parton shower. Similar measurements at the LHC (ATLAS Collaboration, 2017h; CMS Collaboration, 2017e,f)

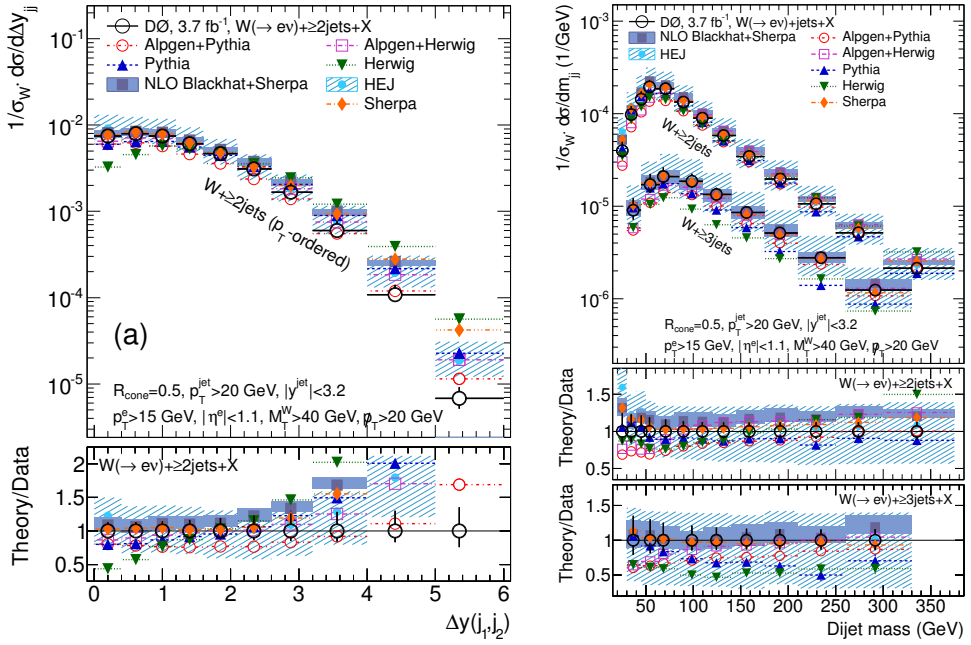

Figure 31 Cross section for the production of $W+\geq 2$ jets as a function of the difference in the rapidity (left) and the dijet invariant mass (right) between the two leading jets, at 1.96 TeV $p\bar{p}$ collisions at the TEVATRON. The figures include comparisons with a fixed-order calculation and MC simulations. Figures taken from (DØ Collaboration, 2013d).

in a restricted phase space, i.e., jet $|y| < 2.4$ and m_{jj} up to 700 GeV – 1 TeV, are compatible with those presented above, but in such a kinematic region do not show significant data-theory discrepancies. In an updated analysis of $W + \geq 2$-jet events at the LHC in the same broad phase space of jet $p_{\mathrm{T}} > 30$ GeV and $|y| < 4.4$, which extends the reach of the m_{jj} distribution to 3 TeV (ATLAS Collaboration, 2018a), a very good agreement is found between data and updated theoretical calculations, while the same level of discrepancy is observed with the older LO SHERPA version (v1.4). These measurements show that the extension of the kinematic reach of the LHC can expose theoretical mismodeling and can be used to improve the theoretical predictions.

The DØ collaboration has also studied in Ref. (DØ Collaboration, 2013d) the probability of emission of a 3^{rd} jet in events with a W and at least two associated jets, as a function of the rapidity separation between the two tagged jets, under various definitions of jet tagging (two most-rapidity-separated jets, the two highest-p_{T} jets, or the two highest-p_{T} jets with a 3^{rd} jet produced in the rapidity gap between them), see Fig. 33. Such a measurement provides a laboratory for studies of rapidity gaps, central jet veto and vector boson fusion jet dynamics. They can test the high-p_{T} and the wide-angle jet production, in a complementary way to studies of dijet events. The results show that in such configurations there are competing effects of increasing phase space for high-p_{T} jet emission between jets and decreasing PDFs at large x. The BFKL-based resummation calculation in HEJ generator describes best the data.

The study of events with a photon and jets is used for searches of new physics signatures, such as heavy resonance states decaying into a photon and a jet. Such new physics processes can produce distinct features in the $\gamma+$jet final state, such as deviation in the invariant mass of the photon and the jet ($m^{\gamma-\mathrm{jet}}$) or angular correlations between the photon and the jet with respect to SM expectations. Figure 34 presents measurements of differential cross sections as a function of $m^{\gamma-\mathrm{jet}}$ in $\gamma+$ jet events at the LHC at 13 TeV center-of-mass energy, and as a function of azimuthal angular separation between the photon and the third leading jet in events with a photon and at least 3 jets in pp collisions at 8 TeV center-of-mass energy. The differential cross section of $d\sigma/dm^{\gamma-\mathrm{jet}}$ shown in Fig. 34 (top) is monotonically decreasing by more than four orders of magnitude up to the highest measured value of $m^{\gamma-\mathrm{jet}} = 3.25$ TeV. Both NLO QCD predictions (fixed-order JETPHOX and SHERPA MC generator that includes the matching of NLO matrix-element with parton showering) describe the data within the experimental and theoretical uncertainties. However, in the highest $m^{\gamma-\mathrm{jet}}$ range a trend of the sim-

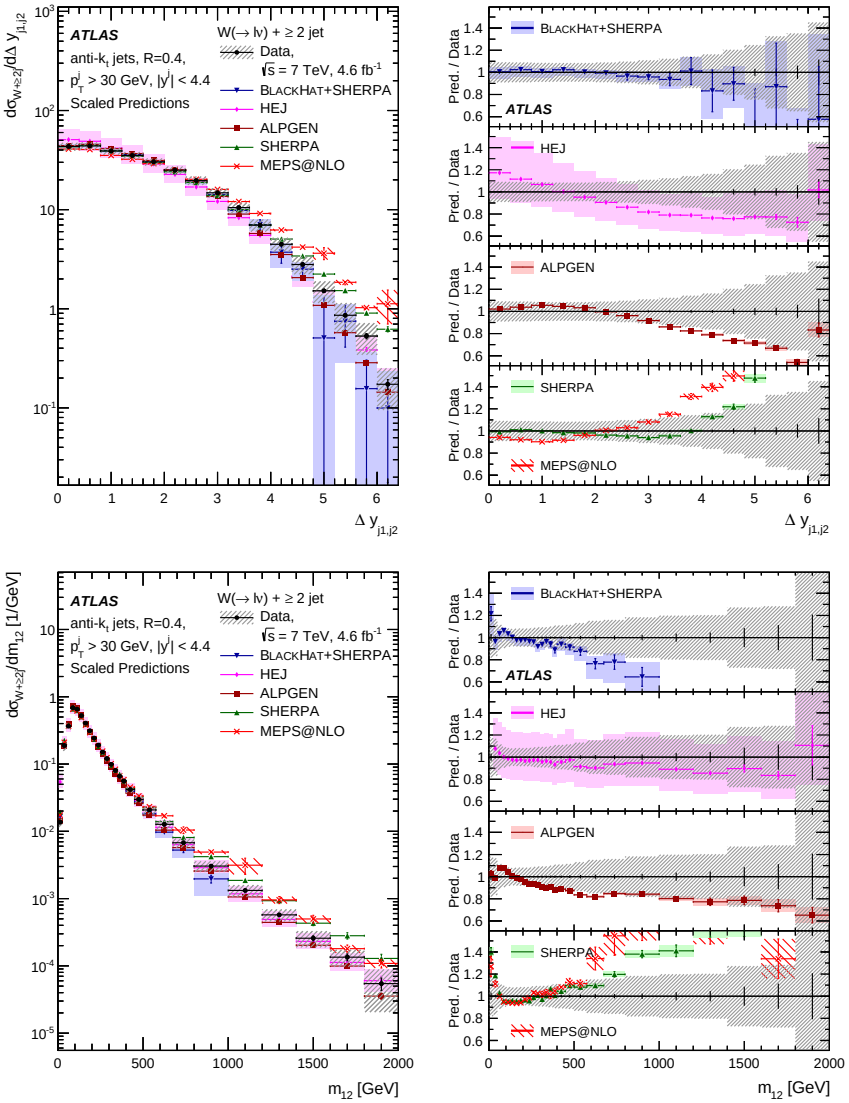

Figure 32 Cross section for the production of $W+\geq 2$ jets as a function of the difference in the rapidity (top) and the dijet invariant mass (bottom) between the two leading jets, at 7 TeV pp collisions at the LHC. The figures include comparisons with a fixed-order calculation and MC simulations. Figures taken from (ATLAS Collaboration, 2015b).

ulation to overestimate the data is seen. Figure 34 (bottom) shows that the cross-section $d\sigma/\Delta\phi^{\gamma-\text{jet3}}$ increases as $\Delta\phi^{\gamma-\text{jet3}}$ increases, indicating the preference for back-to-back configuration between the photon and the third leading jet in $\gamma+$ jet events. The fixed-order NLO pQCD prediction by BLACKHAT gives an adequate description of the angular correlations and their evolution with energy scale, however shows a tendency to systematically overestimate the data.

A recent analysis of γ + 2 jets + X production at 13 TeV at the LHC with 36.1 fb^{-1} of integrated luminosity is carried out in two distinct regions of phase space: one enriched with direct photon production and one with photon fragmentation processes. Experimental cross sections are measured as a function of several observables, including $m^{\text{jet+jet}}$, $m^{\gamma+\text{jet+jet}}$ as well as azimuthal and rapidity differences between the photon and leading jet and between the two jets. Good agreement between data and MC predictions with tree-level multi-jet matrix element merged to parton shower or with NLO accuracy in QCD are observed in the sample enriched with direct photon production, whereas discrepancies are observed in the sample enriched with fragmentation processes. The precision of the measurement is significantly better than the differences between the predictions indicating that theoretical uncertainties are much larger than those of experimental nature (ATLAS Collaboration, 2020c).

The real emission of a vector boson from an

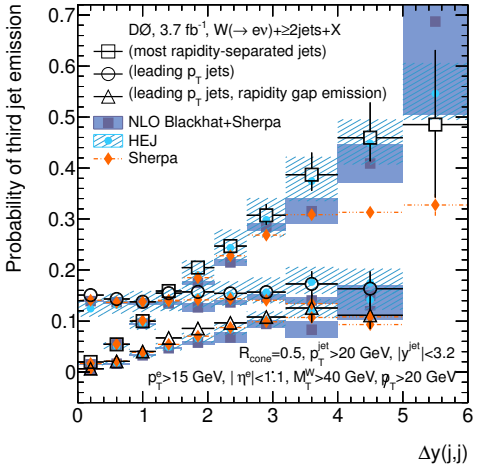

Figure 33 Measurement of the probability for the emission of a third jet in events with $W+ \geq 2$ jets as a function of the dijet rapidity separation of the two tagging jets at 1.96 TeV $p\bar{p}$ collisions at the TEVATRON, and comparisons with theory predictions. The definitions of jet tagging are the two most-rapidity-separated jets, the two highest-p_{T} jets, and the two highest-p_{T} jets with a 3^{rd} jet produced in the rapidity gap between them. Figure taken from (DØ Collaboration, 2013d).

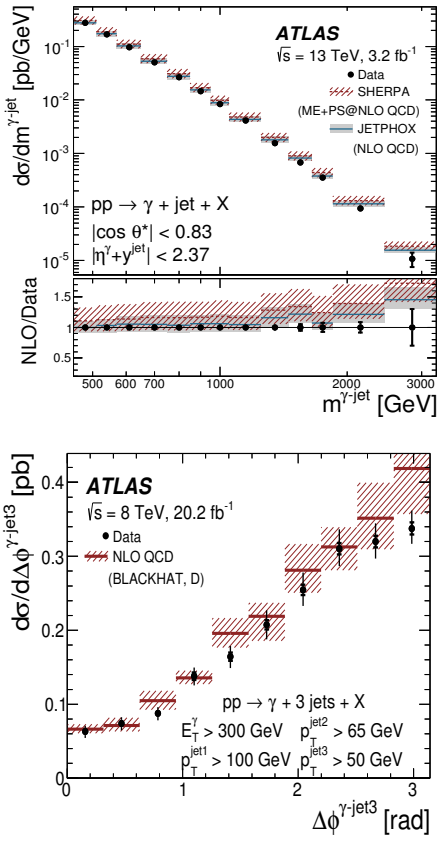

Figure 34 Differential cross sections measured at the LHC for isolated-photon plus jet production as a function of $m^{\gamma-\mathrm{jet}}$ at 13 TeV center-of-mass energy (top), figure taken from (ATLAS Collaboration, 2018c), and for isolated-photon plus three-jet production as a function of $\Delta\phi^{\gamma-\mathrm{jet3}}$ for $E_{\mathrm{T}}^{\gamma} > 300$ GeV at 8 TeV center-of-mass energy (bottom), figure taken from (ATLAS Collaboration, 2017b), and comparisons with theoretical predictions from fixed-order calculations and a MC generator at NLO in pQCD.

initial- or final-state quark has a collinear divergence in the limit of a massless boson. This may be detected as a collinear enhancement in the distribution of the angular separation between the vector boson and the closest jet. Parton shower algorithms are implemented in MC generators to account for QCD and QED emissions in the soft and collinear approximation and an analogous mechanism occurs for the emission of real weak bosons. At very high energies the real emission of weak bosons in dijet events can significantly contribute to the inclusive W + jet measurement. Measurements of W + jet production at the LHC are often insensitive to such an effect as they require large separation between the decay charged lepton and any of the jets. The analysis in Ref. (ATLAS Collaboration, 2017f) studies event configurations in which a muon from a W decay is produced close to a high transverse momentum jet. Figure 35 shows the differential cross section for W+jet events with at least one jet with $p_{\mathrm{T}} > 500$ GeV and higher, and any additional jets with $p_{\mathrm{T}} > 100$ GeV, as a function of the ΔR distance between the W decay muon and the closest jet. An enhancement of the collinear event fraction is expected for increasing values of the leading jet p_{T}, as the W emission from the jet is enhanced. This effect is illustrated in Fig 35: as the value of leading-jet p_{T} increases from $p_{\mathrm{T}} > 500$ GeV to $p_{\mathrm{T}} > 650$ GeV, the fraction of events in the collinear region at low ΔR increases with respect to the fraction of events in the back-to-back configuration. The ALPGEN MC simulation for W + jet production overestimates the data, especially in the collinear region. The prediction by PYTHIA8, which is modified to explicitly include the process of W boson emission as electroweak final-state radiation in the parton shower of a dijet event, underestimates the data in the collinear region. The best agreement over the entire distribution is provided by SHERPA + OPENLOOPS W + 1-jet and W + 2-jet calculation that incorporates NLO QCD and NLO EW corrections. In the high-p_{T} regime the NLO EW corrections have a significant effect, up to about 20%. The "$W+ \geq 1$ jet N_{jetti} NNLO" prediction, which uses a technique based on N-jettiness to split the phase space for the real emission corrections, provides a description very similar to

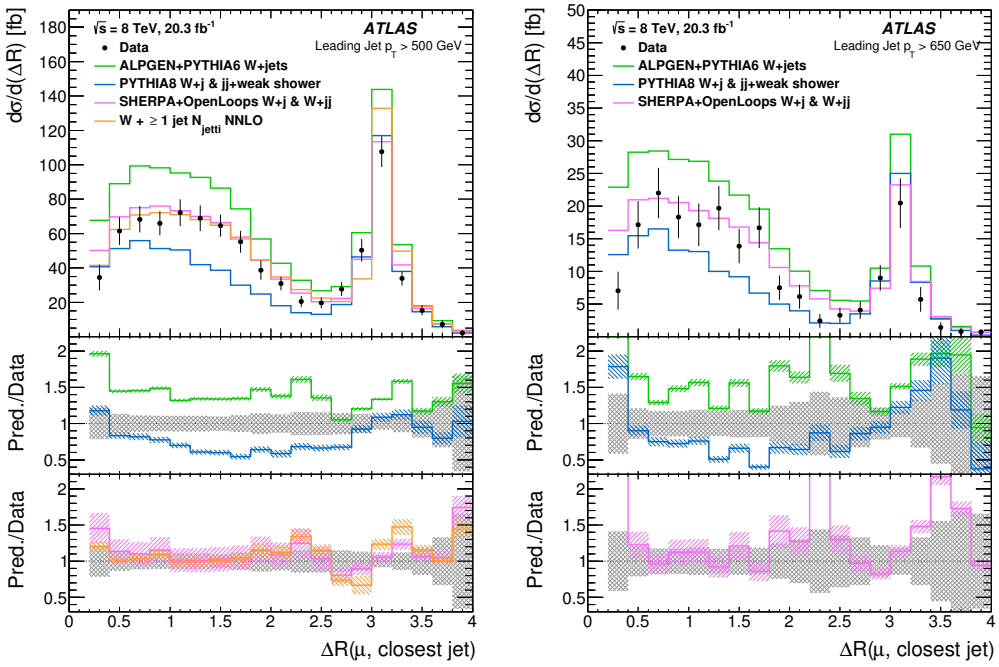

Figure 35 Differential W + jet cross section as a function of the angular separation ΔR between the W decay muon and the closest jet for events with p_{T} (leading jet) $>$ 500 GeV (left) and p_{T} (leading jet) $>$ 650 GeV (right), with 8 TeV pp collisions at the LHC. Several different theoretical predictions from MC generators are compared to experimental data. Figures taken from (ATLAS Collaboration, 2017f).

SHERPA + OPENLOOPS. Such a topology will be more accessible and important with Run-2 data at 13 TeV center-of-mass energy and with larger data sets at the LHC, as well as at higher proton collision energies, for example at future higher-energy proton colliders.

Other studies of correlations between the vector boson and the jets are undertaken as they provide important benchmarks for calculations and for the tuning of MC simulations. One example is the study of the Z boson production in a boosted regime of the Z boson that is important for modeling the background from Z boson decaying into neutrinos in searches of new physics with missing transverse energy in the final state. Figure 36 shows different levels of azimuthal correlations between the Z boson and the three leading jets ($\Delta\phi(Z, j_i)$) in $Z+ \geq 3$ jets events in two different event configurations, i.e., with $p_{\mathrm{T}}^{Z} > 0$ GeV or > 150 GeV. Large correlations are visible between the Z and the leading jet, whereas smaller correlations are present between the Z and the subleading jets. In events with a boosted Z the correlation between the Z boson and the leading jet is enhanced. A good modeling is provided by LO multi-leg (SHERPA, MADGRAPH) and NLO $Z + 1$ jet (POWHEG) generators. The PYTHIA6 prediction, which relies on the parton shower simulation for parton emission shows better modeling in the small $\Delta\phi$ region in the high Z p_{T} regime, where the soft and collinear approximation of the parton shower is most applicable.

Multi-Parton Interactions (MPI) are a necessary ingredient of simulations for the description of particle multiplicities and energy flow, and may contaminate event samples for precision measurements (e.g., for Higgs boson properties) and new physics searches. The greater the $\sqrt{s}$ (thus the lower the parton momentum fraction x), the bigger the impact of MPI at high p_{T}. Therefore, the MPI contribution is generally more significant at the LHC than at the TEVATRON. The impact of MPI in physics processes is difficult to measure as it co-exists with initial and final state radiation, beam remnants and the hard interaction. Experimentally the MPI contribution must also be disentangled from pileup interactions. Double parton scattering (DPS) is a specific case of MPI and its production cross section is typically parameterised as $\sigma_{\mathrm{DPS}} = \frac{\sigma_A \cdot \sigma_B}{\sigma_{\mathrm{eff}}}$, where σ_A and σ_B are the parton level cross sections of the two underlying processes, assumed to be independent, while σ_{eff} is an effective area parameter and is assumed to be independent of phase space and process. These assumptions are tested by measuring σ_{eff} in several processes and at different energy scales. The DPS contribution to the inclusive W production is studied in W + 2-jet events in Refs. (ATLAS Col-

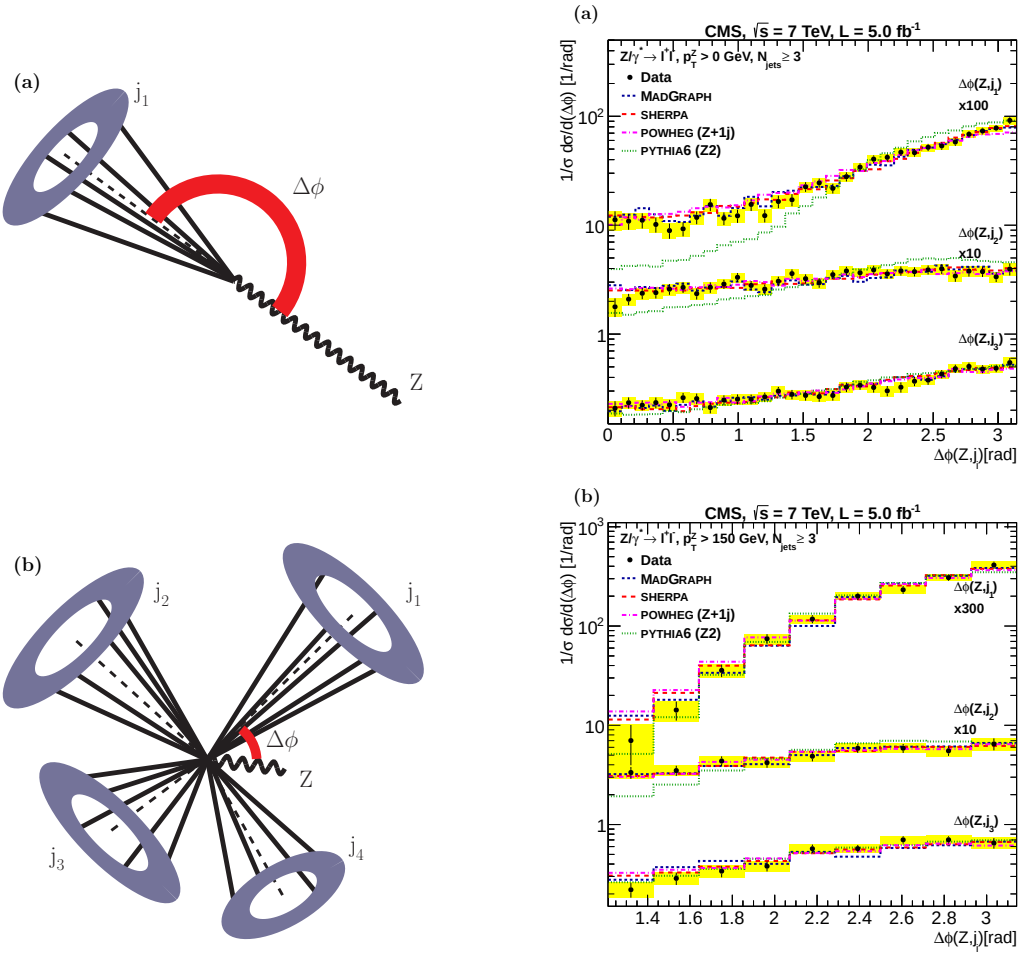

Figure 36 Topology of Z + jet events for $\Delta\phi(Z, j_1) \to \pi$ (top-left), and for $\Delta\phi(Z, j_1) \ll \pi$ (bottom-left). Normalized $\Delta\phi(Z, j_i)$ $(i = 1, 2, 3)$ distributions for the inclusive $N_{\text{jets}} \geq 3$ for $p_{\text{T}}^{Z} > 0$ GeV (top-right) and for $p_{\text{T}}^{Z} > 150$ GeV (bottom-right), with 8 TeV pp collisions at the LHC, compared to theoretical predictions from MC generators. Figures taken from (CMS Collaboration, 2013a).

laboration, 2013b; CMS Collaboration, 2014f). Figure 37 (top) shows examples of the two contributions to the W + 2-jet event sample: DPS (top left) and single parton scattering (SPS) (top right). The fraction of DPS events in W + 2-jet data and σ_{eff} are extracted from a fit of DPS and SPS templates to the normalized transverse momentum balance $\Delta p_{\text{T}}^{\text{rel}} = \frac{|\vec{p}_{\text{T}}^{\,j1} + \vec{p}_{\text{T}}^{\,j2}|}{|\vec{p}_{\text{T}}^{\,j1}| + |\vec{p}_{\text{T}}^{\,j2}|}$. Figure 37 shows the template fit results compared to data. The values of σ_{eff} measured at 7 TeV by the ATLAS and the CMS experiments are 15 ± 3 (stat.)$^{+5}_{-3}$ (syst.) and 20.7 ± 0.8 (stat.) ± 6.6 (syst.) mb, respectively. In order to test the energy dependence of σ_{eff} it is important to repeat such measurements at experiments with greater center-of-mass energies. Moreover, higher $\sqrt{s}$ in future measurements implies a larger phase space available for DPS and thus a greater need for more precise DPS measurements.

For other measurements of V + jet properties, the reader is referred to the following Refs. (ATLAS Collaboration, 2013c,e, 2017e,h; CMS Collaboration, 2011c; DØ Collaboration, 2010b; LHCb Collaboration, 2014b).

4. Cross section ratios

Measurements of production cross sections of individual V + jet processes are limited in high-statistic regions of phase space by systematic uncertainties that are common between processes, while measurements of ratios of different V + jet processes exploit partial cancellations of experimental uncertainties as well as theoretical effects that are common between the two processes in the ratio. Such ratios can provide high-precision tests of the Standard Model, as they are sensitive to non-universal corrections in QCD and electroweak calculations as well as PDFs. In this section several ratios will be presented. In the ratio of W^+ to W^- productions,

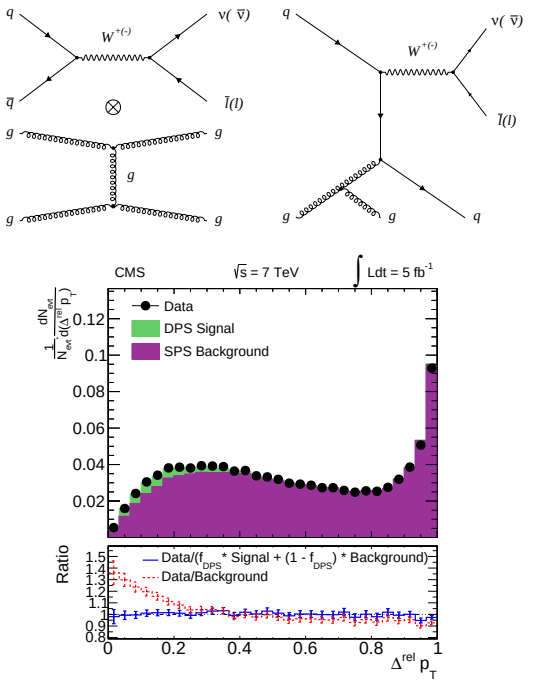

Figure 37 Feynman diagrams for W + 2-jet production from DPS (top-left) and SPS (top-right); fit results for the DPS-sensitive observable $\Delta p_{\mathrm{T}}^{\mathrm{rel}}$ at 7 TeV pp collisions at the LHC (bottom). Figures taken from (CMS Collaboration, 2014f).

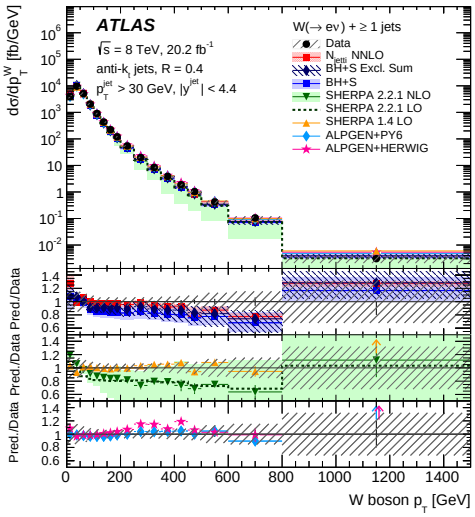

Figure 38 Differential cross section for the production of a W boson as a function of the W p_{T} for events with $N_{\mathrm{jets}} \geq 1$ in pp collisions at 8 TeV center-of-mass energy at the LHC. Experimental results are compared to several theoretical predictions calculated at different orders and with different approximations in pQCD, and with different parton shower implementations. Figure taken from (ATLAS Collaboration, 2018a).

pQCD and electroweak effects cancel to large extent, making this measurement particularly sensitive to PDFs, and specifically to the ratio of up-quark to down-quark at high Bjorken-x. In the W to Z boson ratio, effects from non-perturbative QCD processes largely cancel at high energy scales, whereas other effects do not cancel, such as boson mass effects at low energy scales, quark–gluon and quark–antiquark contributions to V + jet productions, and non-universal electroweak corrections. Such a ratio is therefore useful for validating theoretical predictions used to estimate W+jet or Z+jet backgrounds in searches for new physics. Similarly, in the ratio Z to γ bosons, mass effects cancel at high energy scales, whereas higher-order QCD and electroweak corrections can have large contributions, thus making such a ratio a precise test of higher-order effects in perturbative calculations.

In the analysis presented in Ref. (ATLAS Collaboration, 2018a) measurements are carried out for $W^{\pm}$ production as well as for W^{+} and W^{-} productions and the cross-section ratio of W^{+}/W^{-} in events with the W boson produced association with jets, as a function of a number of variables that are sensitive to higher-order terms and to the PDFs. In the W^{+}/W^{-} ratio in W events with at least one associated jet, many of the experimental and theoretical uncertainties cancel out, making it a more precise test of the theoretical predictions, especially in a kinematic regime with x values higher (approx. up to x =0.1—0.3) than what is typically accessible in measurements of inclusive W production at ATLAS and CMS ($10^{-4} < x < 10^{-1}$). Figure 38 shows the differential cross section as a function of the p_{T} of the W boson for events with $W^{\pm}+ \geq 1$ jet production. Good overall agreement is found between the data and most of LO, NLO and NNLO calculations. Variations in the modeling of different SHERPA generator versions are seen, whereas different parton shower models interfaced to the ALPGEN generator show little impact, with PYTHIA providing a slightly better description of the data. In the W^{+}/W^{-} cross-section ratio in Fig. 39, differences due to QCD and electroweak higher-order effects cancel out to a large extent. In the ratio, the experimental precision is greatly improved and most predictions show a trend to overestimate the data. The data is also compared to different PDF sets with a common calculation by the MCFM program. Sensitivity to PDFs is visible in the variation of agreement between data and the different PDF sets, especially in the region of $p_{\mathrm{T}} \approx 200 - 400$ GeV, where experimental uncertainties are in the 2% – 6% range. In this

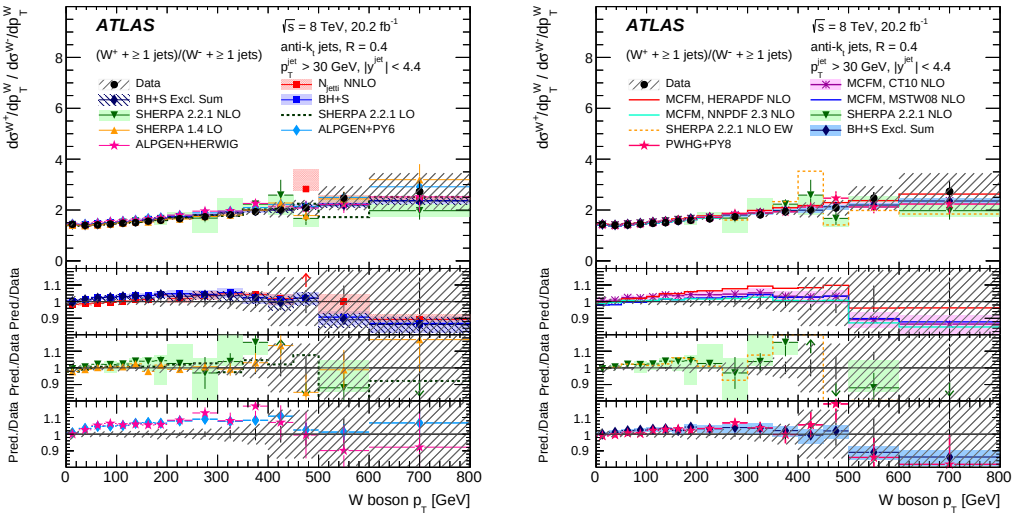

Figure 39 Differential cross section for the W^+/W^- ratio as a function of the W p_{T} for events with $N_{\mathrm{jets}} \geq 1$ in pp collisions at 8 TeV center-of-mass energy at the LHC. Experimental results are compared to several theoretical predictions calculated at different orders, with different approximations in pQCD and with different parton shower implementations as well as to NLO MCFM predictions with four different PDF sets. Figures taken from (ATLAS Collaboration, 2018a).

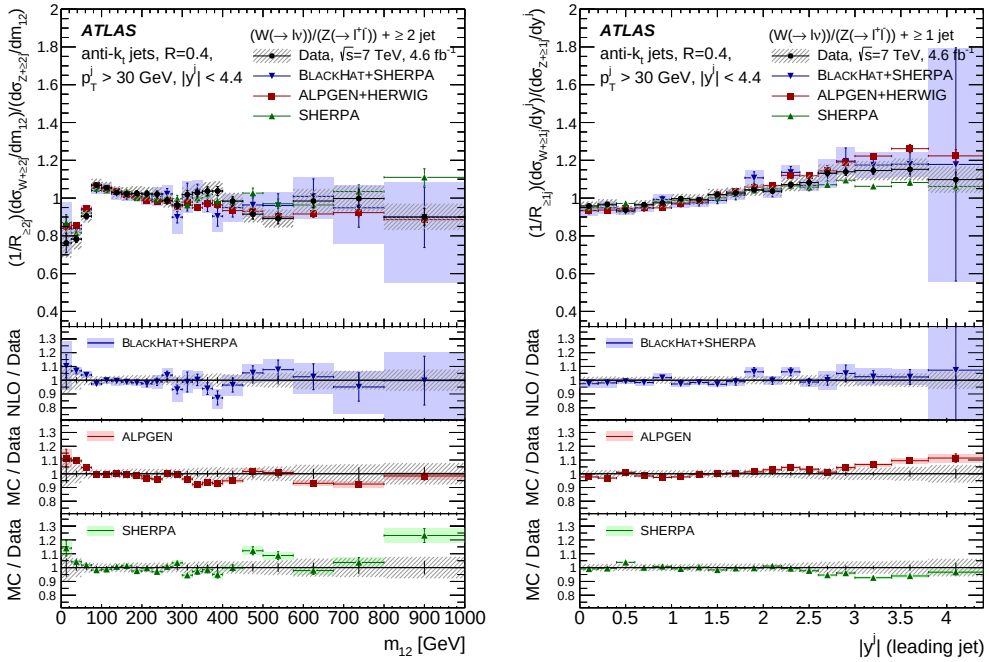

Figure 40 The normalized ratio of W + jet and Z + jet production cross sections, R_{jets}, as a function of the dijet invariant mass, m_{12}, for $N_{\mathrm{jets}} \geq 2$ (left) and the leading-jet absolute rapidity, $|y^j|$, for $N_{\mathrm{jets}} \geq 1$ (right) with 7 TeV pp collisions at the LHC. Experimental results are compared to NLO calculations in pQCD by BLACKHAT as well as to MC generators. Figures taken from (ATLAS Collaboration, 2014a).

region the predictions from different PDF sets may differ by about 2% to 5% and in some cases differ from data up to 2–3 standard deviations.

The production mechanisms of W + jets and Z + jets are very similar once the kinematic effect of the different boson masses and the leptonic branching ratios are taken into account. In ratios of differential cross sections in W + jet and Z + jet events (R_{jets}), the experimental uncertainty cancel significantly, as can be seen in Fig. 18. Theoretical uncertainties, if treated as correlated between the two types of processes, can be significantly reduced too: QCD scale variations, estimated at NLO in pQCD, and

PDF uncertainties overall account for a $2-4\%$ level uncertainty in $R_{\rm jets}$ with at least one jet in the final state with jet $p_{\rm T} \simeq 800$ GeV, to be compared to the 20% level of uncertainties in events with a W boson with at least one associated jet. Such a reduction in theoretical uncertainties is also visible in the phenomenological study presented in Fig. 7 in Sec. II.A.1. Figure 40 shows that the level of mismodeling of the MC simulations that is seen in the cross section measurement as a function of m_{jj} for $W+$jets in Fig. 32 is largely reduced in $R_{\rm jets}$. This effect points towards an underlying cause for the mismodeling in MC generators that has the same effect in both processes. The low part of the m_{jj} distribution in $W+$jet or $Z+$jet events has sensitivity to jet kinematics and nonperturbative effects in soft QCD radiation that differ between W and Z events and do not cancel in the $R_{\rm jets}$ ratio, as can be seen in the $R_{\rm jets}$ values lower than 1 for $m_{jj} < 100$ GeV in Fig. 40 (left). The agreement between predictions and data in the region of high rapidity of the $p_{\rm T}$-leading jet, see Fig. 40 (right), can be affected by the modeling of the parton shower and PDF. Such a ratio measurement is not only important for a better understanding of the theoretical modeling of W/Z+jet processes, but also for the estimation of backgrounds on searches for new physics. For example the calculation of such a ratio is used as *transfer factor* to estimate the $Z(\to \nu\nu)+$jet background yield in a search signal region by extrapolating the measurement of the $W(\to l\nu)$+jet yield from a data control region, see examples in Refs. (ATLAS Collaboration, 2014g,h, 2016h; CMS Collaboration, 2012d, 2017i, 2019f).

The ratio of $\gamma+$jets and $Z+$jets is also of great interest, especially in the high-$p_{\rm T}$ region of the vector bosons, where the Z boson mass effects play a less significant role than in the low-$p_{\rm T}$ region. This ratio can test the impact of QCD and electroweak higher order corrections with greater experimental accuracy, thanks to cancellation of experimental systematic uncertainties such as jet energy calibration and luminosity, see Fig. 41. The NLO pQCD calculation by BlackHat describes well the Z-boson $p_{\rm T}$ spectrum but it tends to underestimate the low part of the γ $p_{\rm T}$ spectrum in events with at least two associated jets. In the LO multi-leg MC generators (MadGraph + Pythia6 and Sherpa) a similar systematic trend of mismodeling the Z $p_{\rm T}$ in $Z+\geq 2$ jets is seen, as well as a significant bias at modeling the shape of the photon $p_{\rm T}$ distribution (see MadGraph + Pythia6 prediction). The $p_{\rm T}$ distribution of the Z/γ ratio flattens at high boson $p_{\rm T}$ values, i.e., greater than 350 GeV. The boson $p_{\rm T}$ shape mismodeling observed in the individual Z and γ production events largely cancels out in the Z/γ ratio and a residual over-estimation of the ratio by a flat 20% is observed in QCD LO multi-leg MC generators (see MadGraph + Pythia6 prediction). A less significant systematic mismodeling is also visible in the NLO fixed-order calculation by BlackHat.

The production of W and Z bosons in association with jets is studied in the forward region of proton-proton collisions with the LHCb experiment. Such measurements provide additional tests of the SM in a region of phase space not directly accessible by ATLAS and CMS at the LHC and provide additional constraints on PDF in a different range of Bjorken-x. As shown in Fig. 42, in the LHCb experiment the charged leptons from the weak boson decay are reconstructed in the forward pseudo-rapidity region of $2.0 < \eta^{\rm l} < 4.5$, while jets in the region $2.2 < \eta^{\rm jet} < 4.2$ with the anti-k_t algorithm with distance parameter $R = 0.5$ and $p_{\rm T}^{\rm jet} > 20$ GeV (LHCb Collaboration, 2016). Cross sections and their respective ratios are measured for $W^+ + \geq 1$ jet, $W^- + \geq 1$ jet and $Z + \geq 1$ jet. In addition, the asymmetry of $W^+ + \geq 1$ jet and $W^- + \geq 1$ jet production and the asymmetry as a function of the charged lepton η are measured. Due to the cancellation of scale uncertainties, the ratios as a function of the charged lepton η are expected to provide sensitivity to the PDFs. Figure 42 shows the broad range of measurements that are carried out in this analysis and the extensive comparisons with predictions from different MC generators and PDFs. Overall a good agreement is seen between data and predictions, however slightly larger values of the asymmetry and the ratio of $W^+ + \geq 1$ jet to $W^- + \geq 1$ jet cross sections are seen in data than in NLO QCD predictions in the first bin of the charged lepton η.

III. ELECTROWEAK PRODUCTION OF A VECTOR BOSON AND TWO JETS

A. Theoretical predictions

The production of a single vector boson in vector boson fusion constitutes an experimental signature of special interest because of its sensitivity to the self-interactions of the electroweak gauge bosons. It presents a prime testbed for searches for new physics signals that are connected to the electroweak symmetry breaking.

The electroweak production of a single vector boson proceeds at $\mathcal{O}(\alpha^4)$ at leading or-

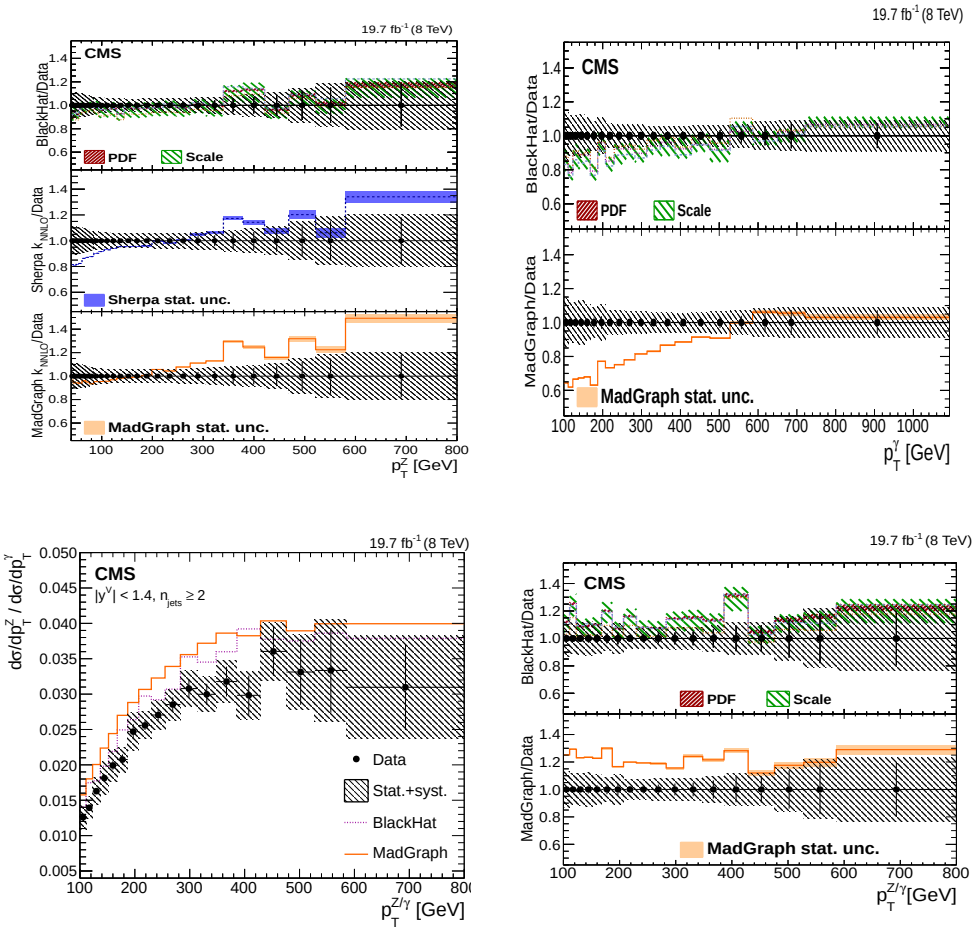

Figure 41 Prediction-to-data ratios of differential cross sections for Z and central ($|y^{\gamma}| < 1.4$) γ productions as a function of the boson p_{T} for inclusive Z + jet and γ + jet processes with a $N_{\mathrm{jets}} \geq 2$ selection, with 8 TeV pp collisions at the LHC (top). Differential cross section ratio of Z + jets over γ + jets and its prediction-to-data ratios as a function of the boson transverse-momentum for central bosons ($|y^{V}| < 1.4$) in the $N_{\mathrm{jets}} \geq 2$ sample (bottom). Experimental results are compared to NLO pQCD calculation by BLACKHAT and to the MADGRAPH MC generator. Figures taken from (CMS Collaboration, 2015b).

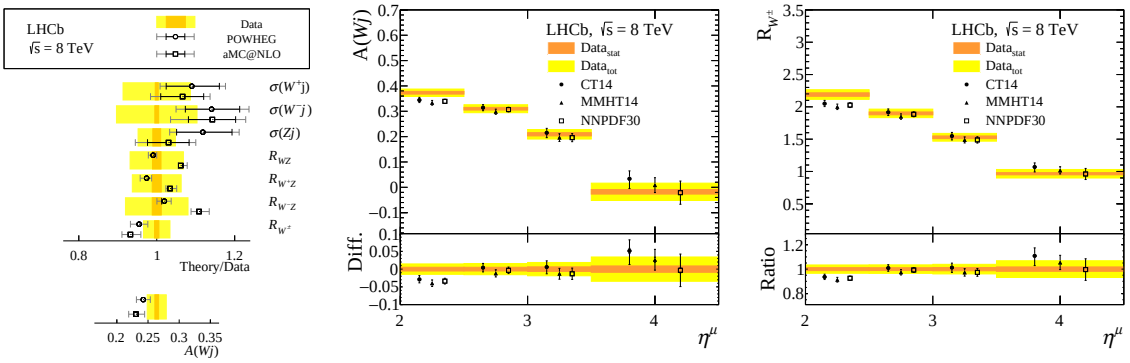

Figure 42 Summary of the W/Z + jet measurements performed in a fiducial region with the LHCb experiment at 8 TeV pp collisions at the LHC (left), compared to predictions from two MC generators. The cross sections for $W^{+}+ \geq 1$ jet, $W^{-}+ \geq$ 1 jet and $Z + \geq 1$ jet are denoted as $\sigma(W^{+}j)$, $\sigma(W^{-}j)$, and $\sigma(Zj)$, respectively, while the ratios $\sigma(Wj)/\sigma(Zj)$, $\sigma(W^{+}j)/\sigma(Zj)$, $\sigma(W^{-}j)/\sigma(Zj)$ and $\sigma(W^{+}j)/\sigma(W^{-}j)$ are denoted as R_{WZ}, $R_{W^{+}Z}$, $R_{W^{-}Z}$ and $R_{W^{\pm}}$, respectively. The asymmetry of $\sigma(W^{+}j)$ and $\sigma(W^{-}j)$ is denoted as $A(Wj)$. The asymmetry $A(Wj)$ (middle) and the ratio $R_{W^{\pm}}$ (right) as a function of the muon pseudorapidity η^{μ}, compared to NLO calculations performed with the FEWZ calculation and three different PDF sets. Figures taken from (LHCb Collaboration, 2016).

der and contains multiple distinct topologies. Of particular interest are: a) the classic vector boson fusion topologies, b) the closely related multi-peripheral topologies, c) bremsstrahlung-like electroweak boson emission off electroweak quark scattering topologies, and d) semileptonic diboson production topologies (s-channel). They are depicted in Fig. 43. Although not all topologies exist for all external flavor configurations, the different diagrams of Fig. 43 interfere and cannot be separated. Nonetheless, in different regions of the phase space, different topologies will dominate and suitable approximations can be constructed. Besides the diboson region, in which both the invariant mass of the lepton pair and the invariant mass of the two final state jets are close to the nominal W and Z boson masses, the vector boson fusion region is of particular interest. This region is characterised by a large invariant mass of the two final-state jets and their large separation in rapidity, typically $m_{jj} > 600\,\text{GeV}$ and $\Delta y > 4.5$. Here, a subclass of the diagrams in Fig. 43(a) dominate the cross section.[6]

The main irreducible background in experimental measurements of the electroweak production of a single vector boson in association with at least two jets is its QCD production channel, proceeding at $\mathcal{O}(\alpha_s^2\alpha^2)$ at LO.[7] As the electroweak production mode is characterised by a color-neutral t-channel exchange, it exhibits reduced hadronic activity in the central region between the leading jets. Such a suppression does not exist in its QCD production mode, and a veto on central or, in fact, any additional jet activity can further enhance the sought after signal. Such jet vetoes, however, are typically badly described by fixed-order perturbation theory due to the emergence of logarithms of the ratio of the hard scale and the jet veto scale and the best available description for this observable is offered by conventional parton showers.

[6] Typically, to maximise data statistics, experimental measurements apply much looser cuts. The suitability of the VBF-approximation in such a phase space must be confirmed if theory predictions calculated in this approximation are to be tested against data.

[7] This distinction between QCD and EW production channels is tied to a leading order interpretation of the process where their interference is small in the VBF phase space region. It breaks down in other regions or at higher-orders.

1. Higher order computations

All higher-order calculations to date have been performed in the above-introduced VBF approximation wherein not only s-channel contributions are neglected but also t-/u-channel interferences are not taken into account. This simplifies the calculation immensely in two ways. Firstly, it separates the two quark lines in color space, thus effectively rendering the calculation a "double-DIS" one. And secondly, it facilitates the calculation of its NLO QCD correction by removing all components at $\mathcal{O}(\alpha_s\alpha^4)$ which possess EW divergences with respect to the $\mathcal{O}(\alpha_s\alpha^3)$ Born process. The production processes of all EW vector bosons, W, Z and γ, in this approximation are implemented in the VBFNLO library (Baglio *et al.*, 2014; Jäger, 2010; Oleari and Zeppenfeld, 2004). Figure 44 displays the results for W and photon production in vector boson fusion, respectively. As can be seen, the NLO QCD corrections are generally small. Complete EW corrections are not known and will have to be calculated for the full $\mathcal{O}(\alpha^4)$ process.

2. Monte Carlo event generators

The above-mentioned fixed-order NLO QCD calculations have been matched to parton showers. Explicit implementations exist in the POWHEG (Jäger *et al.*, 2012; Schissler and Zeppenfeld, 2013) generator, but are also available in the automated NLOPS tools. Figure 45 displays results for Z and W production in vector boson fusion, well reproducing the fixed-order results. Further, multi-jet-merged calculations exist at LO accuracy.

One key aspect in the selection of VBF-type events is the aforementioned rapidity gap. Therefore, a good description of the radiation pattern of the third jet, and any further higher-order radiation, is mandatory. Care must be taken to ensure the initial color and starting scale assignment in the parton showers is correct in order to preserve the unique rapidity gap structure and not spuriously fill it with additional radiation. The supplementation with LO matrix elements in the above matching helps in controlling the associated uncertainties on the level of a few percent, but higher accuracy would be desirable.

B. Experimental results

Initial measurements of the electroweak production of a vector boson and two jets were

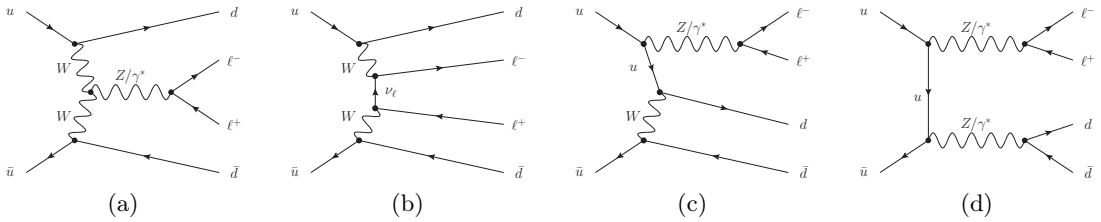

Figure 43 Representative Feynman diagrams for the production of two charged leptons in association with two jets at $\mathcal{O}(\alpha^4)$: vector boson fusion (a), multi-peripheral (b), bremsstrahlung-like (c), and semileptonic diboson production (d).

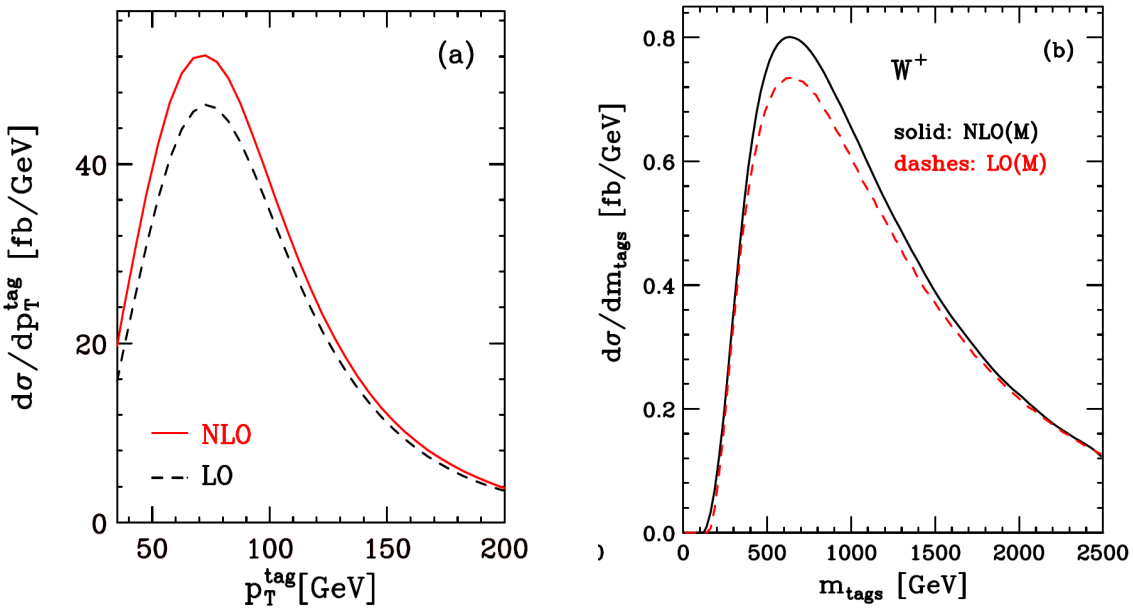

Figure 44 Leading tagging jet transverse momentum in prompt photon production in association with at least two jets through vector boson fusion calculated at LO and NLO QCD accuracy using VBFNLO (left), figure taken from (Jäger, 2010). Invariant mass of the tagging jet pair in the production of a charged lepton and a neutrino in association with at least two jets through vector boson fusion calculated at LO and NLO QCD accuracy using VBFNLO (right), figure taken from (Oleari and Zeppenfeld, 2004).

performed by the CMS collaboration in the final state with two charged leptons and two jets (VBF Z channel) with 7 TeV proton collision data (CMS Collaboration, 2013d). The precision obtained in this first measurement was around 30%, mostly limited by systematic uncertainties on the jet energy scale and the background modeling.

Improved measurements have been obtained with 8 TeV data, by both ATLAS (ATLAS Collaboration, 2014c) and CMS (CMS Collaboration, 2015d), with precisions around 20%, and signal significances just above 5 standard deviations. Measurements of the VBF Z process with 13 TeV have also been performed by ATLAS (ATLAS Collaboration, 2017c) with 2015 data, by CMS (CMS Collaboration, 2018a) with 2016 data, and by ATLAS (ATLAS Collaboration, 2020a) with the full Run 2 data. These ATLAS and CMS measurements reach an overall precision of 20% and 10%, respectively.

It should be noted that the measurements provided by ATLAS and CMS are quite different and complementary. Since the first measurement, CMS has defined the VBF Z signal in an inclusive phase space in the four-fermion final state $\ell\ell$jj, with $m_{\ell\ell} > 50$ GeV and $m_{jj} > 120$ GeV, in which all pure EW diagrams of order $\alpha^4_{\rm EW}$ contribute to the signal definition, whereas ATLAS has performed measurements with the signal defined in higher dijet mass fiducial phase space regions. The ATLAS signal definition is at particle level, where the dijet invariant mass condition is implemented on the two $p_{\rm T}$-leading jets after clustering the final state particles, and the simulation setup includes NLO QCD corrections, implemented with POWHEG (Jäger *et al.*, 2012; Oleari and Zeppenfeld, 2004), and does not include s-channel diboson contributions. Figure 46 (left) shows the dijet invariant mass distribution that is used by ATLAS to extract the signal contri-

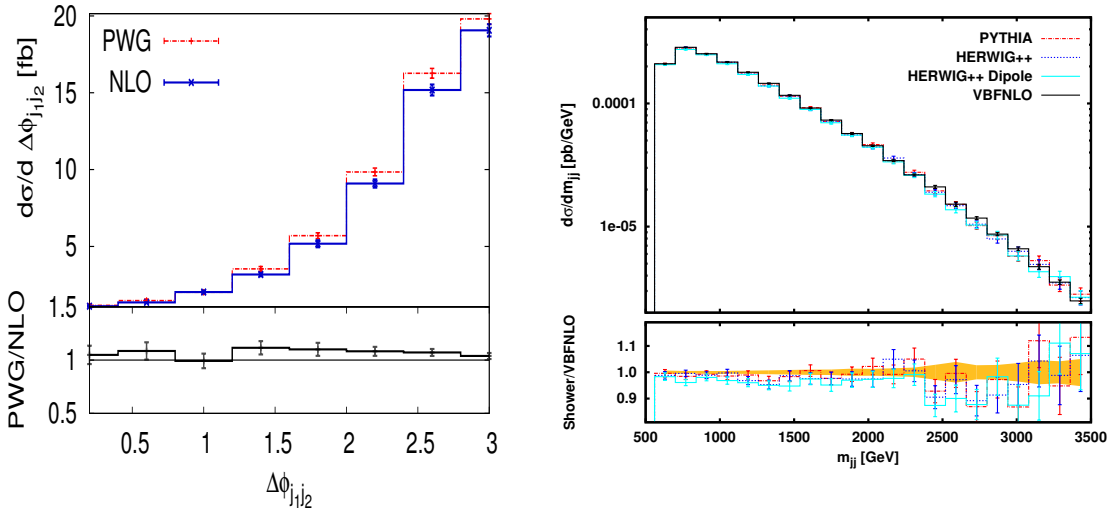

Figure 45 Azimuthal separation of the tagging jets in the production of a pair of charged leptons in association with at least two jets through vector boson fusion calculated at NLO QCD with VBFNLO and at NLO QCD accuracy matched to the parton shower using POWHEG (left), figure taken from (Jäger *et al.*, 2012). Invariant mass of the tagging-jet system in the pair production of a charged lepton and neutrino in association with at least two jets through vector boson fusion calculated at NLO QCD with VBFNLO and at NLO QCD accuracy matched to the parton shower using POWHEG, compared to predictions using PYTHIA and HERWIG++ (right), figure taken from (Schissler and Zeppenfeld, 2013).

m_{jj} cut	$\sqrt{s}$ =7 TeV	$\sqrt{s}$ =8 TeV	$\sqrt{s}$ =13 TeV
120 GeV	154±58 fb (CMS Collaboration, 2013d)	174±43 fb (CMS Collaboration, 2015d)	534±60 fb (CMS Collaboration, 2018a)
250 GeV		54.7 ± 11.2 fb (ATLAS Collaboration, 2014c)	119 ± 26 fb (ATLAS Collaboration, 2017c)
1 TeV		10.7 ± 2.1 fb (ATLAS Collaboration, 2014c)	37.4 ± 6.5 fb (ATLAS Collaboration, 2020a)

Table I Summary of VBF Z production cross sections measured at the LHC in the $\ell\ell$jj final state with different m_{jj} definitions and different proton collision energies. All quoted cross sections are for a single lepton flavor.

bution in the high dijet mass tail with 8 TeV data (ATLAS Collaboration, 2014c). Measurements by CMS are extracted by fitting the dijet invariant mass but also making use of more sophisticated multivariate discriminants with different event observables. Among the CMS multivariate inputs is an internal jet composition discriminator used to separate features of quark- and gluon-initiated jets, applied to the two VBF tagging jets (CMS Collaboration, 2013e, 2017a). The ATLAS measurements include several additional fiducial regions where inclusive cross sections are also measured. Figure 46 (right) shows a summary of such inclusive measurements with 13 TeV data (ATLAS Collaboration, 2017c). The most recent ATLAS results (ATLAS Collaboration, 2020a) focus on differential cross-section measurements, both for the electroweak signal component, and inclusively for the signal and background production, for different observables. Table I shows a summary of inclusive VBF Z cross sections measured to date at the LHC.

Analogous measurements have been performed in the single charged lepton plus dijet final state (VBF W channel) by CMS with 8 TeV collision data (CMS Collaboration, 2016), by ATLAS with 7 TeV and 8 TeV collision data (ATLAS Collaboration, 2017g), and by CMS with 13 TeV collision data (CMS Collaboration, 2020b). A variety of signal definitions has also been chosen for the VBF W channel. The CMS collaboration has used four-fermion LO definitions with $m_{jj} > 120$ GeV (as for VBF Z) and with $m_{jj} > 1$ TeV, while the ATLAS collaboration makes use of NLO signal modeling with $m_{jj} > 0.5, 1, 2$ TeV cuts defined at particle level after parton showering and jet clustering. Figure 47 shows the multivariate output distribution used to measure the inclusive cross section at 13 TeV in the electron channel, and different particle-level

m_{jj} cut	$\sqrt{s}$ =7 TeV	$\sqrt{s}$ =8 TeV	$\sqrt{s}$ =13 TeV
120 GeV			6.23 ± 0.62 pb (CMS Collaboration, 2020b)
500 GeV	2.76 ± 0.67 pb (ATLAS Collaboration, 2017g)	2.89 ± 0.51 pb (ATLAS Collaboration, 2017g)	
1 TeV		0.42 ± 0.10 pb (CMS Collaboration, 2016)	

Table II Summary of VBF W production cross sections measured at the LHC in the $\ell\nu$jj final state with different m_{jj} definitions and different proton collision energies. All quoted cross sections are for a single lepton flavor.

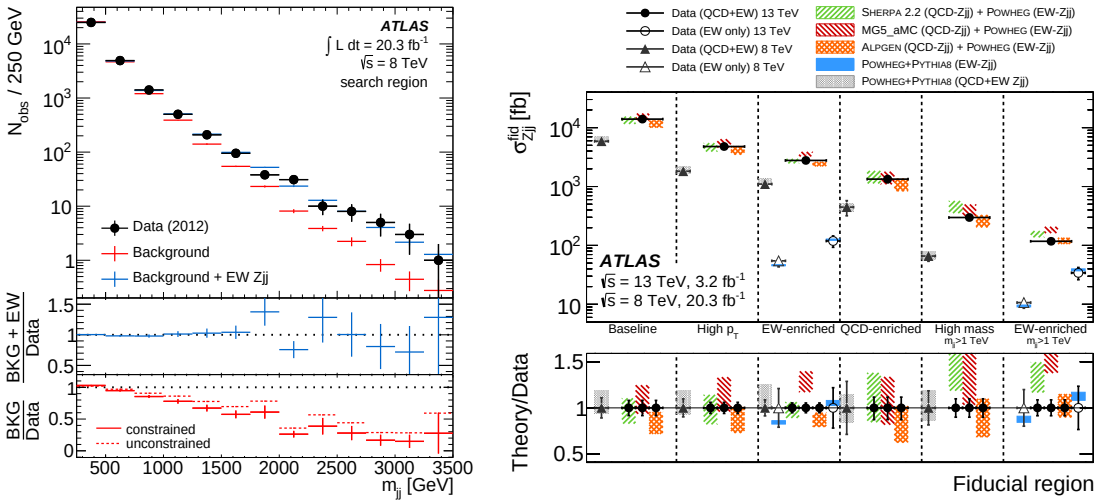

Figure 46 The dijet invariant mass distribution in the search region. The signal and (constrained) background templates are scaled to match the number of events as a result of a fit to data. The lowest panel shows the ratio of constrained and unconstrained background templates to the data (left), figure taken from (ATLAS Collaboration, 2014c). Cross-sections measurements in different fiducial regions at 8 and 13 TeV, compared to theoretical predictions (shaded/hatched bands). The bottom panel shows the ratio of the various theory predictions to data as shaded bands. Relative uncertainties in the measured data are represented by an error bar centered at unity (right), figure taken from (ATLAS Collaboration, 2017c).

fiducial cross sections performed at 8 TeV, respectively in CMS and ATLAS. Table II shows a summary of inclusive VBF W cross sections measured to date at the LHC.

Both the VBF Z and W measurements by ATLAS at 8 TeV (ATLAS Collaboration, 2014c, 2017g) include a large number of differential distributions unfolded to particle level for both inclusive and signal contributions in different fiducial regions, as shown in Fig. 48.

Interference effects between signal and background sources have been evaluated in the range from 2%–12% of the total signal, depending on the channel and the selected phase space, and are generally positive. Results by CMS include a full simulation of interference contributions that are implemented in the cross section extraction fits.

The structure of the WWZ and $WW\gamma$ triple gauge couplings (TGCs) can be explored with VBF Z and W measurements, and anomalous contributions to the TGCs have been searched for by both ATLAS and CMS in the context of the LEP effective Lagrangian approach (Hagiwara *et al.*, 1987) and effective field theory operators in the HISZ basis (Hagiwara *et al.*, 1993). Limits on anomalous coupling parameters have been extracted by ATLAS fitting alternatively the dijet invariant mass and the leading jet p_{T}, in fiducial signal regions (ATLAS Collaboration, 2014c, 2017g). Limits have also been extracted by the CMS collaboration, fitting the p_{T} distributions of the two charged leptons or the single charged lepton in a more inclusive Vjj phase space (CMS Collaboration, 2018a, 2020b), and resulted to be more stringent because of the larger $\sqrt{s}$ of the analyzed data set, and of a larger acceptance in the high p_{T} tails where anomalous TGC effects are generally expected. Examples of kinematic distributions used to fit anomalous TGC contributions are shown in Fig 49. The reported TGC

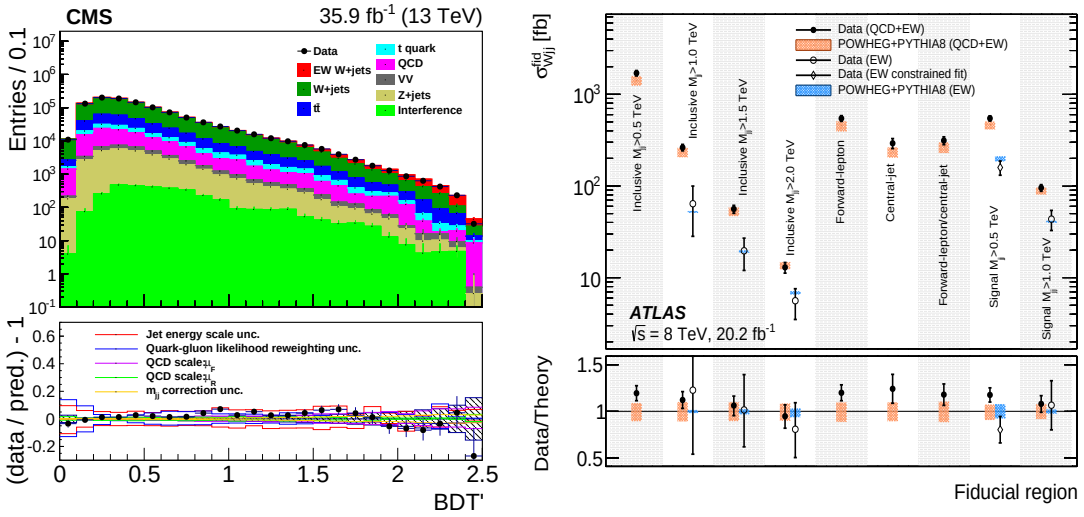

Figure 47 Data and pre-fit MC simulation of the multivariate output distribution used to extract the signal in the electron channel at 13 TeV (left), figure taken from (CMS Collaboration, 2020b). Cross sections for W plus two jets inclusive and EW signal productions in different particle-level fiducial regions at 8 TeV (right), figure taken from (ATLAS Collaboration, 2017g).

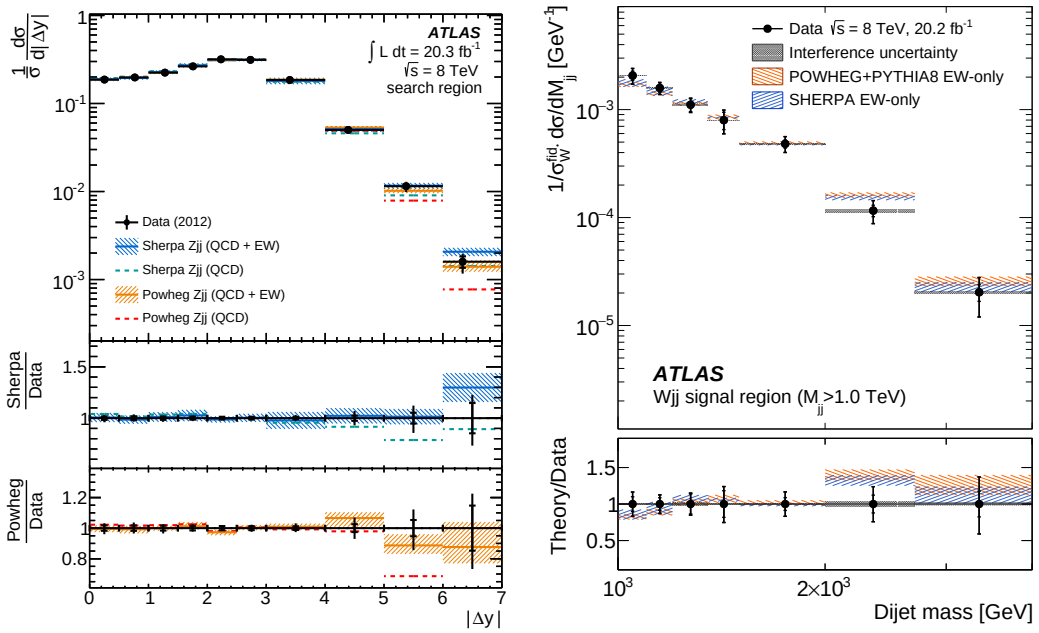

Figure 48 Unfolded normalised differential cross section distribution at 8 TeV as a function of the rapidity separation between the leading jets in the search region. Particle-level predictions are shown for strong and electroweak Zjj production (left), figure taken from (ATLAS Collaboration, 2014c). Unfolded normalized differential EW Wjj production cross sections at 8 TeV as a function of the dijet invariant mass for the signal fiducial region (right), figure taken from (ATLAS Collaboration, 2017g). Both statistical (inner bar) and total (outer bar) measurement uncertainties are shown, as well as ratios of the theoretical predictions to the data.

sensitivities are comparable or even more stringent than some obtained from diboson channels with the same data luminosity, revealing an unexpected high sensitivity of the TGC studies from VBF V measurements.

The full Run 2 ATLAS results (ATLAS Collaboration, 2020a) focus on extracting limits on the interference between the Standard Model and dimension-six scattering amplitudes.

A number of QCD studies of hadronic activity in the selected V plus two jets events have been carried out by CMS and ATLAS with the 7 TeV and 8 TeV data (ATLAS Collaboration, 2014c, 2017g; CMS Collaboration, 2013d, 2015d). Inclusive studies of "radiation patterns" have been performed following the pre-

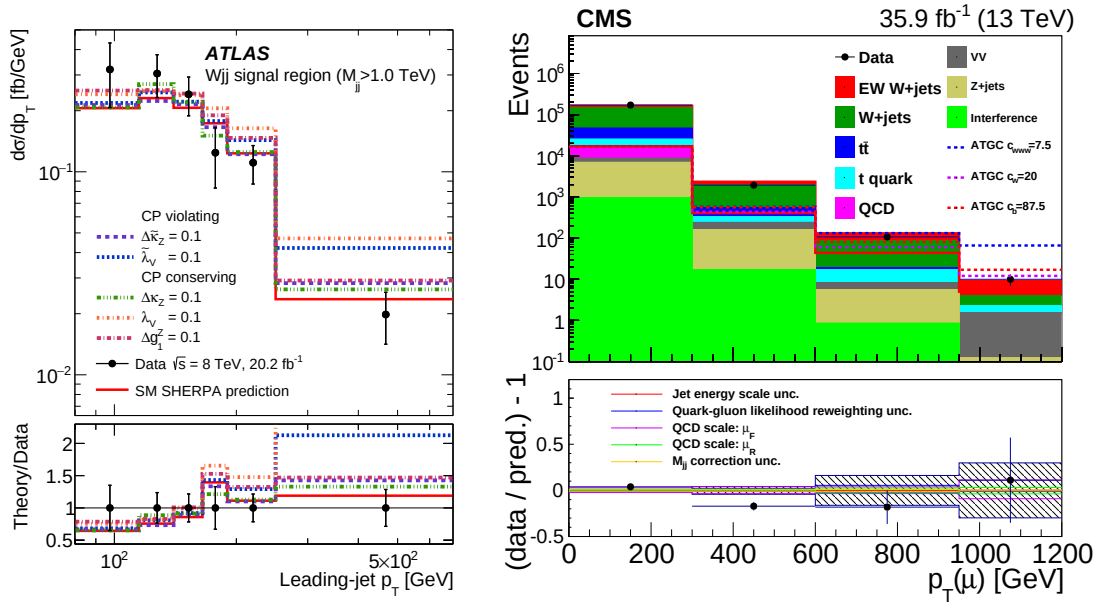

Figure 49 Leading jet p_{T} for the SM (solid line) and with anomalous TGC parameter deviations of 0.1 from the SM values (dashed lines) compared to unfolded differential VBF W cross-section distribution measured in 8 TeV data in the $m_{jj} > 1$ TeV signal region (left), figure taken from (ATLAS Collaboration, 2017g). Muon p_{T} distribution in 13 TeV data and SM backgrounds, and various scenarios for anomalous TGCs. The lower panel shows the ratio between data and prediction minus one with the statistical uncertainty from simulation (gray hatched band) as well as the leading systematic uncertainties (right), figure take from (CMS Collaboration, 2020b).

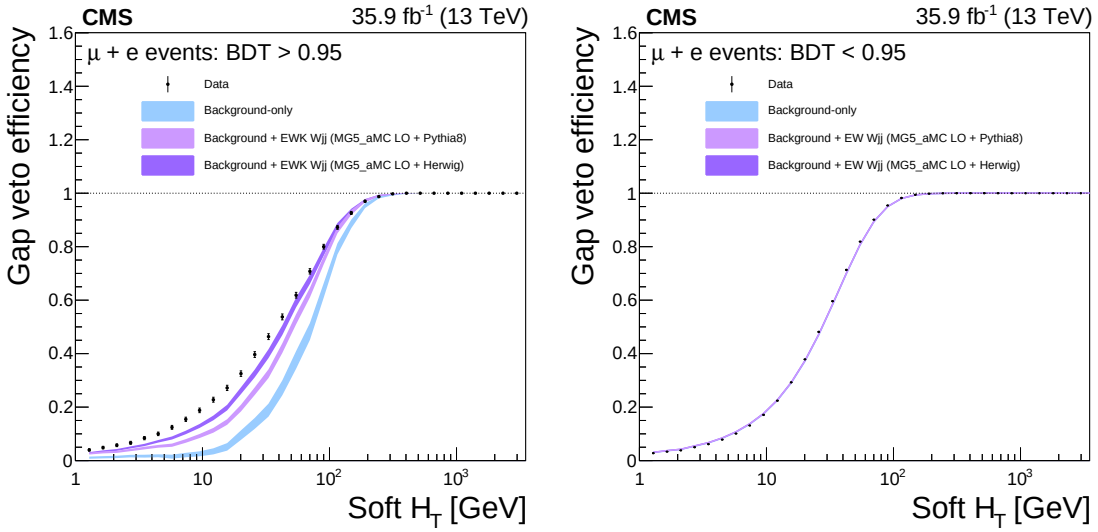

Figure 50 Veto efficiencies of hadronic gap activity at 13 TeV, evaluated with charged particles in signal-enriched (left) and background-enriched (right) regions. The data are compared with the background-only prediction as well as background+signal with PYTHIA (Sjöstrand *et al.*, 2015) or HERWIG (Bähr *et al.*, 2008a) parton showering. Figures taken from (CMS Collaboration, 2020b).

scriptions and suggestions in Ref. (Binoth *et al.*, 2010), where model dependencies are estimated by comparing different generators. The results (CMS Collaboration, 2013d) show a good agreement between data and the predictions by MADGRAPH interfaced to PYTHIA parton shower (ME–PS) for all chosen observables that are sensitive to hadronic activity. Dedicated studies, restricted to the additional hadronic activity in the expected rapidity gap between the two tagging jets, have also been performed. They are particularly interesting when making use of the larger 13 TeV data set (CMS Collaboration, 2018a, 2020b). The hadronic activity in the rapidity gap is measured in signal-enriched regions that have similar signal and background

yields, using as observables the standard reconstructed jets or jets reconstructed by clustering tracks ("soft track jets") from charged particles. The latter are used as they can be effectively cleaned from pileup contributions allowing precise low-p_{T} measurements (CMS Collaboration, 2009, 2010). Monte Carlo based studies of the additional jet activity in VBF W and Z channels revealed interesting differences in the prediction of different parton shower setups (Schissler and Zeppenfeld, 2013).

Figure 50 shows the gap veto efficiency for the "soft" H_{T} observable, i.e., the scalar sum of track jets p_{T} in the rapidity gap region, in signal and background enriched samples. In the background dominated sample the agreement of the data with the predictions is very good. The data in the signal region clearly disfavor the background-only predictions and are in reasonable agreement with the presence of the signal with the HERWIG++ PS predictions for gap activities above 20 GeV, while the signal with PYTHIA PS seems to generally overestimate the gap activity. In the events with very low gap activity, in particular below 10 GeV, as measured with the soft track jets, the data indicates gap activities also below the HERWIG++ PS predictions.

IV. ASSOCIATED PRODUCTION OF A VECTOR BOSON AND HEAVY-FLAVOR JETS

A. Theoretical predictions

The third important class of vector boson production processes is the production in association with heavy quarks, namely b- and c-quarks. The characterizing feature of these quark flavors is their relatively large mass, in comparison with the proton, in combination with a life-time long enough to form hadrons that decay after macroscopic path lengths. Indeed, this feature, leading to the presence of differentiable secondary decay vertices, is used in most tagging algorithms that identify the presence of heavy-flavor hadrons. The top quark associated production features very different dynamics and will not be discussed in this review.

In the following section, the features and availability of calculations for this process class will be reviewed, while a comprehensive review of the calculation techniques can be found in (Febres Cordero and Reina, 2015).

1. Higher order calculations and flavor schemes

Heavy-quark processes in general can be calculated in at least two different approaches. For definiteness, when b-quark associated production is considered either only the $dusc$-quarks are considered massless and the full mass dependence of the b-quark is retained (the four massless flavor scheme, $n_f = 4$, also referred to as 4F) or all five light quark flavors are considered massless (the five massless flavor scheme, $n_f = 5$, also referred to as 5F). While the former correctly describes all effects that are due to the b-mass, the latter allows for the b-quark to be extracted directly from the proton, resumming its contribution to the proton's parton density. By consistency, the b-quark is thus also only included in the running of the strong coupling in the $n_f = 5$ scheme. The choice of scheme, thus, has a non-negligible effect on the value of the strong coupling constant on scales beyond the b-quark mass. In particular, the value of $\alpha_s(m_Z)$ differs in both schemes.[8] Thus, ideally, one would like to have a calculation with both the finite-mass and the resummation effects accounted for. In consequence to these considerations, methods have been formulated that combine both ansatzes, like the FONLL method (Cacciari *et al.*, 1998; Forte *et al.*, 2010). The diagrams contributing in the respective cases are shown in Figures 51 and 52 for W and Z associated heavy flavor production, respectively.

The generalisation for the different mass-dependence treatments of charm quarks is mostly straight-forward (Ball *et al.*, 2016). Because the charm quark's isospin partner, the strange quark, is not mass suppressed, in contrast to the bottom's isospin partner, the top quark, and the respective inter-generational mixing matrix elements V_{cd} are sizeable in comparison to V_{ub} and V_{cb}, additional topologies contribute in W associated charm production that are strongly suppressed in W associated bottom production, cf. Figure 51(c).

One particular aspect of all parton level calculations that has to be kept in mind is that no flavor-jet related observable can be defined in complete analogy to the experimental definitions. This roots in the fact that the identification of heavy flavors in an experimental setting relies on the properties of heavy-flavor

[8] A possible remedy is explored in Ref. (Bertone *et al.*, 2015) where *doped* PDFs are introduced, running α_s in $n_f = 5$ and the evolve the PDFs in $n_f = 4$, which however has not seen a wide-spread use so far.

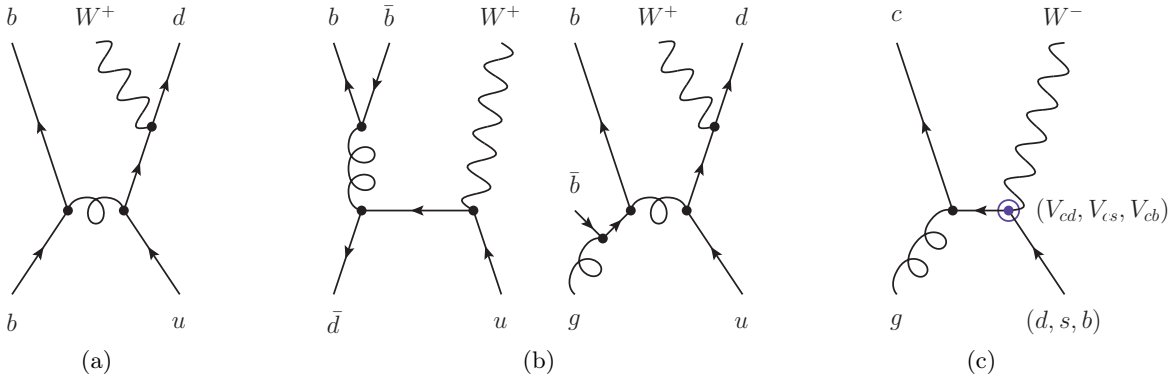

Figure 51 Representative Feynman diagrams for the production of a W boson and (at least) one b quark at LO in the $n_f = 5$ scheme (a), the $n_f = 4$ scheme (b) and additional contributions in the production of (at least) one c quark in association with the W boson (c).

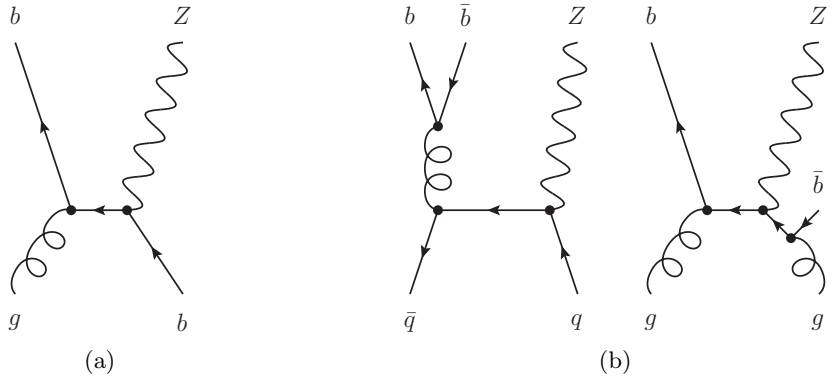

Figure 52 Representative Feynman diagrams for the production of a Z boson and (at least) one b quark at LO in the $n_f = 5$ scheme (a), the $n_f = 4$ scheme (b).

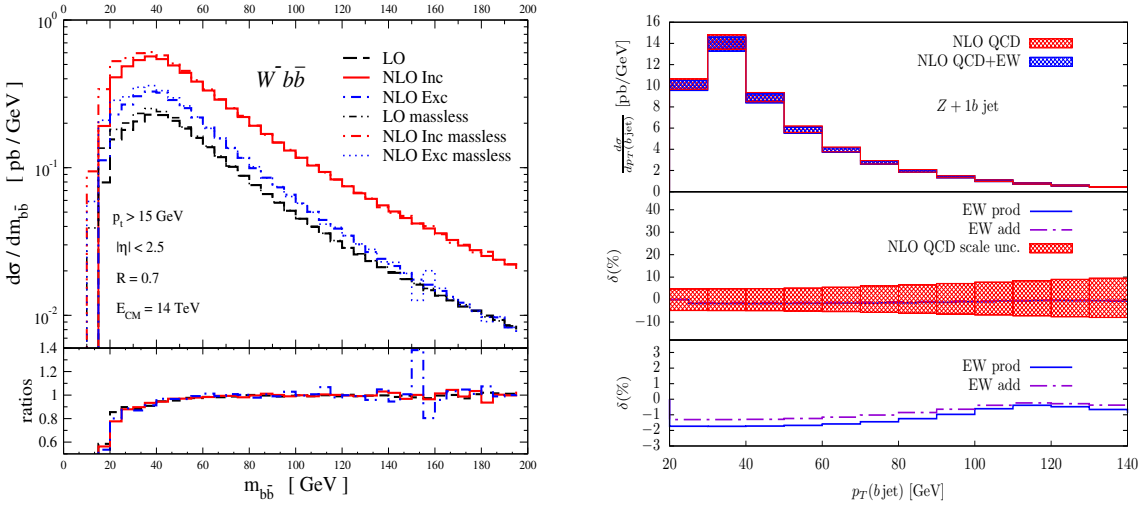

Figure 53 Di-b-jet invariant mass in the pair production of a charged lepton and a neutrino in association with at least two b-jets calculated at LO and NLO QCD in both the $n_f = 4$ and $n_f = 5$ massless quark flavor schemes (left), figure taken from (Febres Cordero *et al.*, 2009). Leading b-jet transverse momentum in the pair production of two charged leptons in association with at least one b-jet calculated at NLO QCD with and without NLO EW corrections in the $n_f = 5$ massless quark flavor scheme (right), figure taken from (Figueroa *et al.*, 2018).

hadrons, in particular their finite lifetime allowing for a measurable spatial separation of production and decay vertices. A parton level heavy-flavor tag, on the other hand, can only involve the partonic jet constituents. The requirement for infrared safety then generally necessitates a signed counting of heavy flavor quanta to guarantee that a collinear $g \to q\bar{q}$ splitting does not alter the jet flavor tag. One useful example here is the flavor-k_{T} algorithm (Banfi *et al.*, 2006). Its anti-k_{T} relative, however, is not infrared safe starting at NNLO as through its cone-like structure, soft wide-angle $g \to q\bar{q}$ splittings carry the possibility of losing one heavy quark thereby again altering the jet flavor tag (Gauld *et al.*, 2020). This is problematic in the limit that the splitting gluon itself comes from a soft $q \to qg$ splitting, rendering the cancellation of its infrared divergence incomplete (Banfi *et al.*, 2006).

Four and five flavor calculations thus exist for $W/Z/\gamma + b$, $W/Z/\gamma + b\bar{b}$ and $W/Z/\gamma + b\bar{b}$ + jet production at NLO QCD (Campbell *et al.*, 2006, 2007; Febres Cordero *et al.*, 2009; Hartanto and Reina, 2014; Stavreva and Owens, 2009) and NLO EW (Figueroa *et al.*, 2018) accuracy. Fig. 53 shows selected calculations for the $W + b\bar{b}$ and $Z + b$ process. A $Z/\gamma + b$ calculation at NNLO QCD accuracy in the $n_f = 5$ scheme became available recently (Gauld *et al.*, 2020), accounting for b-quark mass effects at NLO QCD accuracy with the aforementioned FONLL method and is expected to impact heavy flavour PDF extractions in particular.

2. Monte Carlo event generators

Along with the automation of matching NLO QCD calculations to parton showers, the availability of precision Monte Carlo event generation grew for this process class. Thus, the existing NLO QCD matched results produced by the MC@NLO (Frederix *et al.*, 2011) or POWHEG (Oleari and Reina, 2011) generators represent the state-of-the art for any fixed flavor number scheme. Recently, multi-jet merged predictions at NLO accuracy became available in the MEPS@NLO method combining the $n_f = 4$ and $n_f = 5$ scheme (Höche *et al.*, 2019a). Typically, in the multi-jet merging approach problems arise with double counting of contributions already present in the general V + jets multi-jet merged calculations in the massless limit. Therefore, various strategies have been devised to address this issue. Besides a more phenomenological and not theoretically rigorous approach, known as Heavy Flavor Overlap Removal (Mangano *et al.*, 2002), applied so far to LO-accurate simulations only, more rigorous approaches use schemes equivalent to the FONLL approach (Höche *et al.*, 2019a). Figure 54 shows the result of both approaches.

B. Experimental results

Processes involving vector bosons in association with bottom or charm quarks provide stringent tests of QCD predictions and are the largest backgrounds in studies of the Higgs boson decaying to two b quarks, in measurements of the properties of the productions of single or pairs of top quarks, and in numerous searches for physics beyond the SM.

1. Heavy-flavor identification in jets

The identification of jets originating from b or c quarks (heavy-flavor jets) is of primary importance for many measurements and searches with proton collision data. Detectors with precise charged-particle tracking as well as electron and muon identification are well suited to identify heavy-flavor jets, exploiting mainly the presence of displaced tracks from which a secondary vertex (SV) may be reconstructed. Figure 55 shows examples of distributions of combined multivariate algorithms and reconstructed secondary vertex mass used to identify and separate heavy-flavor jets in association with vector bosons. The heavy-flavor identifications algorithms and their performances have been described in detail for LHC 7 and 8 TeV proton collision data (ATLAS Collaboration, 2016f; CMS Collaboration, 2013b), and for 13 TeV collision data (ATLAS Collaboration, 2018e; CMS Collaboration, 2018b).

In simulated events different procedures can be applied to assign a flavor to a jet. A simple parton-level angular association was mostly used by TEVATRON and LHC Run 1 data. A particle-level definition commonly employed for LHC Run 2 data makes use of a ghost association (Cacciari and Salam, 2008) of heavy-flavor hadrons to generator-level particle jets. In all definitions, precedence is first given to the b-quark flavor, and then to c-quark flavor.

Both parton- and particle-based heavy-flavor definitions have been used to define the V plus heavy-flavor jet measurements described in the following.

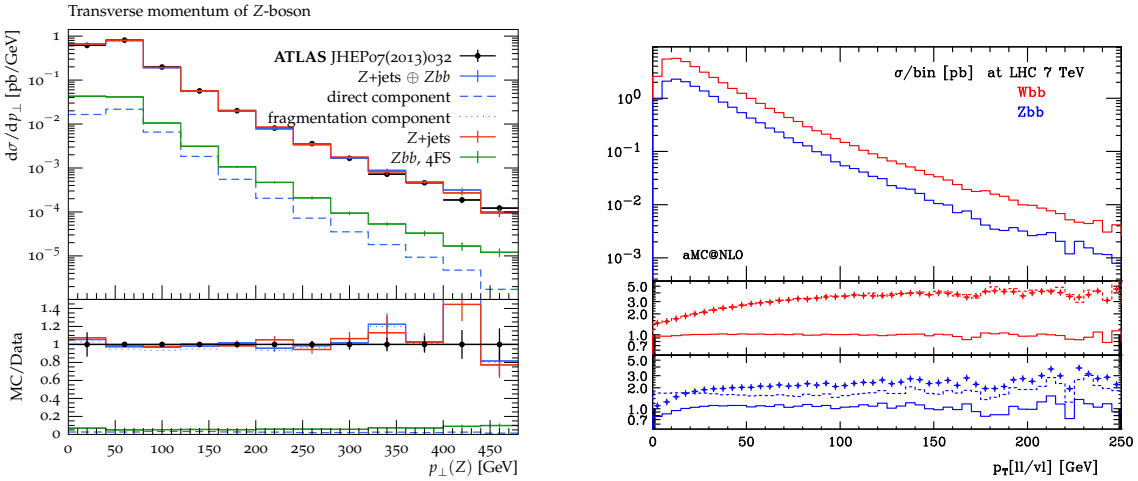

Figure 54 Reconstructed Z boson transverse momentum in the pair production of two charged leptons in association with at least one b jet calculated using the fusing method to combine $n_f = 4$ and $n_f = 5$ schemes in the MEPS@NLO method in SHERPA (left), figure taken from (Höche *et al.*, 2019a). Reconstructed vector boson transverse momentum in the production of a pair of charged leptons, and a charged lepton and neutrino in association with a pair of b jets calculated at NLO QCD matched to the parton shower in aMC@NLO (right). The insets show the ratios of the aMC@NLO result over the corresponding NLO (solid), aMC@LO (dashed) and LO (crosses) results. Figure taken from (Frederix *et al.*, 2011).

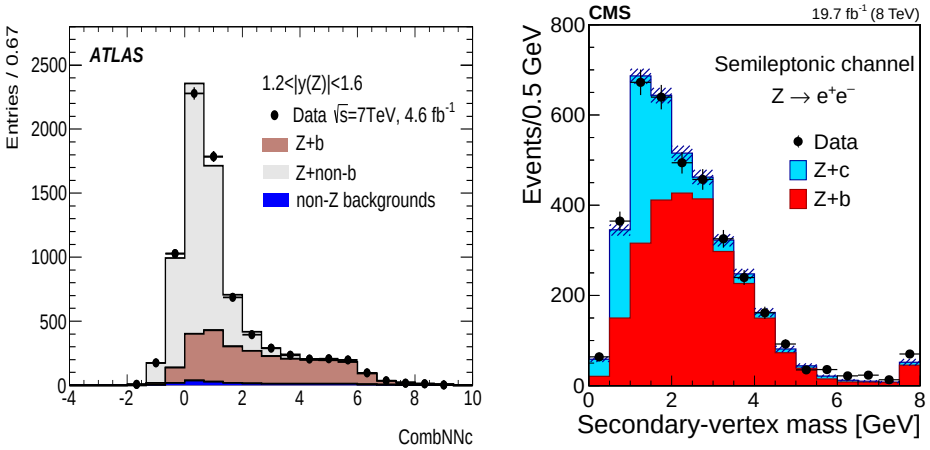

Figure 55 Combined neural network output distribution providing separation between jet flavors in Z+jet events at 7 TeV(left), figure taken from (ATLAS Collaboration, 2014b). Secondary-vertex mass distributions for jets associated to a Z boson decaying to electrons, after background subtraction, at 8 TeV (right), figure taken from (CMS Collaboration, 2018c).

2. $V + b$-quark productions

Studies of the production of prompt photons in association with b quarks have been performed with TEVATRON data and compared to various QCD predictions. Measurements by DØ (DØ Collaboration, 2009a, 2012, 2013a) were performed differentially in the photon p_{T}, and in the photon and jet rapidity for both γ+b and γ+c productions, separating the jet flavors with a combined displaced track jet probability. Similar results have been produced by CDF (CDF Collaboration, 2010a, 2013b), alternatively making use of the invariant mass of reconstructed secondary vertices to separate jet flavors. All results showed a need for higher-order perturbative QCD corrections beyond NLO, in the larger $p_{\mathrm{T}} > 70$ GeV regions.

The ATLAS collaboration has measured isolated-photon plus heavy-flavor jet production in 8 TeV proton collisions (ATLAS Collaboration, 2018b). Results are provided differentially in the transverse energy of the photon and in two photon pseudorapidity regions, and compared to LO and NLO QCD calculation with 5F and 4F schemes, as shown in Fig 56. The NLO predictions underestimate the data in the kinematic region with $E_{\mathrm{T}}^{\gamma} \geq 125$ GeV with the 4F scheme, and in the kinematic region with $E_{\mathrm{T}}^{\gamma} \geq 200$ GeV with the 5F scheme. The 4F

predictions for the cross-section ratios overestimate the data for $E_{\mathrm{T}}^{\gamma} \geq 65$ GeV. The best description of the data is provided by SHERPA predictions, which include up to three additional partons and are computed in the 5F scheme.

The first measurement of the associated production of a Z boson with a b-jet was performed by DØ (DØ Collaboration, 2005) indicating a ratio to light jets around 2%, in agreement with existing NLO QCD predictions. Similar results where derived also by CDF (CDF Collaboration, 2006), including a fiducial $Z + b$ cross section with a total uncertainty around 40%.

A subsequent CDF analysis with a larger data sample reported similar results for the fractions of associated b-jets, with improved precision, and differential distributions in jet E_{T}, jet η, Z boson transverse momentum, number of jets, and number of b-jets (CDF Collaboration, 2009b). Results were consistent with predictions from LO Monte Carlo generators and NLO QCD calculations within uncertainties. The invariant mass distribution of the tracks forming the secondary vertex was used to extract the b-jet fractions.

More recent measurements by DØ determined the b-jet ratios to light jets with a precision around 10% using a peculiar technique that combines the properties of the tracks associated to the jet (DØ Collaboration, 2011a). A more recent DØ publication reported the fractions of b-to-light jet associated production as a function of the Z boson transverse momentum, jet transverse momentum, jet pseudorapidity, and the azimuthal angle between the Z boson and the jet (DØ Collaboration, 2013c). Existing predictions from Monte Carlo event generators did not provide a consistent description of all the examined variables.

In the meantime first measurements of $Z + b$ productions with LHC data were performed by ATLAS (ATLAS Collaboration, 2012b) with 7 TeV proton collision data, reporting both a fiducial cross section and the ratio to the inclusive Z cross section in the same fiducial region, both with a precision around 30%. Similar measurements were then performed by CMS (CMS Collaboration, 2012c) with a larger data sample, allowing the precision to improve to better than 20%. The measured cross sections and the kinematic distributions of the b-jet and charged leptons were found to be in reasonable agreement with existing predictions.

Dedicated measurements of the production of two b-hadrons (B) together with a Z boson were performed with 7 TeV data by CMS with particular focus on the angular correlations between the b-hadrons and the Z boson (CMS Collaboration, 2013c). The b-hadrons are identified by means of displaced secondary vertices, without the use of reconstructed jets, permitting the study of b-hadron pair production with an angular separation smaller than the jet radius. The results shown in Fig. 57 indicate that the 5F description may not be well suited to describe the collinear production of b-hadrons.

Other measurements of total cross sections, separately for a Z boson produced with exactly one b-jet and with at least two b-jets have been produced by CMS (CMS Collaboration, 2014d). For those results data favor the predictions in the five-flavor scheme, where b-quarks are assumed massless, while predictions in the four-flavor scheme show a clear disagreement in the $Z + 1$ b-jet final state.

The LHCb collaboration has produced complementary measurements of $Z+b$-jet cross section in the forward pseudorapidity range $2.0< \eta$ 4.5 and with jet p_{T} above 10 or 20 GeV (LHCb Collaboration, 2015c). The results yield a 25-30% precision and are in reasonable agreement with both massless and massive bottom-quark calculations.

Further differential measurements of $Z + b$-jet productions have been performed by ATLAS with 7 TeV data (ATLAS Collaboration, 2014b), and by CMS with 8 TeV data (CMS Collaboration, 2017g). The ATLAS total cross section results are generally in good agreement with predictions from MCFM. Predictions obtained using MADGRAPH5_aMC@NLO with a 4F scheme underestimate the $Z + 1$ b cross sections, while predictions with the 5F scheme seem to underestimate the $Z+2$ b yields. Interesting disagreements between predictions and data are also reported in the differential distributions, as for example the angular separation between the Z boson and the b-jet shown in Fig. 58, where missing higher order QCD corrections in the predictions might explain the discrepancies.

The CMS results for $Z + b$ productions with 8 TeV collision data have also been compared with a variety of predictions, yielding fair agreement with the data results. Predictions with 4F scheme seem to underestimate the total $Z+1$ b cross sections and fail to describe simultaneously both the low- and high-p_{T} b-jet regions. In the case of Z boson in association with two b-jets, the data distributions are generally well reproduced by the predictions, as for example the dijet mass shown in Fig. 58.

Measurements of $Z+b$ and $Z+bb$ productions with 13 TeV collision data have been performed by ATLAS (ATLAS Collaboration, 2020d). A summary of the total measured cross sections

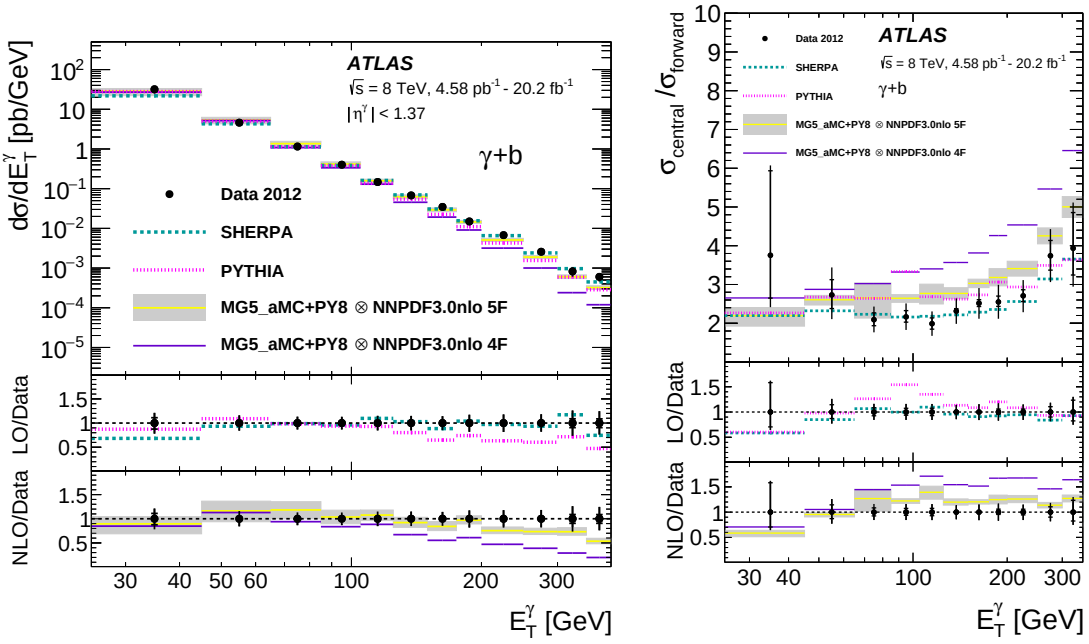

Figure 56 Measured $\gamma + b$ cross sections at 8 TeV. Differential cross sections as a function of the photon transverse energy in the central region ($|\eta^{\gamma}| < 1.37$) (left). Cross-section ratios of the central region, $|\eta^{\gamma}| < 1.37$, to the forward region, $1.56 < |\eta^{\gamma}| < 2.37$, as a function of the photon transverse energy (right). Figures taken from (ATLAS Collaboration, 2018b).

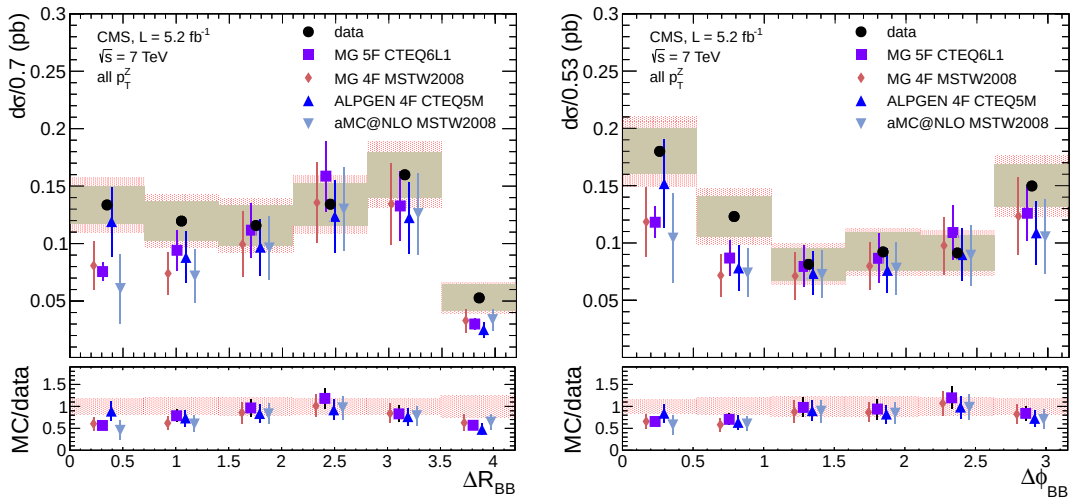

Figure 57 Measured $Z + BB$ differential cross sections at 7 TeV as a function of $\Delta R(BB)$ (left) and $\Delta\phi(BB)$ (right). Measurements are compared to the hadron-level predictions by MadGraph in the four- and five-flavor schemes. Figures taken from (CMS Collaboration, 2013c).

and comparisons with different predictions is shown in Fig. 59. It can be seen that the 5F scheme predictions at NLO accuracy agree better with data than 4F scheme ones, and that the 4F predictions underestimate data in events with at least one b-jet.

Early measurements of $W + b$ rates by CDF (CDF Collaboration, 2010b) with Tevatron data revealed some excess over the existing predictions with LO multijet-merged (Mangano *et al.*, 2002) and NLO accurate calculations (Campbell *et al.*, 2009, 2007; Febres Cordero *et al.*, 2006) that were not confirmed by subsequent similar DØ measurements (DØ Collaboration, 2013b).

Meanwhile, first measurements of $W + b$ productions with Lhc data were performed by Atlas (ATLAS Collaboration, 2012c) with 7 TeV proton collision data. Events are required to have exactly one b-tagged jet reducing sig-

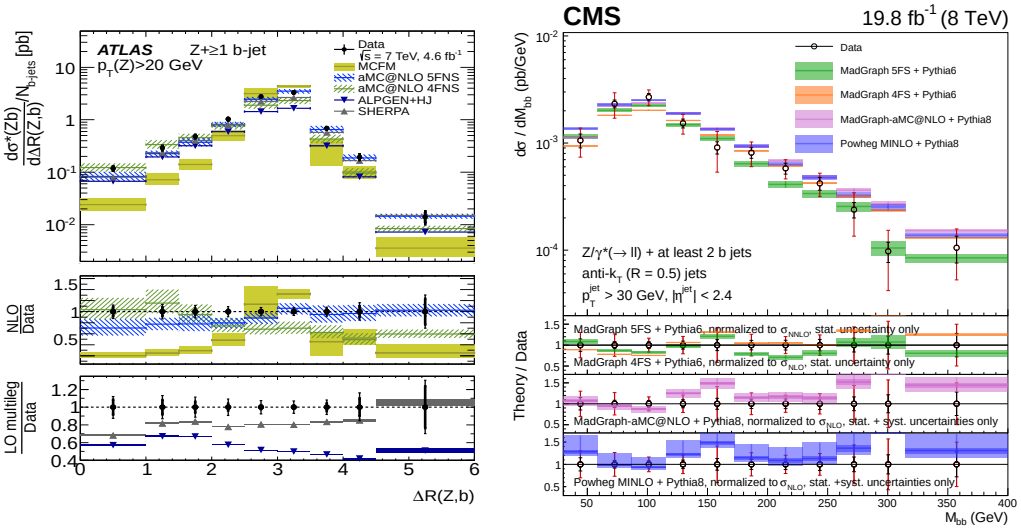

Figure 58 Measured $Z + b$ differential cross sections at 7 TeV (left) and 8 TeV (right). The Z plus b-jet cross section as a function of $\Delta R(Z, b)$ (left), figure taken from (ATLAS Collaboration, 2014b). The Z plus 2 b-jets cross section as a function of the invariant mass of the b-jet pair (right), figure taken from (CMS Collaboration, 2017g).

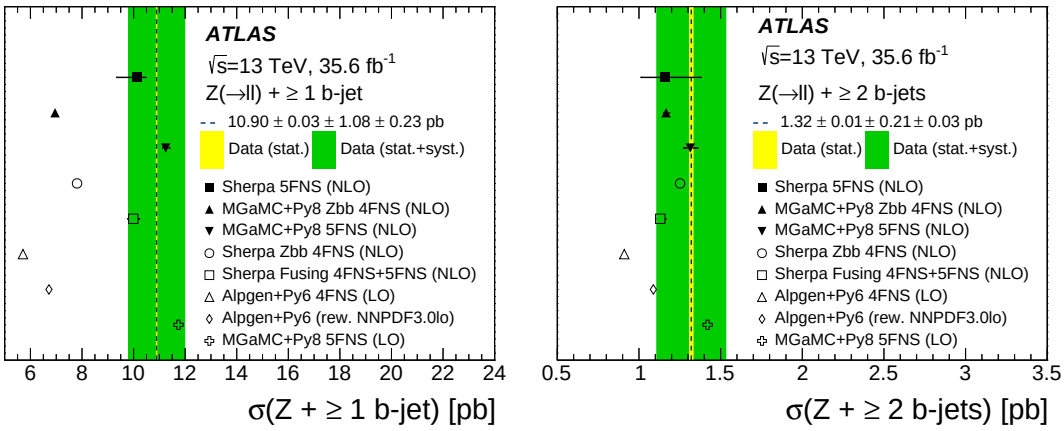

Figure 59 Measured cross-sections for $Z + \geq 1$ b-jet (left) and $Z + \geq 2$ b-jets (right). The data are compared to different predictions in the 4F and 5F approximations. The yellow band corresponds to the statistical uncertainty of the data, and the green band to statistical and systematic uncertainties of the data, added in quadrature. The error bars on the SHERPA 5F (NLO) predictions correspond to the statistical and theoretical uncertainties added in quadrature. Only statistical uncertainties are shown for the other predictions. Figures taken from (ATLAS Collaboration, 2020d).

nificantly the top-quark background. Results are unfolded to a fiducial phase space at particle level, where b-jets are defined by the presence of a b-hadron associated to the jet, and are compared to QCD NLO predictions performed in the 5 flavor scheme (Campbell *et al.*, 2012) and to other leading order predictions. Results with a larger data set have been subsequently produced by ATLAS (ATLAS Collaboration, 2013d) allowing for an improved precision and differential measurements as a function of the b-jet p_{T}, shown in Fig. 60.

Dedicated measurements of the production of a W boson and two b-jets have been performed by CMS with both 7 TeV (CMS Collaboration, 2014c) and 8 TeV (CMS Collaboration, 2017d) proton collision data. Events are required to have exactly two b-tagged jets, and top-quark background is reduced requiring no additional jets nor isolated electrons or muons. Fig. 61 (left) shows the data and post-fit Monte Carlo distributions for $\Delta R(b, b)$. Results are given in terms of a fiducial $W + bb$ cross section and are in good agreement with several predictions from MCFM, corrected for DPS and hadronization effects, and from MADGRAPH +PYTHIA, with different PDF flavor schemes, as shown in Fig. 61 (right).

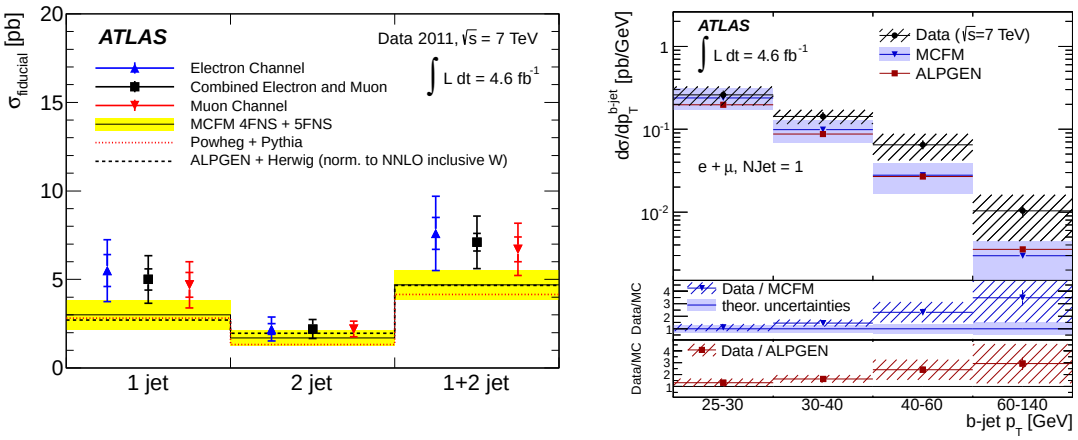

Figure 60 $W + b(b)$ fiducial and differential cross sections at 7 TeV. Total cross sections in the 1, 2, and 1+2 jet exclusive bins with the statistical (inner error bar) and statistical plus systematic (outer error bar) uncertainty in the electron, muon, and combined electron plus muon channel (left). Differential $W + b$-jet cross-sections with total uncertainties as a function of the b-jet p_{T} in the 1-jet fiducial region, compared to the MCFM and ALPGEN predictions (right). Figures taken from (ATLAS Collaboration, 2013d).

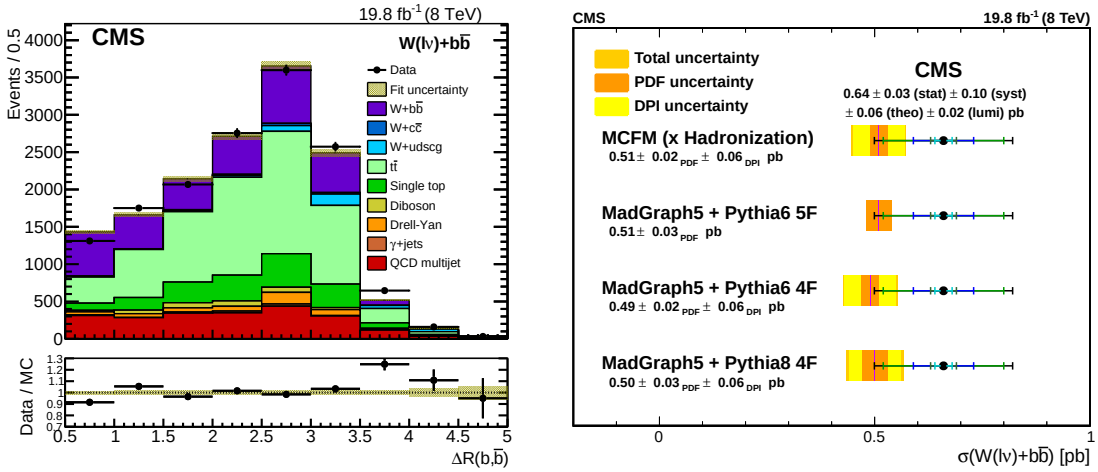

Figure 61 $W + bb$ production at 8 TeV. Post-fit $\Delta R(b, b)$ distribution (left). Comparison between the measured cross section and various QCD predictions (right). Figures taken from (CMS Collaboration, 2014c, 2017d).

It can be finally remarked that in the context of the measurements of the Higgs boson decays to bottom quarks in the associated VH production mode, both the ATLAS and CMS collaborations determine normalization "scale factors" for the W/Z $+b(b)$ background sources, with respect to NLO QCD predictions, and with a precision in the 10–20% range (ATLAS Collaboration, 2018f; CMS Collaboration, 2018f). In this specific phase space of the Higgs to bottom-quark measurements, CMS reported significantly large scale factors for $W+b(b)$ productions, up to a factor two with respect to the reference NLO QCD predictions, while ATLAS normalizations are consistent with predictions.

3. $V + c$-quark productions

First measurements of associated production of Z bosons with charm-quark jets were performed by DØ (DØ Collaboration, 2014) reporting an integrated fraction of c-jets of 8% with a 10% relative uncertainty, and a ratio to b-jet production of about 4 with a 15% relative uncertainty. The cross section ratios were also measured differentially as a function of jet and Z boson transverse momenta showing significant deviations from existing perturbative QCD calculations and event generators predictions.

The first observation of $Z + c$ production at LHC was reported by LHCb in the forward region $2 < y < 4$ with data from proton collisions

at 7 TeV, making use of fully reconstructed D^0 and $D^{\pm}$ decays (LHCb Collaboration, 2014a).

The CMS collaboration has performed a measurement of associated Z + charm production in proton collisions at 8 TeV (CMS Collaboration, 2018c). The selection of event candidates relies on the identification of semileptonic decays of c or b hadrons with a muon in the final state and through the reconstruction of exclusive decay channels of $D^{\pm}$ and $D^{*\pm}(2010)$ mesons. The total $Z + c$ cross section is measured with a precision of 10% while the cross section ratio $Z + c/Z + b$ is determined to be 2.0 ± 0.3. Differential cross sections are measured as a function of the transverse momentum of the Z boson and the heavy-flavor jet. The measurements are in agreement with NLO QCD predictions, including parton shower development and non-perturbative effects. Results in the highest transverse momentum regions are compatible with predictions using PDF sets with no intrinsic charm component. Results with 13 TeV collision data have been released recently, making use of jet secondary vertex mass distributions to separate light, charm and bottom flavor components (CMS Collaboration, 2020a,c). Results are given in terms of b/light, c/light and c/b production ratios, both inclusively and differentially with respect to the Z boson p_{T} and the jet p_{T}. The experimental results are in reasonable agreement with current theoretical predictions that however carry a larger uncertainty. Figure 62 shows $Z+c$ cross section measurements at 8 TeV and c/b cross section ratio measurements at 13 TeV, both as a function of the heavy-flavor jet p_{T}.

Measurements of the production of a W boson and charm quarks are carried out determining the charge sign of the W boson and the charm quark, and separating events with same-sign (SS) and opposite-sign (OS) charges. Contributions from W+c processes are inferred after performing a subtraction of SS events from OS ones, that effectively removes most background sources.

Initial $W + c$ measurements were performed by CDF (CDF Collaboration, 2008a) and subsequently reached an overall 20% precision (CDF Collaboration, 2013c) with results compatible with existing theoretical expectations. A 15% constraint on the $|V_{cs}|$ CKM quark mixing matrix element was also derived from these results.

The first measurements of $W+c$ productions at the LHC were performed with 7 TeV proton collision data by CMS (CMS Collaboration, 2014a), where hadronic and inclusive semileptonic decays of charm hadrons are used to select the presence of c-jets. Cross sections and cross section ratios were measured inclusively to precisions of 3–7%, and differentially with respect to the absolute value of the pseudorapidity of the charged lepton from the W-boson decay, shown in Fig 63. Results are directly sensitive to the strange quark content of the proton, and are consistent with the predictions based on global fits of parton distribution functions (see Sec. V).

The ATLAS collaboration performed measurements of $W + c$ production at 7 TeV where the charm quark is similarly tagged either by a semileptonic decay or by the presence of a charmed meson (ATLAS Collaboration, 2014e). Results where also found in good agreement with theoretical predictions for the cross sections with different choices of the PDF set, with a preference for PDFs with an SU(3)-symmetric light-quark sea, as discussed in Sec. V.

The CMS collaboration has also produced $W+c$ measurements with 13 TeV collision data using only charm quarks tagged via the full reconstruction of D-mesons (CMS Collaboration, 2019b). Figure 64 shows differential $W+c$ cross sections measured at 13 TeV by CMS.

Measurements of W boson productions in association with b- and c-quarks have also been carried out in the forward regions of proton collisions at 7 and 8 TeV by LHCb (LHCb Collaboration, 2015d). A dedicated secondary vertex tagger is used to identify and separate the presence of heavy-flavor jets. Results are generally in agreement with QCD predictions and do not support a large contribution from intrinsic b-quark content in the proton but the precision is not sufficient to rule out such a contribution at O(10%).

V. THEORETICAL INTERPRETATIONS OF DATA FROM VECTOR BOSON PRODUCTION WITH ASSOCIATED JETS

The production of high statistics V + jet Monte Carlo samples is key to much of the TEVATRON and the LHC physics programs. The validation of MC event generators available with different levels of approximations in pQCD and different non-perturbative QCD model implementations require careful comparisons between predictions and with data. Several investigations into the tuning of related MC parameters and evaluations of uncertainties on their predictions have been carried out by both communities of experimentalists and theorists based on V+jet processes. Examples of validation and tuning studies of V+jet MC event generators are included in Refs. (ATLAS Collabo-

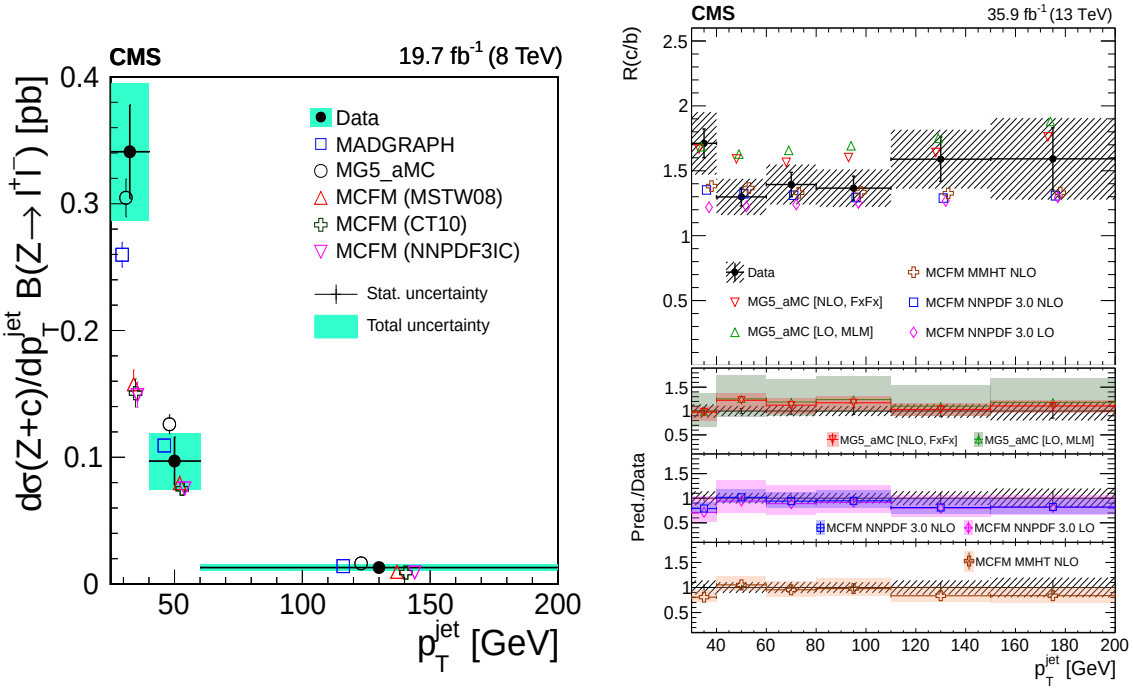

Figure 62 Differential $Z + c$ cross section as a function of the transverse momentum of the c-jet at 8 TeV (left), figure taken from (CMS Collaboration, 2018c). $(Z + c)/(Z + b)$ cross section ratio as a function of the transverse momentum of the jet at 13 TeV (right), figure taken from (CMS Collaboration, 2020c).

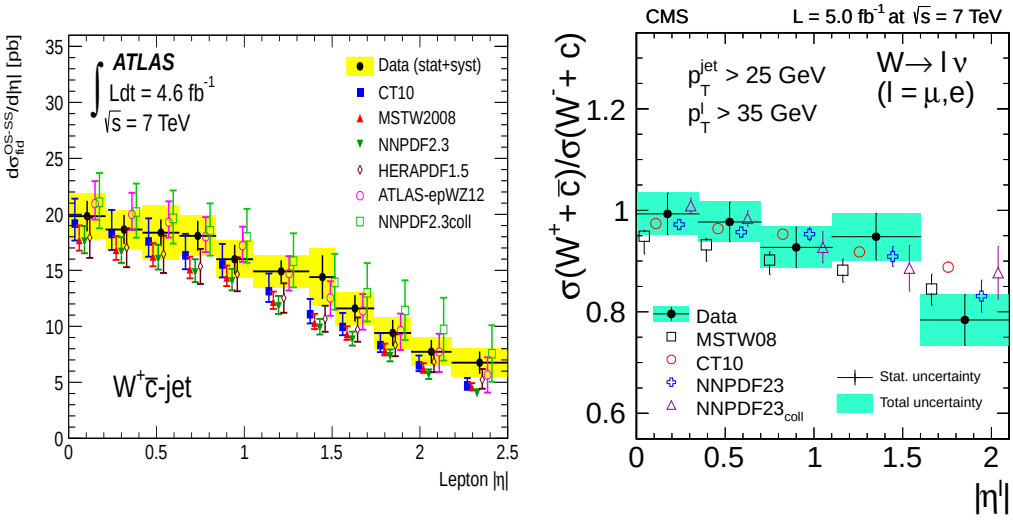

Figure 63 Measurements of $W + c$ production in proton collisions at 7 TeV. The measured differential cross section (left), figure taken from (ATLAS Collaboration, 2014e), and the cross section ratio $\sigma(W^+ + c)/\sigma(W^- + c)$ as functions of the charged lepton $|\eta|$ (right) are compared to predictions obtained using various PDF sets, figure taken from (CMS Collaboration, 2014a).

ration, 2014f, 2016a,d,i, 2017a; Cooper *et al.*, 2012).

An example is the comparison of the MC generators used by LHC experiments in Run-2 analyses with V + jet measurements performed at 7 TeV center-of mass energy in Run-1 (ATLAS Collaboration, 2016d). The same generators were then used to simulate events at the Run-2 center-of-mass energy of 13 TeV to investigate further the differences between the predictions and assess the theoretical uncertainties. Given the increase in cross section for the W/Z + jet production processes in Run-2 with respect to Run-1, it was important to carefully assess the accuracy of the MC generators in the new kinematic regime. Predicted differential cross sections were compared to unfolded distributions in data using the RIVET package (Bierlich *et al.*, 2020; Buckley *et al.*, 2013). Although an overall good description of

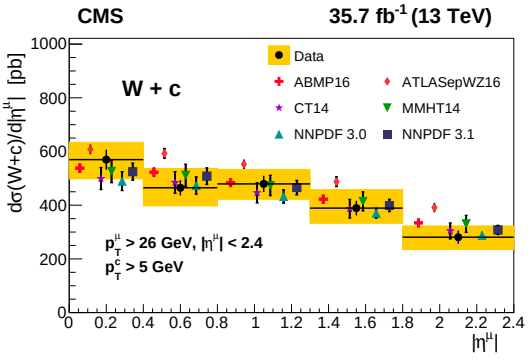

Figure 64 Differential cross sections of $W + c$ production, measured as a function of the charged lepton pseudorapidity at 13 TeV The measurements are compared to the QCD predictions at NLO using different PDF sets. Figure taken from (CMS Collaboration, 2019b).

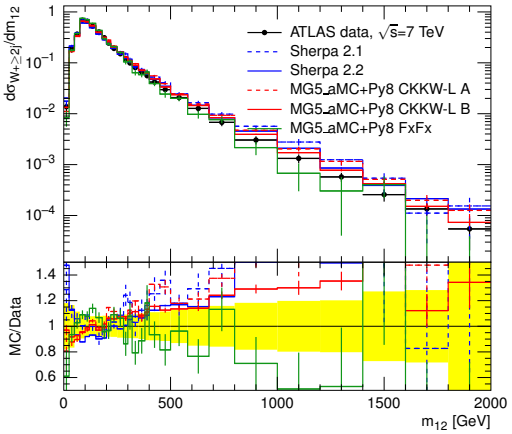

Figure 65 Comparison between different MC generator models and data for events with a W and at least two jets, in the distribution of the invariant mass of the two leading jets, at 7 TeV pp collisions, figure taken from (ATLAS Collaboration, 2016d).

the data is provided by all considered generators, as Fig. 65 shows, some clear differences between prediction and data at 7 TeV were visible in some observables. This type of studies has prompted a new tuning of model parameters (ATLAS Collaboration, 2014f) and improvements in the calculations. Comparisons were also made in phase space regions and for processes that became more relevant for Run-2 analyses due to the larger statistics, e.g. the production of vector bosons in association with heavy-flavor jets and for electroweak $V + 2$ jets production (ATLAS Collaboration, 2017a). As a result of these studies the uncertainties associated to the normalization and shapes of the predictions of the MC generators for V+jet processes have been routinely assessed on different MC event generators, including variations of matching and merging schemes, parton shower realisations as well as fragmentation and underlying event models, the strong coupling constant and PDFs.

The understanding of the proton PDF, and specifically the flavor composition of the quark sea is important for the LHC physics program as a whole. For instance the strange quark PDF has a direct impact on the measurement of the W boson mass. In addition to measurements of charm production in deep inelastic scattering experiments with neutrinos, the strange quark content of the nucleon can be obtained from the measurements of inclusive differential W and Z boson cross sections, W + charm production as well as W/Z+jets. Inclusive differential W and Z boson cross sections at $\sqrt{s} = 7$ TeV (ATLAS Collaboration, 2012d, 2017i; CMS Collaboration, 2012b, 2014b) allowed the strange content of the sea to be measured rather than assumed to be a fixed fraction of the light sea quarks.

A QCD interpretation of inclusive W and Z boson production data by the ATLAS Collaboration together with data from deep-inelastic scattering at HERA presented in Ref (ATLAS Collaboration, 2012a) shows the sensitivity to the light-quark sea composition of the proton at the LHC. The ratio of the strange-to-down sea quark distributions was determined to be consistent with one at momentum transfer squared $Q^2 = 1.9$ GeV^2 and Bjorken $x = 0.023$, therefore supporting a symmetric composition of the light-quark sea at low x. The CMS $W + c$ measurement at $\sqrt{s} = 7$ TeV (CMS Collaboration, 2014a) identified processes where a c quark is produced in association with a W boson and was used for the determination of the strange-quark distribution in the proton. This analysis was followed recently by a measurement at 13 TeV center-of-mass energy (CMS Collaboration, 2019b). The CMS results point towards a strangeness suppression with respect to light sea-quark densities in agreement with measurements in neutrino scattering experiments. These results are hence in tension with ATLAS studies based on the analysis of inclusive W and Z boson production (ATLAS Collaboration, 2017i) and W + charm production at $\sqrt{s} = 7$ TeV (ATLAS Collaboration, 2014e), which are found to be consistently and significantly better described by an unsuppressed strange sea at low-x values. Figure 66 shows the cross section measured by the CMS experiment for the production of $W + c$, compared to various PDF fits, including the one by the ATLAS collaboration (ATLASepWZ16) that makes use of inclusive W and Z cross section data as an input.

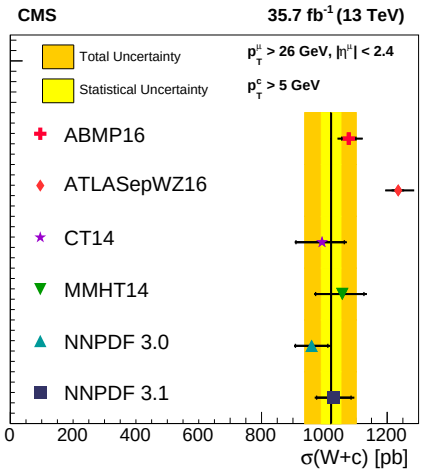

Figure 66 The fiducial cross section for $W + c$ production at 13 TeV with the CMS detector at the LHC. The measurement is compared to predictions using several PDF sets. With the exception of ATLASepWZ16, which is obtained at NNLO in pQCD, all other PDF sets are obtained at NLO. Figure taken from (CMS Collaboration, 2019b).

The cross section ratio $R_c^{\pm} = \sigma(W^+ + \bar{c})/\sigma(W^- + c)$ can be sensitive to the s-$\bar{s}$ asymmetry in the PDFs that was suggested by neutrino data (Goncharov *et al.*, 2001). The results by CMS (see Fig. 63) and ATLAS (see Fig. 12 in Ref. (ATLAS Collaboration, 2014e)) are compatible, within one standard deviation, with predictions obtained using PDF parameterisations with no asymmetry or a small asymmetry in the order of few percent. Those LHC measurements of the $R_c^{\pm}$ ratio at 7 TeV were limited by statistical uncertainties. Given the far larger data set collected by LHC experiments at higher center-of-mass energies, it will be very interesting to see such measurements repeated with greater precision.

As discussed in Sec. II.B.4 the study of W or Z boson production with jets allows to access the high-x region of the parton phase space that is of great importance for PDF fitting, as it is to-date poorly constrained by data and subject to non-perturbative effects with large uncertainties from phenomenological models. The TEVATRON $W^{\pm}$ asymmetry data is not subject to such uncertainties, however the results from CDF and DØ experiments are in tension (CDF Collaboration, 2009a; DØ Collaboration, 2015). The production of W/Z + jets at the LHC provides a new and independent data set that can be used as input to PDF fits to access partons at high x. Given the ATLAS and CMS tension on the strange-quark PDF, it is therefore of particular interest to check the impact of the new W + jet data on the strange-quark density. Figure 67 shows the results of the PDF analysis of the ATLAS measurement of the W boson p_{T} spectrum (ATLAS Collaboration, 2018a) in W + jet events at a center-of-mass energy of 8 TeV, as shown in Fig. 39, fitted together with ATLAS inclusive W and Z production measurements at 7 TeV and HERA deep-inelastic scattering data. The PDF fit is performed at NNLO in pQCD, and was made possible by recent theoretical developments providing NNLO predictions for such processes (Boughezal *et al.*, 2015b; Gehrmann-De Ridder *et al.*, 2016b). The fraction of the strange-quark density in the proton can be defined by the quantity $R_s = (s+\bar{s})/(\bar{u}+\bar{d})$, that is shown in Fig. 67. The effect of the W + jet data is most significant in the kinematic region $x > 0.02$, where the uncertainty is significantly lower and the fit results in the R_s distribution that falls from about 1 at $x \approx 0.01$ to about 0.3 at $x \approx 0.1$. At low x, i.e. $x < 0.023$, the fit with the W + jet data is compatible with the unsuppressed strange-quark density found in previous ATLAS analyses with different data sets.

Further measurements at the LHC with even greater precision, including W/Z + jets, aided by the completion of the NNLO $W + c$ calculation, will help to understand this apparent tension between different experimental data sets in the determination of the strange-quark content of the proton.

VI. CONCLUSIONS AND OUTLOOK

This article has reviewed achievements in the understanding of the production of vector bosons in association with light- or heavy-flavor jets, with a focus on the LHC results. These processes are of great importance for the success of physics programs at hadron colliders since they are major backgrounds to new physics searches and are ideal testing grounds for new calculations and models in the QCD and electroweak sectors of the Standard Model. This review has summarized theoretical techniques developed to describe experimental results in $p\bar{p}$ collisions at the TEVATRON and in pp collisions at the LHC, and has highlighted a few of the several measurements that were carried out by the CDF and DØ collaborations at the TEVATRON as well as the ATLAS, CMS and LHCb collaborations at the LHC at different center-or-mass energies. Detailed comparisons between the experimental results and cutting-edge predictions have been presented together with discussions of differences in phase spaces and production mechanisms between the TEVATRON and the

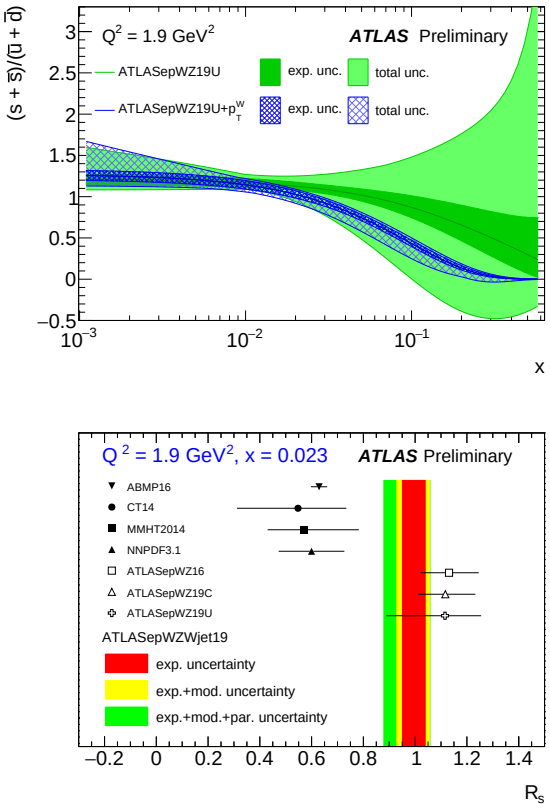

Figure 67 The R_s distribution, evaluated at Q^2 = 1.9 GeV^2, as determined from a fit that includes W + jet data as a function of W p_{T}, in comparison to a similar fit without W + jet data as input (top). The R_s ratio evaluated at x = 0.023 and Q^2 = 1.9 GeV^2, for the ATLAS PDF set that includes the W + jet data as input, in comparison to other PDF sets (bottom). Figures taken from (ATLAS Collaboration, 2019e).

LHC.

The modeling of V + jet processes improved significantly at the TEVATRON, and measurements of such processes have prompted the development of high-order QCD calculations and new techniques for their modeling in MC generators. TEVATRON data sets were used to tune theoretical predictions and MC generators, and those tunes turned out to be also accurate at describing the first V + jet data results at the LHC Run-1, despite the large difference in center-of-mass energies. TEVATRON data still provides an important legacy for V + jet analyses at the LHC. The measurements carried out by the LHC experimental collaborations, thanks to the greater statistics in V + jet samples, have urged further developments in the theoretical description of such processes both in the QCD and the electroweak sectors. These processes have been at the center of both the so-called next-to-leading and next-to-next-to-leading order revolutions in perturbative QCD calculations and their implementations in MC generators.

In several kinematic regions the experimental uncertainties are significantly smaller than the uncertainties in the predictions. Such a high experimental precision has allowed to test and constrain theoretical predictions and models, including parton density functions, in a broad kinematic region, including extreme regions of phase space, that are relevant for new physics searches.

Despite the great theoretical progress in the past decades and the many years in understanding of the V + jet production mechanism there are still theory uncertainties that can be further reduced in future developments, for example higher order QCD and electroweak contributions in hard scattering matrix elements, parton-showers and their matching algorithms, or be better constrained by data like PDFs and underlying event modeling. Improvements in the understanding of these sources of uncertainties in V + jet processes are critical for improvements in the precision of measurements and in the reach of searches at the LHC and at future collider experiments.

a. Outlook

Studies of V + jet physics will necessarily continue in future LHC runs and at possible future colliders, as the success of the physics programs of such experiments will critically rely on the good understanding of such processes. The higher and higher expected statistics, precision and extended phase space, e.g., to higher jet multiplicities or higher energy scales, will challenge theoretical predictions to perform calculations at higher orders in QCD, i.e., at N^{3}LO,[9] to systematically include higher-order electroweak corrections in MC generators together with mixed electroweak-QCD terms and to improve MC generators for more accurate estimation of the various sources of uncertainties in the modeling.

Studies of the QCD production of V + jets will remain critical for the understanding of QCD dynamics as well as for a better understanding of electroweak corrections, as they will become more significant at higher energy scales. Experimental analyses are expected to become more sophisticated in studying statistical and systematic correlations between differential cross

[9] A first result for lepton pair production via virtual photon exchange has been presented in (Duhr *et al.*, 2020a,b).

sections in the same and in different V + jet processes, such that several observables can be used simultaneously as inputs to PDF global fits, MC tunes, and indirect searches for new physics. With more accurate and precise theoretical predictions new measurements will become interesting, for example the extraction of the strong coupling α_s from jet rates in V + jet events.[10]

It is expected that electroweak analyses will become predominant in the future to search for anomalies in the gauge structure of the Standard Model. A good understanding of vector boson fusion production of V+jets is important for studies of Higgs production, and for a thorough investigation of anomalies in the gauge couplings a comprehensive and simultaneous analysis of several electroweak processes will be beneficial. An example of an electroweak process that has not been investigated due to experimental challenges is the eletroweak production of two jets in association with a photon. This process will provide a new window in the studies of anomalous couplings. Developments in the separation of jets induced by quarks or gluons may have a significant impact in the discrimination of electroweak V+jet processes from QCD-induced background in future analyses, and may impact the constraints on quark and gluon PDFs. At higher center-of-mass energies the study of the emission of massive vector bosons collinearly with jets in W/Z+jets will become more important and the development and testing of electroweak showering models more relevant than it has been so far.

As experimental results become more precise, preservation and sharing of analysis details are more important. Future studies are expected to include multiple differential cross section measurements and such a large amount of experimental results will be a wealth for the understanding of the SM and beyond SM physics. The analysis algorithms as well as the experimental results must be preserved for current and future generations. The LHC experimental data with their uncertainties are stored in the HEPDATA repository (Maguire *et al.*, 2017), which has become an essential tool for archiving detailed experimental results, for comparisons against MC predictions, and for tuning and constraining of theoretical models, e.g., underlying event and PDFs. In recent years the RIVET project (Robust Independent Validation of Experiment and Theory) (Bierlich *et al.*, 2020; Buckley *et al.*, 2013) has been asserted as *the* repository for analysis algorithms (a combination of fiducial phase space definitions and physics objects). This project was originally intended as a toolkit for validation of MC event generators, however, thanks to its large (and ever growing) set of experimental analyses and its link to the HEPDATA repository for experimental data points from the collider experiments, it has become very useful also as a long term repository of analysis algorithms. RIVET also provides useful algorithms to extract observable quantities from different MC generators in a model independent way, i.e., without prior knowledge of specific algorithm implementations or specific event record definitions. Such repositories and analysis tools will become more critical in multi-process fits, e.g., PDF, EFT, including for storing information about correlations between measurements.

[10] A precursor to this has been presented in (Johnson and Maître, 2018).

ACKNOWLEDGMENTS

The work of Alessandro Tricoli is supported by the U.S.A. Department of Energy under grant contact DE-SC0012704. Marek Schönherr is funded by the Royal Society through a University Research Fellowship and acknowledges support from the European Unions Horizon 2020 research and innovation programme as part of the Marie Sklodowska-Curie Innovative Training Network MCnetITN3 (grant agreement no. 722104).

REFERENCES

Aaij, R, *et al.* (2019), "A comprehensive real-time analysis model at the LHCb experiment," JINST **14** (04), P04006, arXiv:1903.01360 [hep-ex].

Actis, S, A. Denner, L. Hofer, A. Scharf, and S. Uccirati (2013), "Recursive generation of one-loop amplitudes in the Standard Model," JHEP **04**, 037, arXiv:1211.6316 [hep-ph].

Alcaraz Maestre, J, *et al.* (SM and NLO MULTILEG Working Group, SM MC Working Group) (2012), "The SM and NLO Multileg and SM MC Working Groups: Summary Report," in *Proceedings, 7th Les Houches Workshop on Physics at TeV Colliders: Les Houches, France, May 30-June 17, 2011*, pp. 1–220, arXiv:1203.6803 [hep-ph].

Alioli, Simone, Christian W. Bauer, Calvin Berggren, Frank J. Tackmann, and Jonathan R. Walsh (2015), "Drell-Yan production at NNLL′+NNLO matched to parton showers," Phys. Rev. D **92** (9), 094020, arXiv:1508.01475 [hep-ph].

Alioli, Simone, Paolo Nason, Carlo Oleari, and Emanuele Re (2008), "NLO vector-boson pro-

duction matched with shower in POWHEG," JHEP **07**, 060, arXiv:0805.4802 [hep-ph].
Alioli, Simone, Paolo Nason, Carlo Oleari, and Emanuele Re (2011), "Vector boson plus one jet production in POWHEG," JHEP **01**, 095, arXiv:1009.5594 [hep-ph].
Altarelli, Guido, R. Keith Ellis, and G. Martinelli (1979), "Large Perturbative Corrections to the Drell-Yan Process in QCD," Nucl. Phys. B **157**, 461–497.
Alwall, J, R. Frederix, S. Frixione, V. Hirschi, F. Maltoni, O. Mattelaer, H. S. Shao, T. Stelzer, P. Torrielli, and M. Zaro (2014), "The automated computation of tree-level and next-to-leading order differential cross sections, and their matching to parton shower simulations," JHEP **07**, 079, arXiv:1405.0301 [hep-ph].
Alwall, Johan, *et al.* (2008), "Comparative study of various algorithms for the merging of parton showers and matrix elements in hadronic collisions," Eur. Phys. J. C **53**, 473–500, arXiv:0706.2569 [hep-ph].
Anastasiou, Charalampos, Lance J. Dixon, Kirill Melnikov, and Frank Petriello (2004), "High precision QCD at hadron colliders: Electroweak gauge boson rapidity distributions at NNLO," Phys. Rev. D **69**, 094008, arXiv:hep-ph/0312266 [hep-ph].
Andersson, Bo, G. Gustafson, G. Ingelman, and T. Sjöstrand (1983), "Parton Fragmentation and String Dynamics," Phys. Rept. **97**, 31–145.
Appel, J A, *et al.* (1986), "Measurement of $W^{\pm}$ and Z^0 properties at the CERN $\bar{p}p$ collider," Z. Phys. C **30** (1), 1–22.
Arnison, G, *et al.* (1983a), "Experimental observation of isolated large transverse energy electrons with associated missing energy at s=540 GeV," Phys. Lett. B **122** (1), 103 – 116.
Arnison, G, *et al.* (1983b), "Experimental observation of lepton pairs of invariant mass around 95 GeV/c^2 at the CERN SPS collider," Phys. Lett. B **126** (5), 398 – 410.
Arnison, G, *et al.* (1983c), "Further Evidence for Charged Intermediate Vector Bosons at the SPS Collider," Phys. Lett. B **129** (3), 273–282.
Arnison, G, *et al.* (1984a), "Observation of muonic Z^0-decay at the $\bar{p}p$ collider," Phys. Lett. B **147** (1), 241 – 248.
Arnison, G, *et al.* (1984b), "Observation of the muonic decay of the charged intermediate vector boson," Phys. Lett. B **134** (6), 469 – 476.
ATLAS Collaboration, (2011a), "Measurement of the inclusive isolated prompt photon cross-section in pp collisions at $\sqrt{s} = 7$ TeV using 35 pb^{-1} of ATLAS data," Phys. Lett. B **706**, 150–167, arXiv:1108.0253 [hep-ex].
ATLAS Collaboration, (2011b), "Measurement of the inclusive isolated prompt photon cross section in pp collisions at $\sqrt{s} = 7$ TeV with the ATLAS detector," Phys. Rev. D **83**, 052005, arXiv:1012.4389 [hep-ex].
ATLAS Collaboration, (2011c), "Measurement of the production cross section for W-bosons in association with jets in pp collisions at $\sqrt{s} = 7$ TeV with the ATLAS detector," Phys. Lett. B **698**, 325–345, arXiv:1012.5382 [hep-ex].
ATLAS Collaboration, (2012a), "Determination of the strange quark density of the proton from ATLAS measurements of the $W \to \ell\nu$ and $Z \to \ell\ell$ cross sections," Phys. Rev. Lett. **109**, 012001, arXiv:1203.4051 [hep-ex].
ATLAS Collaboration, (2012b), "Measurement of the cross-section for b-jets produced in association with a Z boson at $\sqrt{s} = 7$ TeV with the ATLAS detector," Phys. Lett. B **706**, 295–313, arXiv:1109.1403 [hep-ex].
ATLAS Collaboration, (2012c), "Measurement of the cross section for the production of a W boson in association with b-jets in pp collisions at $\sqrt{s} =$ 7 TeV with the ATLAS detector," Phys. Lett. B **707**, 418, arXiv:1109.1470 [hep-ex].
ATLAS Collaboration, (2012d), "Measurement of the inclusive $W^{\pm}$ and Z/γ^* cross sections in the e and μ decay channels in pp collisions at $\sqrt{s} =$ 7 TeV with the ATLAS detector," Phys. Rev. D **85**, 072004, arXiv:1109.5141 [hep-ex].
ATLAS Collaboration, (2012e), "Measurement of the polarisation of W bosons produced with large transverse momentum in pp collisions at $\sqrt{s} = 7$ TeV with the ATLAS experiment," Eur. Phys. J. C **72** (5), 2001, arXiv:1203.2165 [hep-ex].
ATLAS Collaboration, (2012f), "Measurement of the production cross section for Z/γ^* in association with jets in pp collisions at $\sqrt{s} = 7$ TeV with the ATLAS detector," Phys. Rev. D **85**, 032009, arXiv:1111.2690 [hep-ex].
ATLAS Collaboration, (2012g), "Measurement of the production cross section of an isolated photon associated with jets in proton-proton collisions at $\sqrt{s} = 7$ TeV with the ATLAS detector," Phys. Rev. D **85**, 092014, arXiv:1203.3161 [hep-ex].
ATLAS Collaboration, (2012h), "Study of jets produced in association with a W boson in pp collisions at $\sqrt{s} = 7$ TeV with the ATLAS detector," Phys. Rev. D **85**, 092002, arXiv:1201.1276 [hep-ex].
ATLAS Collaboration, (2013a), "Dynamics of isolated-photon plus jet production in pp collisions at $\sqrt{s} = 7$ TeV with the ATLAS detector," Nucl. Phys. B **875**, 483–535, arXiv:1307.6795 [hep-ex].
ATLAS Collaboration, (2013b), "Measurement of hard double-parton interactions in $W(\to l\nu)+$ 2 jet events at $\sqrt{s} = 7$ TeV with the ATLAS detector," New J. Phys. **15**, 033038, arXiv:1301.6872 [hep-ex].
ATLAS Collaboration, (2013c), "Measurement of k_t splitting scales in $W \to \ell\nu$ events at $\sqrt{s} = 7$ TeV with the ATLAS detector," Eur. Phys. J. C **73** (5), 2432, arXiv:1302.1415 [hep-ex].
ATLAS Collaboration, (2013d), "Measurement of the cross-section for W boson production in association with b-jets in pp collisions at $\sqrt{s} = 7$ TeV with the ATLAS detector," JHEP **06**, 084, arXiv:1302.2929 [hep-ex].
ATLAS Collaboration, (2013e), "Measurement of the production cross section of jets in association with a Z boson in pp collisions at $\sqrt{s} = 7$ TeV with the ATLAS detector," JHEP **07**, 032, arXiv:1304.7098 [hep-ex].
ATLAS Collaboration, (2014a), "A measurement of

the ratio of the production cross sections for W and Z bosons in association with jets with the ATLAS detector," Eur. Phys. J. C **74** (12), 3168, arXiv:1408.6510 [hep-ex].

ATLAS Collaboration, (2014b), "Measurement of differential production cross-sections for a Z boson in association with b-jets in 7 TeV proton-proton collisions with the ATLAS detector," JHEP **10**, 141, arXiv:1407.3643 [hep-ex].

ATLAS Collaboration, (2014c), "Measurement of the electroweak production of dijets in association with a Z boson and distributions sensitive to vector boson fusion in proton-proton collisions at $\sqrt{s} = 8$ TeV using the ATLAS detector," JHEP **04**, 031, arXiv:1401.7610 [hep-ex].

ATLAS Collaboration, (2014d), "Measurement of the inclusive isolated prompt photons cross section in pp collisions at $\sqrt{s} = 7$ TeV with the ATLAS detector using 4.6 fb^{-1}," Phys. Rev. D **89** (5), 052004, arXiv:1311.1440 [hep-ex].

ATLAS Collaboration, (2014e), "Measurement of the production of a W boson in association with a charm quark in pp collisions at $\sqrt{s} = 7$ TeV with the ATLAS detector," JHEP **05**, 068, arXiv:1402.6263 [hep-ex].

ATLAS Collaboration, (2014f), "Measurement of the Z/γ^* boson transverse momentum distribution in pp collisions at $\sqrt{s} = 7$ TeV with the ATLAS detector," JHEP **2014** (9), 145, arXiv:1406.3660 [hep-ex].

ATLAS Collaboration, (2014g), "Search for pair-produced third-generation squarks decaying via charm quarks or in compressed supersymmetric scenarios in pp collisions at $\sqrt{s} = 8$ TeV with the ATLAS detector," Phys. Rev. D **90** (5), 052008, arXiv:1407.0608 [hep-ex].

ATLAS Collaboration, (2014h), "Search for strong production of supersymmetric particles in final states with missing transverse momentum and at least three b-jets at $\sqrt{s} = 8$ TeV proton-proton collisions with the ATLAS detector," JHEP **2014** (10), 24, arXiv:1407.0600 [hep-ex].

ATLAS Collaboration, (2015a), "Measurement of the forward-backward asymmetry of electron and muon pair-production in pp collisions at $\sqrt{s} = 7$ TeV with the ATLAS detector," JHEP **09**, 049, arXiv:1503.03709 [hep-ex].

ATLAS Collaboration, (2015b), "Measurements of the W production cross sections in association with jets with the ATLAS detector," Eur. Phys. J. C **75** (2), 82, arXiv:1409.8639 [hep-ex].

ATLAS Collaboration, (2015c), *Proposal for truth particle observable definitions in physics measurements*, Tech. Rep. ATL-PHYS-PUB-2015-013 (CERN, Geneva).

ATLAS Collaboration, (2016a), "Measurement of event-shape observables in $Z \to \ell^+\ell^-$ events in pp collisions at $\sqrt{s} = 7$ TeV with the ATLAS detector at the LHC," Eur. Phys. J. C **76** (7), 375, arXiv:1602.08980 [hep-ex].

ATLAS Collaboration, (2016b), "Measurement of the angular coefficients in Z-boson events using electron and muon pairs from data taken at $\sqrt{s} =$ 8 TeV with the ATLAS detector," JHEP **08**, 159, arXiv:1606.00689 [hep-ex].

ATLAS Collaboration, (2016c), "Measurement of the inclusive isolated prompt photon cross section in pp collisions at $\sqrt{s} = 8$ TeV with the ATLAS detector," JHEP **08**, 005, arXiv:1605.03495 [hep-ex].

ATLAS Collaboration, (2016d), *Monte Carlo Generators for the Production of a W or Z/γ^* Boson in Association with Jets at ATLAS in Run 2*, Tech. Rep. ATL-PHYS-PUB-2016-003 (CERN, Geneva).

ATLAS Collaboration, (2016e), "Muon reconstruction performance of the ATLAS detector in proton–proton collision data at $\sqrt{s} = 13$ TeV," Eur. Phys. J. C **76** (5), 292, arXiv:1603.05598 [hep-ex].

ATLAS Collaboration, (2016f), "Performance of b-jet identification in the ATLAS Experiment," JINST **11** (04), P04008, arXiv:1512.01094 [hep-ex].

ATLAS Collaboration, (2016g), "Performance of pile-up mitigation techniques for jets in pp collisions at $\sqrt{s} = 8$ TeV using the ATLAS detector," Eur. Phys. J. C **76** (11), 581, arXiv:1510.03823 [hep-ex].

ATLAS Collaboration, (2016h), "Search for invisible decays of a Higgs boson using vector-boson fusion in pp collisions at $\sqrt{s} = 8$ TeV with the ATLAS detector," JHEP **01**, 172, arXiv:1508.07869 [hep-ex].

ATLAS Collaboration, (2016i), *Validation of Monte Carlo event generators in the ATLAS Collaboration for LHC Run 2*, Tech. Rep. ATL-PHYS-PUB-2016-001 (CERN, Geneva).

ATLAS Collaboration, (2017a), *ATLAS simulation of boson plus jets processes in Run 2*, Tech. Rep. ATL-PHYS-PUB-2017-006 (CERN, Geneva).

ATLAS Collaboration, (2017b), "High-E_{T} isolated-photon plus jets production in pp collisions at $\sqrt{s} = 8$ TeV with the ATLAS detector," Nucl. Phys. B **918**, 257–316, arXiv:1611.06586 [hep-ex].

ATLAS Collaboration, (2017c), "Measurement of the cross-section for electroweak production of dijets in association with a Z boson in pp collisions at $\sqrt{s} = 13$ TeV with the ATLAS detector," Phys. Lett. B **775**, 206, arXiv:1709.10264 [hep-ex].

ATLAS Collaboration, (2017d), "Measurement of the cross section for inclusive isolated-photon production in pp collisions at $\sqrt{s} = 13$ TeV using the ATLAS detector," Phys. Lett. B **770**, 473–493, arXiv:1701.06882 [hep-ex].

ATLAS Collaboration, (2017e), "Measurement of the k_{t} splitting scales in $Z \to \ell\ell$ events in pp collisions at $\sqrt{s} = 8$ TeV with the ATLAS detector," JHEP **08**, 026, arXiv:1704.01530 [hep-ex].

ATLAS Collaboration, (2017f), "Measurement of W boson angular distributions in events with high transverse momentum jets at $\sqrt{s} = 8$ TeV using the ATLAS detector," Phys. Lett. B **765**, 132–153, arXiv:1609.07045 [hep-ex].

ATLAS Collaboration, (2017g), "Measurements of electroweak Wjj production and constraints on anomalous gauge couplings with the ATLAS detector," Eur. Phys. J. C **77**, 474, arXiv:1703.04362 [hep-ex].

ATLAS Collaboration, (2017h), "Measurements of

the production cross section of a Z boson in association with jets in pp collisions at $\sqrt{s} = 13$ TeV with the ATLAS detector," Eur. Phys. J. C **77** (6), 361, arXiv:1702.05725 [hep-ex].

ATLAS Collaboration, (2017i), "Precision measurement and interpretation of inclusive W^+ , W^- and Z/γ^* production cross sections with the ATLAS detector," Eur. Phys. J. C **77** (6), 367, arXiv:1612.03016 [hep-ex].

ATLAS Collaboration, (2018a), "Measurement of differential cross sections and W^+/W^- cross-section ratios for W boson production in association with jets at $\sqrt{s} = 8$ TeV with the ATLAS detector," JHEP **05**, 077, arXiv:1711.03296 [hep-ex].

ATLAS Collaboration, (2018b), "Measurement of differential cross sections of isolated-photon plus heavy-flavour jet production in pp collisions at $\sqrt{s} = 8$ TeV using the ATLAS detector," Phys. Lett. B **776**, 295–317, arXiv:1710.09560 [hep-ex].

ATLAS Collaboration, (2018c), "Measurement of the cross section for isolated-photon plus jet production in pp collisions at $\sqrt{s} = 13$ TeV using the ATLAS detector," Phys. Lett. B **780**, 578–602, arXiv:1801.00112 [hep-ex].

ATLAS Collaboration, (2018d), *Measurement of the effective leptonic weak mixing angle using electron and muon pairs from Z-boson decay in the ATLAS experiment at $\sqrt{s} = 8$ TeV*, Tech. Rep. ATLAS-CONF-2018-037 (CERN, Geneva).

ATLAS Collaboration, (2018e), "Measurements of b-jet tagging efficiency with the ATLAS detector using $t\bar{t}$ events at $\sqrt{s} = 13$ TeV," JHEP **08**, 089, arXiv:1805.01845 [hep-ex].

ATLAS Collaboration, (2018f), "Observation of $H \to b\bar{b}$ decays and VH production with the ATLAS detector," Phys. Lett. B **786**, 59–86, arXiv:1808.08238 [hep-ex].

ATLAS Collaboration, (2018g), "Performance of missing transverse momentum reconstruction with the ATLAS detector using proton-proton collisions at $\sqrt{s} = 13$ TeV," Eur. Phys. J. C **78** (11), 903, arXiv:1802.08168 [hep-ex].

ATLAS Collaboration, (2019a), "Electron and photon performance measurements with the ATLAS detector using the 2015–2017 LHC proton-proton collision data," JINST **14** (12), P12006, arXiv:1908.00005 [hep-ex].

ATLAS Collaboration, (2019b), "Measurement of the inclusive cross-section for the production of jets in association with a Z boson in proton-proton collisions at 8 TeV using the ATLAS detector," Eur. Phys. J. C **79** (10), 847, arXiv:1907.06728 [hep-ex].

ATLAS Collaboration, (2019c), "Measurement of the inclusive isolated-photon cross section in pp collisions at $\sqrt{s} = 13$ TeV using 36 fb^{-1} of ATLAS data," JHEP **10**, 203, arXiv:1908.02746 [hep-ex].

ATLAS Collaboration, (2019d), "Measurement of the ratio of cross sections for inclusive isolated-photon production in pp collisions at $\sqrt{s} = 13$ and 8 TeV with the ATLAS detector," JHEP **04**, 093, arXiv:1901.10075 [hep-ex].

ATLAS Collaboration, (2019e), *QCD analysis of ATLAS $W^{\pm}$ boson production data in association with jets*, Tech. Rep. ATL-PHYS-PUB-2019-016 (CERN, Geneva).

ATLAS Collaboration, (2019f), *Standard Model Summary Plots Summer 2019*, Tech. Rep. ATL-PHYS-PUB-2019-024 (CERN, Geneva).

ATLAS Collaboration, (2020a), "Differential cross-section measurements for the electroweak production of dijets in association with a Z boson in proton-proton collisions at ATLAS," submitted to Eur. Phys. J. C 10.3204/PUBDB-2020-02663, arXiv:2006.15458 [hep-ex].

ATLAS Collaboration, (2020b), "Jet energy scale and resolution measured in proton-proton collisions at $\sqrt{s} = 13$ TeV with the ATLAS detector," Submitted to Eur. Phys. J. C 10.3204/PUBDB-2020-02665, arXiv:2007.02645 [hep-ex].

ATLAS Collaboration, (2020c), "Measurement of isolated-photon plus two-jet production in pp collisions at $\sqrt{s} = 13$ TeV with the ATLAS detector," JHEP **03**, 179, arXiv:1912.09866 [hep-ex].

ATLAS Collaboration, (2020d), "Measurements of the production cross-section for a Z boson in association with b-jets in proton-proton collisions at $\sqrt{s} = 13$ TeV with the ATLAS detector," JHEP **07**, 044, arXiv:2003.11960 [hep-ex].

ATLAS Collaboration, (2020e), "Performance of electron and photon triggers in ATLAS during LHC Run 2," Eur. Phys. J. C **80** (1), 47, arXiv:1909.00761 [hep-ex].

Aurenche, Patrick, Michel Fontannaz, Jean-Philippe Guillet, Eric Pilon, and Monique Werlen (2006), "A New critical study of photon production in hadronic collisions," Phys. Rev. D **73**, 094007, arXiv:hep-ph/0602133 [hep-ph].

Bacchetta, Alessandro, Valerio Bertone, Chiara Bissolotti, Giuseppe Bozzi, Filippo Delcarro, Fulvio Piacenza, and Marco Radici (2020), "Transverse-momentum-dependent parton distributions up to N^{3}LL from Drell-Yan data," JHEP **07**, 117, arXiv:1912.07550 [hep-ph].

Baglio, J, *et al.* (2014), "Release Note - VBFNLO 2.7.0. ," arXiv:1404.3940 [hep-ph].

Bagnaia, P, *et al.* (1983), "Evidence for $Z^0 \to e^+e^-$ at the CERN $\bar{p}p$ Collider," Phys. Lett. B **129** (1), 130 – 140.

Bagnaia, P, *et al.* (1984), "A study of high transverse momentum electrons produced in $\bar{p}p$ collisions at 540 GeV," Z. Phys. C **24** (1), 1–17.

Bähr, M, *et al.* (2008a), "Herwig++ physics and manual," Eur. Phys. J. C **58**, 639, arXiv:0803.0883 [hep-ph].

Bähr, Manuel, Stefan Gieseke, and Michael H. Seymour (2008b), "Simulation of multiple partonic interactions in Herwig++," JHEP **07**, 076, arXiv:0803.3633 [hep-ph].

Balazs, C, and C. P. Yuan (1997), "Soft gluon effects on lepton pairs at hadron colliders," Phys. Rev. D **56**, 5558–5583, arXiv:hep-ph/9704258 [hep-ph].

Ball, Richard D, Valerio Bertone, Marco Bonvini, Stefano Forte, Patrick Groth Merrild, Juan Rojo, and Luca Rottoli (2016), "Intrinsic charm in a matched general-mass scheme," Phys. Lett. B **754**, 49–58, arXiv:1510.00009 [hep-ph].

Banfi, A, S. Redford, M. Vesterinen, P. Waller, and T. R. Wyatt (2011a), "Optimisation of variables

for studying dilepton transverse momentum distributions at hadron colliders," Eur. Phys. J. C **71**, 1600, arXiv:1009.1580 [hep-ex].

Banfi, Andrea, Mrinal Dasgupta, and Simone Marzani (2011b), "QCD predictions for new variables to study dilepton transverse momenta at hadron colliders," Phys. Lett. B **701**, 75–81, arXiv:1102.3594 [hep-ph].

Banfi, Andrea, Pier Francesco Monni, Gavin P. Salam, and Giulia Zanderighi (2012), "Higgs and Z-boson production with a jet veto," Phys. Rev. Lett. **109**, 202001, arXiv:1206.4998 [hep-ph].

Banfi, Andrea, Gavin P. Salam, and Giulia Zanderighi (2006), "Infrared safe definition of jet flavor," Eur. Phys. J. C **47**, 113–124, arXiv:hep-ph/0601139.

Banner, M, *et al.* (1983), "Observation of single isolated electrons of high transverse momentum in events with missing transverse energy at the CERN $\bar{p}p$ collider," Phys. Lett. B **122** (5), 476 – 485.

Barberio, Elisabetta, Bob van Eijk, and Zbigniew Wąs (1991), "PHOTOS: A Universal Monte Carlo for QED radiative corrections in decays," Comput. Phys. Commun. **66**, 115–128.

Barzè, Luca, Guido Montagna, Paolo Nason, Oreste Nicrosini, and Fulvio Piccinini (2012), "Implementation of electroweak corrections in the POWHEG BOX: single W production," JHEP **04**, 037, arXiv:1202.0465 [hep-ph].

Barzè, Luca, Guido Montagna, Paolo Nason, Oreste Nicrosini, Fulvio Piccinini, and Alessandro Vicini (2013), "Neutral current Drell-Yan with combined QCD and electroweak corrections in the POWHEG BOX," Eur. Phys. J. C **73** (6), 2474, arXiv:1302.4606 [hep-ph].

Becher, Thomas, and Matthias Neubert (2011), "Drell-Yan Production at Small q_T, Transverse Parton Distributions and the Collinear Anomaly," Eur. Phys. J. C **71**, 1665, arXiv:1007.4005 [hep-ph].

Bellm, Johannes, Stefan Gieseke, and Simon Plätzer (2018), "Merging NLO Multi-jet Calculations with Improved Unitarization," Eur. Phys. J. C **78** (3), 244, arXiv:1705.06700 [hep-ph].

Bellm, Johannes, *et al.* (2016), "Herwig 7.0/Herwig++ 3.0 release note," Eur. Phys. J. C **76** (4), 196, arXiv:1512.01178 [hep-ph].

Berends, Frits A, W.T. Giele, H. Kuijf, R. Kleiss, and W.James Stirling (1989), "Multi - Jet Production in W, Z Events at $p\bar{p}$ Colliders," Phys. Lett. B **224**, 237–242.

Berger, C F, Z. Bern, Lance J. Dixon, F. Febres Cordero, D. Forde, T. Gleisberg, H. Ita, D. A. Kosower, and D. Maître (2010), "Next-to-Leading Order QCD Predictions for Z, γ^* + 3-Jet Distributions at the Tevatron," Phys. Rev. D **82**, 074002, arXiv:1004.1659 [hep-ph].

Berger, C F, Z. Bern, Lance J. Dixon, F. Febres Cordero, D. Forde, T. Gleisberg, H. Ita, D. A. Kosower, and D. Maître (2011), "Precise Predictions for W + 4 Jet Production at the Large Hadron Collider," Phys. Rev. Lett. **106**, 092001, arXiv:1009.2338 [hep-ph].

Berger, C F, Z. Bern, Lance J. Dixon, Fernando Febres Cordero, D. Forde, T. Gleisberg, H. Ita, D. A. Kosower, and D. Maître (2009), "Precise Predictions for W + 3 Jet Production at Hadron Colliders," Phys. Rev. Lett. **102**, 222001, arXiv:0902.2760 [hep-ph].

Berger, CF, Z. Bern, L.J. Dixon, F. Febres Cordero, D. Forde, H. Ita, D.A. Kosower, and D. Maître (2008), "An Automated Implementation of On-Shell Methods for One-Loop Amplitudes," Phys. Rev. D **78**, 036003, arXiv:0803.4180 [hep-ph].

Bermudez Martinez, A, *et al.* (2019), "Production of Z-bosons in the parton branching method," Phys. Rev. D **100** (7), 074027, arXiv:1906.00919 [hep-ph].

Bern, Z, G. Diana, L. J. Dixon, F. Febres Cordero, S. Höche, H. Ita, D. A. Kosower, D. Maître, and K. J. Ozeren (2011), "Driving Missing Data at Next-to-Leading Order," Phys. Rev. D **84**, 114002, arXiv:1106.1423 [hep-ph].

Bern, Z, L. J. Dixon, F. Febres Cordero, S. Höche, H. Ita, D. A. Kosower, D. Maître, and K. J. Ozeren (2013), "Next-to-Leading Order W + 5-Jet Production at the LHC," Phys. Rev. D **88** (1), 014025, arXiv:1304.1253 [hep-ph].

Bernaciak, C, and D. Wackeroth (2012), "Combining NLO QCD and Electroweak Radiative Corrections to W boson Production at Hadron Colliders in the POWHEG Framework," Phys. Rev. D **85**, 093003, arXiv:1201.4804 [hep-ph].

Bertone, Valerio, Stefano Carrazza, and Juan Rojo (2015), "Doped Parton Distributions," in *27th Rencontres de Blois on Particle Physics and Cosmology*, arXiv:1509.04022 [hep-ph].

Bierlich, Christian, *et al.* (2020), "Robust Independent Validation of Experiment and Theory: Rivet version 3," SciPost Phys. **8**, 026, arXiv:1912.05451 [hep-ph].

Binoth, T, *et al.* (SM and NLO Multileg Working Group) (2010), "The SM and NLO Multileg Working Group: Summary report," in *Physics at TeV colliders. Proceedings, 6th Workshop, dedicated to Thomas Binoth, Les Houches, France, June 8-26, 2009*, pp. 21–189, arXiv:1003.1241 [hep-ph].

Bizoń, Wojciech, Xuan Chen, Aude Gehrmann-De Ridder, Thomas Gehrmann, Nigel Glover, Alexander Huss, Pier Francesco Monni, Emanuele Re, Luca Rottoli, and Paolo Torrielli (2018), "Fiducial distributions in Higgs and Drell-Yan production at N^{3}LL+NNLO," JHEP **12**, 132, arXiv:1805.05916 [hep-ph].

Bizoń, Wojciech, Aude Gehrmann-De Ridder, Thomas Gehrmann, Nigel Glover, Alexander Huss, Pier Francesco Monni, Emanuele Re, Luca Rottoli, and Duncan M. Walker (2019), "The transverse momentum spectrum of weak gauge bosons at N^{3}LL + NNLO," Eur. Phys. J. C **79** (10), 868, arXiv:1905.05171 [hep-ph].

Blazey, Gerald C, *et al.* (2000), "Run II jet physics," in *Physics at Run II: QCD and Weak Boson Physics Workshop: Final General Meeting*, pp. 47–77, arXiv:hep-ex/0005012.

Bloch, F, and A. Nordsieck (1937), "Note on the Radiation Field of the electron," Phys. Rev. **52**, 54–59.

Bothmann, Enrico, *et al.* (2019), "Event Genera-

tion with SHERPA 2.2," SciPost Phys. **7**, 34, arXiv:1905.09127 [hep-ph].

Boughezal, Radja, John M. Campbell, R. Keith Ellis, Christfried Focke, Walter T. Giele, Xiaohui Liu, and Frank Petriello (2016a), "Z-boson production in association with a jet at next-to-next-to-leading order in perturbative QCD," Phys. Rev. Lett. **116** (15), 152001, arXiv:1512.01291 [hep-ph].

Boughezal, Radja, Christfried Focke, Walter Giele, Xiaohui Liu, and Frank Petriello (2015a), "Higgs boson production in association with a jet at NNLO using jettiness subtraction," Phys. Lett. B **748**, 5–8, arXiv:1505.03893 [hep-ph].

Boughezal, Radja, Christfried Focke, Xiaohui Liu, and Frank Petriello (2015b), "W-boson production in association with a jet at next-to-next-to-leading order in perturbative QCD," Phys. Rev. Lett. **115** (6), 062002, arXiv:1504.02131 [hep-ph].

Boughezal, Radja, Xiaohui Liu, and Frank Petriello (2016b), "Phenomenology of the Z-boson plus jet process at NNLO," Phys. Rev. D **94** (7), 074015, arXiv:1602.08140 [hep-ph].

Boughezal, Radja, Xiaohui Liu, and Frank Petriello (2016c), "W-boson plus jet differential distributions at NNLO in QCD," Phys. Rev. D **94** (11), 113009, arXiv:1602.06965 [hep-ph].

Bozzi, Giuseppe, Stefano Catani, Giancarlo Ferrera, Daniel de Florian, and Massimiliano Grazzini (2011), "Production of Drell-Yan lepton pairs in hadron collisions: Transverse-momentum resummation at next-to-next-to-leading logarithmic accuracy," Phys. Lett. B **696**, 207–213, arXiv:1007.2351 [hep-ph].

Buckley, Andy, Jonathan Butterworth, Leif Lonnblad, David Grellscheid, Hendrik Hoeth, James Monk, Holger Schulz, and Frank Siegert (2013), "Rivet user manual," Comput. Phys. Commun. **184**, 2803–2819, arXiv:1003.0694 [hep-ph].

Butterworth, J M, Jeffrey R. Forshaw, and M. H. Seymour (1996), "Multiparton interactions in photoproduction at HERA," Z. Phys. C **72**, 637–646, arXiv:hep-ph/9601371 [hep-ph].

Cacciari, Matteo, Mario Greco, and Paolo Nason (1998), "The p_T spectrum in heavy flavor hadroproduction," JHEP **05**, 007, arXiv:hep-ph/9803400 [hep-ph].

Cacciari, Matteo, and Gavin P. Salam (2008), "Pileup subtraction using jet areas," Phys. Lett. B **659**, 119–126, arXiv:0707.1378 [hep-ph].

Cacciari, Matteo, Gavin P. Salam, and Gregory Soyez (2008), "The anti-k_t jet clustering algorithm," JHEP **04**, 063, arXiv:0802.1189 [hep-ph].

Campbell, J M, F. Caola, F. Febres Cordero, L. Reina, and D. Wackeroth (2012), "NLO QCD predictions for $W+1$ jet and $W+2$ jet production with at least one b jet at the 7 TeV LHC," Phys. Rev. D **86**, 034021, arXiv:1107.3714 [hep-ph].

Campbell, John M, and R. Keith Ellis (2002), "Next-to-Leading Order Corrections to $W+2$ jet and $Z+2$ Jet Production at Hadron Colliders," Phys. Rev. D **65**, 113007, arXiv:hep-ph/0202176 [hep-ph].

Campbell, John M, R. Keith Ellis, F. Febres Cordero, F. Maltoni, L. Reina, D. Wackeroth, and S. Willenbrock (2009), "Associated Production of a W Boson and One b Jet," Phys. Rev. D **79**, 034023, arXiv:0809.3003 [hep-ph].

Campbell, John M, R. Keith Ellis, F. Maltoni, and S. Willenbrock (2004), "Associated production of a Z Boson and a single heavy quark jet," Phys. Rev. D **69**, 074021, arXiv:hep-ph/0312024 [hep-ph].

Campbell, John M, R. Keith Ellis, F. Maltoni, and S. Willenbrock (2006), "Production of a Z boson and two jets with one heavy-quark tag," Phys. Rev. D **73**, 054007, [Erratum: Phys. Rev.D77,019903(2008)], arXiv:hep-ph/0510362 [hep-ph].

Campbell, John M, R. Keith Ellis, F. Maltoni, and S. Willenbrock (2007), "Production of a W boson and two jets with one b-quark tag," Phys. Rev. D **75**, 054015, arXiv:hep-ph/0611348 [hep-ph].

Campbell, John M, R. Keith Ellis, Paolo Nason, and Giulia Zanderighi (2013), "W and Z Bosons in Association with Two Jets Using the POWHEG Method," JHEP **08**, 005, arXiv:1303.5447 [hep-ph].

Campbell, John M, R. Keith Ellis, and Ciaran Williams (2017a), "Direct Photon Production at Next-to–Next-to-Leading Order," Phys. Rev. Lett. **118** (22), 222001, [Erratum: Phys.Rev.Lett. 124, 259901 (2020)], arXiv:1612.04333 [hep-ph].

Campbell, John M, R. Keith Ellis, and Ciaran Williams (2017b), "Driving missing data at the LHC: NNLO predictions for the ratio of $\gamma + j$ and $Z + j$," Phys. Rev. D **96** (1), 014037, arXiv:1703.10109 [hep-ph].

Campbell, John M, and R.K. Ellis (2010), "MCFM for the Tevatron and the LHC," Nucl. Phys. B Proc. Suppl. **205-206**, 10–15, arXiv:1007.3492 [hep-ph].

Campbell, John M, Juan Rojo, Emma Slade, and Ciaran Williams (2018), "Direct photon production and PDF fits reloaded," Eur. Phys. J. C **78** (6), 470, arXiv:1802.03021 [hep-ph].

Catani, S, Yuri L. Dokshitzer, M.H. Seymour, and B.R. Webber (1993), "Longitudinally invariant K_t clustering algorithms for hadron hadron collisions," Nucl. Phys. B **406**, 187–224.

Catani, S, M. Fontannaz, J.P. Guillet, and E. Pilon (2002), "Cross-section of isolated prompt photons in hadron hadron collisions," JHEP **05**, 028, arXiv:hep-ph/0204023.

Catani, S, F. Krauss, R. Kuhn, and B. R. Webber (2001), "QCD matrix elements + parton showers," JHEP **11**, 063, arXiv:hep-ph/0109231 [hep-ph].

Catani, Stefano, Leandro Cieri, Giancarlo Ferrera, Daniel de Florian, and Massimiliano Grazzini (2009), "Vector boson production at hadron colliders: a fully exclusive QCD calculation at NNLO," Phys. Rev. Lett. **103**, 082001, arXiv:0903.2120 [hep-ph].

Catani, Stefano, Leandro Cieri, Daniel de Florian, Giancarlo Ferrera, and Massimiliano Grazzini (2014), "Universality of transverse-momentum resummation and hard factors at the NNLO,"

Nucl. Phys. B **881**, 414–443, arXiv:1311.1654 [hep-ph].
Catani, Stefano, Simone Devoto, Massimiliano Grazzini, Stefan Kallweit, Javier Mazzitelli, and Hayk Sargsyan (2019), "Top-quark pair hadroproduction at next-to-next-to-leading order in QCD," Phys. Rev. D **99** (5), 051501, arXiv:1901.04005 [hep-ph].
Catani, Stefano, and Massimiliano Grazzini (2007), "An NNLO subtraction formalism in hadron collisions and its application to Higgs boson production at the LHC," Phys. Rev. Lett. **98**, 222002, arXiv:hep-ph/0703012 [hep-ph].
CDF and D0 Collaborations, (2018), "Tevatron Run II combination of the effective leptonic electroweak mixing angle," Phys. Rev. D **97** (11), 112007, arXiv:1801.06283 [hep-ex].
CDF Collaboration, (2006), "Measurement of the b jet cross-section in events with a Z boson in $p\bar{p}$ collisions at $\sqrt{s} = 1.96$ TeV," Phys. Rev. D **74**, 032008, arXiv:hep-ex/0605099 [hep-ex].
CDF Collaboration, (2008a), "First measurement of the production of a W boson in association with a single charm quark in $p\bar{p}$ collisions at $\sqrt{s} = 1.96$ TeV," Phys. Rev. Lett. **100**, 091803, arXiv:0711.2901 [hep-ex].
CDF Collaboration, (2008b), "Measurement of inclusive jet cross-sections in $Z/\gamma^* \to e^+e^-$ + jets production in $p\bar{p}$ collisions at $\sqrt{s} = 1.96$-TeV," Phys. Rev. Lett. **100**, 102001, arXiv:0711.3717 [hep-ex].
CDF Collaboration, (2008c), "Measurement of the cross section for W-boson production in association with jets in $p\bar{p}$ collisions at $\sqrt{s} = 1.96$-TeV," Phys. Rev. D **77**, 011108, arXiv:0711.4044 [hep-ex].
CDF Collaboration, (2009a), "Direct Measurement of the W Production Charge Asymmetry in $p\bar{p}$ Collisions at $\sqrt{s} = 1.96$ TeV," Phys. Rev. Lett. **102**, 181801, arXiv:0901.2169 [hep-ex].
CDF Collaboration, (2009b), "Measurement of cross sections for b jet production in events with a Z boson in $\bar{p}p$ collisions at $\sqrt{s} = 1.96$ TeV," Phys. Rev. D **79**, 052008, arXiv:0812.4458 [hep-ex].
CDF Collaboration, (2010a), "A Study of the associated production of photons and b-quark jets in $\bar{p}p$ collisions at $\sqrt{s} = 1.96$ TeV," Phys. Rev. D **81**, 052006, arXiv:0912.3453 [hep-ex].
CDF Collaboration, (2010b), "First Measurement of the b-jet Cross Section in Events with a W Boson in $\bar{p}p$ Collisions at $\sqrt{s} = 1.96$ TeV," Phys. Rev. Lett. **104**, 131801, arXiv:0909.1505 [hep-ex].
CDF Collaboration, (2011), "First Measurement of the Angular Coefficients of Drell-Yan e^+e^- pairs in the Z Mass Region from $p\bar{p}$ Collisions at $\sqrt{s} = 1.96$ TeV," Phys. Rev. Lett. **106**, 241801, arXiv:1103.5699 [hep-ex].
CDF Collaboration, (2013a), "Indirect Measurement of $\sin^2\theta_W$ (M_W) Using e^+e^- Pairs in the Z-Boson Region with $p\bar{p}$ Collisions at a Center-of-Momentum Energy of 1.96 TeV," Phys. Rev. D **88** (7), 072002, [Erratum: Phys.Rev.D 88, 079905 (2013)], arXiv:1307.0770 [hep-ex].
CDF Collaboration, (2013b), "Measurement of the cross section for direct-photon production in association with a heavy quark in $p\bar{p}$ collisions at $\sqrt{s} = 1.96$ TeV," Phys. Rev. Lett. **111** (4), 042003, arXiv:1303.6136 [hep-ex].
CDF Collaboration, (2013c), "Observation of the production of a W boson in association with a single charm quark," Phys. Rev. Lett. **110**, 071801, arXiv:1209.1921 [hep-ex].
CDF Collaboration, (2015), "Measurement of Differential Production Cross Section for Z/γ^* Bosons in Association with Jets in $p\bar{p}$ Collisions at $\sqrt{s} = 1.96$ TeV," Phys. Rev. D **91** (1), 012002, arXiv:1409.4359 [hep-ex].
Chen, Xuan, Thomas Gehrmann, Nigel Glover, Marius Höfer, and Alexander Huss (2020), "Isolated photon and photon+jet production at NNLO QCD accuracy," JHEP **04**, 166, arXiv:1904.01044 [hep-ph].
Chiesa, Mauro, Nicolas Greiner, and Francesco Tramontano (2016), "Automation of electroweak corrections for LHC processes," J. Phys. G **43** (1), 013002, arXiv:1507.08579 [hep-ph].
Chiesa, Mauro, Guido Montagna, Luca Barzè, Mauro Moretti, Oreste Nicrosini, Fulvio Piccinini, and Francesco Tramontano (2013), "Electroweak Sudakov Corrections to New Physics Searches at the LHC," Phys. Rev. Lett. **111** (12), 121801, arXiv:1305.6837 [hep-ph].
Christiansen, Jesper Roy, and Torbjörn Sjöstrand (2014), "Weak Gauge Boson Radiation in Parton Showers," JHEP **04**, 115, arXiv:1401.5238 [hep-ph].
Cieri, Leandro, Giancarlo Ferrera, and German F. R. Sborlini (2018), "Combining QED and QCD transverse-momentum resummation for Z boson production at hadron colliders," JHEP **08**, 165, arXiv:1805.11948 [hep-ph].
CMS Collaboration, (2009), *Performance of Jet Reconstruction with Charged Tracks only*, Tech. Rep. CMS-PAS-JME-08-001 (CERN, Geneva).
CMS Collaboration, (2010), *Commissioning of TrackJets in pp Collisions at 7 TeV*, Tech. Rep. CMS-PAS-JME-10-006 (CERN, Geneva).
CMS Collaboration, (2011a), "Measurement of the Differential Cross Section for Isolated Prompt Photon Production in pp Collisions at 7 TeV," Phys. Rev. D **84**, 052011, arXiv:1108.2044 [hep-ex].
CMS Collaboration, (2011b), "Measurement of the Isolated Prompt Photon Production Cross Section in pp Collisions at $\sqrt{s} = 7$ TeV," Phys. Rev. Lett. **106**, 082001, arXiv:1012.0799 [hep-ex].
CMS Collaboration, (2011c), "Measurement of the Polarization of W Bosons with Large Transverse Momenta in W+Jets Events at the LHC," Phys. Rev. Lett. **107**, 021802, arXiv:1104.3829 [hep-ex].
CMS Collaboration, (2011d), "Measurement of the weak mixing angle with the Drell-Yan process in proton-proton collisions at the LHC," Phys. Rev. D **84**, 112002, arXiv:1110.2682 [hep-ex].
CMS Collaboration, (2012a), "Jet Production Rates in Association with W and Z Bosons in pp Collisions at $\sqrt{s} = 7$ TeV," JHEP **01**, 010, arXiv:1110.3226 [hep-ex].
CMS Collaboration, (2012b), "Measurement of the

Electron Charge Asymmetry in Inclusive W Production in pp Collisions at $\sqrt{s} = 7$ TeV," Phys. Rev. Lett. **109**, 111806, arXiv:1206.2598 [hep-ex].
CMS Collaboration, (2012c), "Measurement of the Z/γ^*+b-jet cross section in pp collisions at $\sqrt{s} = 7$ TeV," JHEP **06**, 126, arXiv:1204.1643 [hep-ex].
CMS Collaboration, (2012d), "Search for supersymmetry in hadronic final states using MT2 in pp collisions at $\sqrt{s} = 7$ TeV," JHEP **2012** (10), 18, arXiv:1207.1798 [hep-ex].
CMS Collaboration, (2013a), "Event Shapes and Azimuthal Correlations in Z + Jets Events in pp Collisions at $\sqrt{s} = 7$ TeV," Phys. Lett. B **722**, 238–261, arXiv:1301.1646 [hep-ex].
CMS Collaboration, (2013b), "Identification of b-quark jets with the CMS experiment," JINST **8**, P04013, arXiv:1211.4462 [hep-ex].
CMS Collaboration, (2013c), "Measurement of the Cross Section and Angular Correlations for Associated Production of a Z Boson with b Hadrons in pp Collisions at $\sqrt{s} = 7$ TeV," JHEP **12**, 039, arXiv:1310.1349 [hep-ex].
CMS Collaboration, (2013d), "Measurement of the hadronic activity in events with a Z and two jets and extraction of the cross section for the electroweak production of a Z with two jets in pp collisions at $\sqrt{s} = 7$ TeV," JHEP **10**, 062, arXiv:1305.7389 [hep-ex].
CMS Collaboration, (2013e), *Performance of quark/gluon discrimination in 8 TeV pp data*, Tech. Rep. CMS-PAS-JME-13-002 (CERN, Geneva).
CMS Collaboration, (2013f), "Rapidity distributions in exclusive Z + jet and γ + jet events in pp collisions at $\sqrt{s} = 7$ TeV," Phys. Rev. D **88** (11), 112009, arXiv:1310.3082 [hep-ex].
CMS Collaboration, (2014a), "Measurement of associated W+charm production in pp collisions at $\sqrt{s} = 7$ TeV," JHEP **02**, 013, arXiv:1310.1138 [hep-ex].
CMS Collaboration, (2014b), "Measurement of the muon charge asymmetry in inclusive $pp \to W + X$ production at $\sqrt{s} = 7$ TeV and an improved determination of light parton distribution functions," Phys. Rev. D **90**, 032004, arXiv:1312.6283 [hep-ex].
CMS Collaboration, (2014c), "Measurement of the production cross section for a W boson and two b jets in pp collisions at $\sqrt{s} = 7$ TeV," Phys. Lett. B **735**, 204–225, arXiv:1312.6608 [hep-ex].
CMS Collaboration, (2014d), "Measurement of the production cross sections for a Z boson and one or more b jets in pp collisions at $\sqrt{s} = 7$ TeV," JHEP **06**, 120, arXiv:1402.1521 [hep-ex].
CMS Collaboration, (2014e), "Measurement of the triple-differential cross section for photon+jets production in proton-proton collisions at $\sqrt{s} = 7$ TeV," JHEP **06**, 009, arXiv:1311.6141 [hep-ex].
CMS Collaboration, (2014f), "Study of double parton scattering using W + 2-jet events in proton-proton collisions at $\sqrt{s} = 7$ TeV," JHEP **03**, 032, arXiv:1312.5729 [hep-ex].
CMS Collaboration, (2015a), "Angular coefficients of Z bosons produced in pp collisions at $\sqrt{s} = 8$ TeV and decaying to $\mu^+\mu^-$ as a function of transverse momentum and rapidity," Phys. Lett. B **750**, 154–175, arXiv:1504.03512 [hep-ex].
CMS Collaboration, (2015b), "Comparison of the Z/γ^* + jets to γ + jets cross sections in pp collisions at $\sqrt{s} = 8$ TeV," JHEP **10**, 128, [Erratum: JHEP04,010(2016)], arXiv:1505.06520 [hep-ex].
CMS Collaboration, (2015c), "Differential cross section measurements for the production of a W boson in association with jets in proton–proton collisions at $\sqrt{s} = 7$ TeV," Phys. Lett. B **741**, 12–37, arXiv:1406.7533 [hep-ex].
CMS Collaboration, (2015d), "Measurement of electroweak production of two jets in association with a Z boson in proton-proton collisions at $\sqrt{s} = 8$ TeV," Eur. Phys. J. C **75**, 66, arXiv:1410.3153 [hep-ex].
CMS Collaboration, (2015e), "Measurements of jet multiplicity and differential production cross sections of Z+ jets events in proton-proton collisions at $\sqrt{s} = 7$ TeV," Phys. Rev. D **91** (5), 052008, arXiv:1408.3104 [hep-ex].
CMS Collaboration, (2015f), "Performance of Electron Reconstruction and Selection with the CMS Detector in Proton-Proton Collisions at $\sqrt{s} = 8$ TeV," JINST **10** (06), P06005, arXiv:1502.02701 [physics.ins-det].
CMS Collaboration, (2015g), "Performance of Photon Reconstruction and Identification with the CMS Detector in Proton-Proton Collisions at $\sqrt{s} = 8$ TeV," JINST **10** (08), P08010, arXiv:1502.02702 [physics.ins-det].
CMS Collaboration, (2016), "Measurement of electroweak production of a W boson and two forward jets in proton-proton collisions at $\sqrt{s} = 8$ TeV," JHEP **11**, 147, arXiv:1607.06975 [hep-ex].
CMS Collaboration, (2017a), *Jet algorithms performance in 13 TeV data*, Tech. Rep. CMS-PAS-JME-16-003 (CERN, Geneva).
CMS Collaboration, (2017b), "Jet energy scale and resolution in the CMS experiment in pp collisions at 8 TeV," JINST **12** (02), P02014, arXiv:1607.03663 [hep-ex].
CMS Collaboration, (2017c), "Measurement of the differential cross sections for the associated production of a W boson and jets in proton-proton collisions at $\sqrt{s} = 13$ TeV," Phys. Rev. D **96** (7), 072005, arXiv:1707.05979 [hep-ex].
CMS Collaboration, (2017d), "Measurement of the production cross section of a W boson in association with two b jets in pp collisions at $\sqrt{s} = 8$ TeV," Eur. Phys. J. C **77** (2), 92, arXiv:1608.07561 [hep-ex].
CMS Collaboration, (2017e), "Measurements of differential cross sections for associated production of a W boson and jets in proton-proton collisions at $\sqrt{s} = 8$ TeV," Phys. Rev. D **95**, 052002, arXiv:1610.04222 [hep-ex].
CMS Collaboration, (2017f), "Measurements of differential production cross sections for a Z boson in association with jets in pp collisions at $\sqrt{s} = 8$ TeV," JHEP **04**, 022, arXiv:1611.03844 [hep-ex].
CMS Collaboration, (2017g), "Measurements of the associated production of a Z boson and b jets in pp collisions at $\sqrt{s} = 8$ TeV," Eur. Phys. J. C **77** (11), 751, arXiv:1611.06507 [hep-ex].
CMS Collaboration, (2017h), "Particle-flow recon-

struction and global event description with the CMS detector," JINST **12** (10), P10003–P10003, arXiv:1706.04965 [physics.ins-det].
CMS Collaboration, (2017i), "Searches for invisible decays of the Higgs boson in pp collisions at $\sqrt{s}$ = 7, 8, and 13 TeV," JHEP **02**, 135, arXiv:1610.09218 [hep-ex].
CMS Collaboration, (2017j), "The CMS trigger system," JINST **12** (01), P01020, arXiv:1609.02366 [physics.ins-det].
CMS Collaboration, (2018a), "Electroweak production of two jets in association with a Z boson in proton-proton collisions at $\sqrt{s}$ = 13 TeV," Eur. Phys. J. C **78**, 589, arXiv:1712.09814 [hep-ex].
CMS Collaboration, (2018b), "Identification of heavy-flavour jets with the CMS detector in pp collisions at 13 TeV," JINST **13** (05), P05011, arXiv:1712.07158 [physics.ins-det].
CMS Collaboration, (2018c), "Measurement of associated Z + charm production in proton-proton collisions at $\sqrt{s}$ = 8 TeV," Eur. Phys. J. C **78** (4), 287, arXiv:1711.02143 [hep-ex].
CMS Collaboration, (2018d), "Measurement of differential cross sections for Z boson production in association with jets in proton-proton collisions at $\sqrt{s}$ = 13 TeV," Eur. Phys. J. C **78** (11), 965, arXiv:1804.05252 [hep-ex].
CMS Collaboration, (2018e), "Measurement of the weak mixing angle using the forward-backward asymmetry of Drell-Yan events in pp collisions at 8 TeV," Eur. Phys. J. C **78** (9), 701, arXiv:1806.00863 [hep-ex].
CMS Collaboration, (CMS) (2018f), "Observation of Higgs boson decay to bottom quarks," Phys. Rev. Lett. **121** (12), 121801, arXiv:1808.08242 [hep-ex].
CMS Collaboration, (2019a), "Displays of candidate VHcc events," .
CMS Collaboration, (2019b), "Measurement of associated production of a W boson and a charm quark in proton-proton collisions at $\sqrt{s}$ = 13 TeV," Eur. Phys. J. C **79** (3), 269, arXiv:1811.10021 [hep-ex].
CMS Collaboration, (2019c), "Measurement of differential cross sections for inclusive isolated-photon and photon+jet production in proton-proton collisions at $\sqrt{s}$ = 13 TeV," Eur. Phys. J. C **79** (1), 20, arXiv:1807.00782 [hep-ex].
CMS Collaboration, (2019d), "Measurements of triple-differential cross sections for inclusive isolated-photon+jet events in pp collisions at $\sqrt{s}$ = 8 TeV," Eur. Phys. J. C **79** (11), 969, arXiv:1907.08155 [hep-ex].
CMS Collaboration, (2019e), "Performance of missing transverse momentum reconstruction in proton-proton collisions at $\sqrt{s}$ = 13 TeV using the CMS detector," JINST **14** (07), P07004, arXiv:1903.06078 [hep-ex].
CMS Collaboration, (2019f), "Search for invisible decays of a Higgs boson produced through vector boson fusion in proton-proton collisions at $\sqrt{s}$ = 13 TeV," Phys. Lett. B **793**, 520–551, arXiv:1809.05937 [hep-ex].
CMS Collaboration, (2020a), "Measurement of differential cross sections for Z bosons produced in association with charm jets in pp collisions at $\sqrt{s}$ = 13 TeV," arXiv:2012.04119 [hep-ex].
CMS Collaboration, (2020b), "Measurement of electroweak production of a W boson in association with two jets in proton-proton collisions at $\sqrt{s}$ = 13 TeV," Eur. Phys. J. C **80** (1), 43, arXiv:1903.04040 [hep-ex].
CMS Collaboration, (2020c), "Measurement of the associated production of a Z boson with charm or bottom quark jets in proton-proton collisions at $\sqrt{s}$ = 13 TeV," Phys. Rev. D **102** (3), 032007, arXiv:2001.06899 [hep-ex].
CMS Collaboration, (2020d), "Performance of the reconstruction and identification of high-momentum muons in proton-proton collisions at $\sqrt{s}$ = 13 TeV," JINST **15** (02), P02027, arXiv:1912.03516 [physics.ins-det].
CMS Collaboration, (2020e), "Pileup mitigation at CMS in 13 TeV data," JINST **15** (09), P09018, arXiv:2003.00503 [hep-ex].
CMS Collaboration, (2020f), "Summaries of CMS cross section measurements," https://twiki.cern.ch/twiki/bin/view/CMSPublic/PhysicsResultsCombined.
DØ Collaboration, (2005), "A measurement of the ratio of inclusive cross sections $\sigma(pp \to Z + b - \text{jet})/\sigma(pp \to Z + jet)$ at $\sqrt{s}$ = 1.96 TeV," Phys. Rev. Lett. **94**, 161801, arXiv:hep-ex/0410078 [hep-ex].
DØ Collaboration, (2008a), "Measurement of differential Z/γ^* + jet + X cross sections in $p\bar{p}$ collisions at $\sqrt{s}$ = 1.96 TeV," Phys. Lett. B **669**, 278–286, arXiv:0808.1296 [hep-ex].
DØ Collaboration, (2008b), "Measurement of the Differential Cross-Section for the Production of an Isolated Photon with Associated Jet in $p\bar{p}$ Collisions at $\sqrt{s}$ = 1.96 TeV," Phys. Lett. B **666**, 435–445, arXiv:0804.1107 [hep-ex].
DØ Collaboration, (2009a), "Measurement of $\gamma + b$ + X and $\gamma + c$ + X production cross sections in p anti-p collisions at $\sqrt{s}$ = 1.96 TeV," Phys. Rev. Lett. **102**, 192002, arXiv:0901.0739 [hep-ex].
DØ Collaboration, (2009b), "Measurements of differential cross sections of Z/γ^*+jets+X events in proton anti-proton collisions at $\sqrt{s}$ = 1.96 TeV," Phys. Lett. B **678**, 45–54, arXiv:0903.1748 [hep-ex].
DØ Collaboration, (2010a), "Double parton interactions in γ+3 jet events in pp^- bar collisions $\sqrt{s}$ = 1.96 TeV." Phys. Rev. D **81**, 052012, arXiv:0912.5104 [hep-ex].
DØ Collaboration, (2010b), "Measurement of Z/γ^*+jet+X angular distributions in $\bar{p}p$ collisions at $\sqrt{s}$ = 1.96 TeV," Phys. Lett. B **682**, 370–380, arXiv:0907.4286 [hep-ex].
DØ Collaboration, (2011a), "A measurement of the ratio of inclusive cross sections $\sigma($ $\to$ +b jet$)/\sigma($ $\to$ + jet) at $\sqrt{s}$ = 1.96 TeV," Phys. Rev. D **83**, 031105, arXiv:1010.6203 [hep-ex].
DØ Collaboration, (2011b), "Azimuthal decorrelations and multiple parton interactions in γ+2 jet and γ+3 jet events in $p\bar{p}$ collisions at $\sqrt{s}$ = 1.96 TeV," Phys. Rev. D **83**, 052008, arXiv:1101.1509 [hep-ex].
DØ Collaboration, (2011c), "Measurements of inclusive W+jets production rates as a function of jet transverse momentum in $p\bar{p}$ collisions at

$\sqrt{s} = 1.96$ TeV," Phys. Lett. B **705**, 200–207, arXiv:1106.1457 [hep-ex].

DØ Collaboration, (2012), "Measurement of the photon+b-jet production differential cross section in $p\bar{p}$ collisions at $\sqrt{s} = 1.96$ TeV," Phys. Lett. B **714**, 32–39, arXiv:1203.5865 [hep-ex].

DØ Collaboration, (2013a), "Measurement of the differential photon + c-jet cross section and the ratio of differential photon+ c and photon+ b cross sections in proton-antiproton collisions at $\sqrt{s} = 1.96$ TeV," Phys. Lett. B **719**, 354–361, arXiv:1210.5033 [hep-ex].

DØ Collaboration, (2013b), "Measurement of the $p\bar{p} \to W + b + X$ production cross section at $\sqrt{s} = 1.96$ TeV," Phys. Lett. B **718**, 1314–1320, arXiv:1210.0627 [hep-ex].

DØ Collaboration, (2013c), "Measurement of the ratio of differential cross sections $\sigma(p\bar{p} \to Z + bjet)/\sigma(p\bar{p} \to Z + jet)$ in $p\bar{p}$ collisions at $\sqrt{s} = 1.96$ TeV," Phys. Rev. D **87** (9), 092010, arXiv:1301.2233 [hep-ex].

DØ Collaboration, (2013d), "Studies of W boson plus jets production in $p\bar{p}$ collisions at $\sqrt{s} = 1.96$ TeV," Phys. Rev. D **88** (9), 092001, arXiv:1302.6508 [hep-ex].

DØ Collaboration, (2014), "Measurement of associated production of Z bosons with charm quark jets in $\bar{p}p$ collisions at $\sqrt{s} = 1.96$ TeV," Phys. Rev. Lett. **112**, 042001, arXiv:1308.4384 [hep-ex].

DØ Collaboration, (2015), "Measurement of the electron charge asymmetry in $p\bar{p} \to W + X \to e\nu + X$ decays in $p\bar{p}$ collisions at $\sqrt{s} = 1.96$ TeV," Phys. Rev. D **91** (3), 032007, [Erratum: Phys.Rev.D 91, 079901 (2015)], arXiv:1412.2862 [hep-ex].

Collins, John C, Davison E. Soper, and George F. Sterman (1985), "Transverse Momentum Distribution in Drell-Yan Pair and W and Z Boson Production," Nucl. Phys. B **250**, 199–224.

Cooper, B, J. Katzy, M. L. Mangano, A. Messina, L. Mijovič, and P. Skands (2012), "Importance of a consistent choice of α_S in the matching of AlpGen and Pythia," Eur. Phys. J. C **72** (7), 10.1140/epjc/s10052-012-2078-y, arXiv:1109.5295 [hep-ph].

Coradeschi, Francesco, and Thomas Cridge (2019), "reSolve — A transverse momentum resummation tool," Comput. Phys. Commun. **238**, 262–294, arXiv:1711.02083 [hep-ph].

Corke, Richard, and Torbjorn Sjostrand (2010), "Multiparton Interactions and Rescattering," JHEP **01**, 035, arXiv:0911.1909 [hep-ph].

Currie, James, E. W. N. Glover, and Steven Wells (2013), "Infrared Structure at NNLO Using Antenna Subtraction," JHEP **04**, 066, arXiv:1301.4693 [hep-ph].

Davidson, N, T. Przedzinski, and Z. Wąs (2016), "PHOTOS interface in C++: Technical and Physics Documentation," Comput. Phys. Commun. **199**, 86–101, arXiv:1011.0937 [hep-ph].

Denner, Ansgar, Stefan Dittmaier, Tobias Kasprzik, and Alexander Mück (2011), "Electroweak corrections to dilepton + jet production at hadron colliders," JHEP **06**, 069, arXiv:1103.0914 [hep-ph].

Denner, Ansgar, Stefan Dittmaier, Tobias Kasprzik, and Alexander Mück (2013), "Electroweak corrections to monojet production at the LHC," Eur. Phys. J. C **73** (2), 2297, arXiv:1211.5078 [hep-ph].

Denner, Ansgar, Lars Hofer, Andreas Scharf, and Sandro Uccirati (2015), "Electroweak corrections to lepton pair production in association with two hard jets at the LHC," JHEP **01**, 094, arXiv:1411.0916 [hep-ph].

Denner, Ansgar, and Stefano Pozzorini (2001a), "One loop leading logarithms in electroweak radiative corrections. 1. Results," Eur. Phys. J. C **18**, 461–480, arXiv:hep-ph/0010201 [hep-ph].

Denner, Ansgar, and Stefano Pozzorini (2001b), "One loop leading logarithms in electroweak radiative corrections. 2. Factorization of collinear singularities," Eur. Phys. J. C **21**, 63–79, arXiv:hep-ph/0104127 [hep-ph].

Dittmaier, Stefan, Alexander Huss, and Christian Schwinn (2014), "Mixed QCD-electroweak $\mathcal{O}(\alpha_s\alpha)$ corrections to Drell-Yan processes in the resonance region: pole approximation and non-factorizable corrections," Nucl. Phys. B **885**, 318–372, arXiv:1403.3216 [hep-ph].

Dittmaier, Stefan, Alois Kabelschacht, and Tobias Kasprzik (2008), "Polarized QED splittings of massive fermions and dipole subtraction for non-collinear-safe observables," Nucl. Phys. B **800**, 146–189, arXiv:0802.1405 [hep-ph].

Dokshitzer, Yuri L, G.D. Leder, S. Moretti, and B.R. Webber (1997), "Better jet clustering algorithms," JHEP **08**, 001, arXiv:hep-ph/9707323.

Duhr, Claude, Falko Dulat, and Bernhard Mistlberger (2020a), "Charged Current Drell-Yan Production at N3LO," arXiv:2007.13313 [hep-ph].

Duhr, Claude, Falko Dulat, and Bernhard Mistlberger (2020b), "The Drell-Yan cross section to third order in the strong coupling constant," Phys. Rev. Lett. **125** (17), 172001, arXiv:2001.07717 [hep-ph].

Ebert, Markus A, and Frank J. Tackmann (2017), "Resummation of Transverse Momentum Distributions in Distribution Space," JHEP **02**, 110, arXiv:1611.08610 [hep-ph].

Ellis, R Keith, Kirill Melnikov, and Giulia Zanderighi (2009), "W+3 jet production at the Tevatron," Phys. Rev. D **80**, 094002, arXiv:0906.1445 [hep-ph].

Ellis, Stephen D, and Davison E. Soper (1993), "Successive combination jet algorithm for hadron collisions," Phys. Rev. D **48**, 3160–3166, arXiv:hep-ph/9305266.

Febres Cordero, F, and L. Reina (2015), "Electroweak Gauge-Boson Production in Association with b Jets at Hadron Colliders," Int. J. Mod. Phys. A **30** (16), 1530042, arXiv:1504.07177 [hep-ph].

Febres Cordero, F, L. Reina, and D. Wackeroth (2006), "NLO QCD corrections to W boson production with a massive b-quark jet pair at the Tevatron p anti-p collider," Phys. Rev. D **74**, 034007, arXiv:hep-ph/0606102 [hep-ph].

Febres Cordero, Fernando, L. Reina, and D. Wackeroth (2009), "W- and Z-boson

production with a massive bottom-quark pair at the Large Hadron Collider," Phys. Rev. D **80**, 034015, arXiv:0906.1923 [hep-ph].
Field, R D, and R. P. Feynman (1977), "Quark Elastic Scattering as a Source of High Transverse Momentum Mesons," Phys. Rev. D **15**, 2590–2616.
Field, Richard D, and Stephen Wolfram (1983), "A QCD Model for e+ e- Annihilation," Nucl. Phys. B **213**, 65–84.
Figueroa, D, S. Honeywell, S. Quackenbush, L. Reina, C. Reuschle, and D. Wackeroth (2018), "Electroweak and QCD corrections to Z-boson production with one b jet in a massive five-flavor scheme," Phys. Rev. D **98** (9), 093002, arXiv:1805.01353 [hep-ph].
de Florian, Daniel, Manuel Der, and Ignacio Fabre (2018), "QCD⊕QED NNLO corrections to Drell Yan production," Phys. Rev. D **98** (9), 094008, arXiv:1805.12214 [hep-ph].
Forte, Stefano, Eric Laenen, Paolo Nason, and Juan Rojo (2010), "Heavy quarks in deep-inelastic scattering," Nucl. Phys. **B834**, 116–162, arXiv:1001.2312 [hep-ph].
Frederix, Rikkert, and Stefano Frixione (2012), "Merging meets matching in MC@NLO," JHEP **12**, 061, arXiv:1209.6215 [hep-ph].
Frederix, Rikkert, Stefano Frixione, Valentin Hirschi, Fabio Maltoni, Roberto Pittau, and Paolo Torrielli (2011), "W and Z/γ^* boson production in association with a bottom-antibottom pair," JHEP **09**, 061, arXiv:1106.6019 [hep-ph].
Frederix, Rikkert, Stefano Frixione, Valentin Hirschi, Fabio Maltoni, Roberto Pittau, and Paolo Torrielli (2012), "aMC@NLO predictions for Wjj production at the Tevatron," JHEP **02**, 048, arXiv:1110.5502 [hep-ph].
Frederix, Rikkert, Stefano Frixione, Andreas Papaefstathiou, Stefan Prestel, and Paolo Torrielli (2016), "A study of multi-jet production in association with an electroweak vector boson," JHEP **02**, 131, arXiv:1511.00847 [hep-ph].
Frixione, Stefano (1998), "Isolated photons in perturbative QCD," Phys. Lett. B **429**, 369–374, arXiv:hep-ph/9801442 [hep-ph].
Frixione, Stefano, Paolo Nason, and Carlo Oleari (2007), "Matching NLO QCD computations with Parton Shower simulations: the POWHEG method," JHEP **11**, 070, arXiv:0709.2092 [hep-ph].
Frixione, Stefano, and Bryan R. Webber (2002), "Matching NLO QCD computations and parton shower simulations," JHEP **06**, 029, arXiv:hep-ph/0204244 [hep-ph].
Frixione, Stefano, and Bryan R. Webber (2004), "The MC@NLO 2.3 event generator," arXiv:hep-ph/0402116 [hep-ph].
Garland, L W, T. Gehrmann, E. W. Nigel Glover, A. Koukoutsakis, and E. Remiddi (2002a), "The Two loop QCD matrix element for $e^+e^- \to 3$ jets," Nucl. Phys. B **627**, 107–188, arXiv:hep-ph/0112081 [hep-ph].
Garland, L W, T. Gehrmann, E. W. Nigel Glover, A. Koukoutsakis, and E. Remiddi (2002b), "Two loop QCD helicity amplitudes for $e^+e^- \to 3$ jets," Nucl. Phys. B **642**, 227–262, arXiv:hep-ph/0206067 [hep-ph].
Gauld, R, A. Gehrmann-De Ridder, T. Gehrmann, E. W. N. Glover, and A. Huss (2017), "Precise predictions for the angular coefficients in Z-boson production at the LHC," JHEP **11**, 003, arXiv:1708.00008 [hep-ph].
Gauld, R, A. Gehrmann-De Ridder, E.W. N. Glover, A. Huss, and I. Majer (2020), "Predictions for Z-boson production in association with a b-jet at $\mathcal{O}(\alpha_s^3)$," arXiv:2005.03016 [hep-ph].
Gaunt, Jonathan, Maximilian Stahlhofen, Frank J. Tackmann, and Jonathan R. Walsh (2015), "N-jettiness Subtractions for NNLO QCD Calculations," JHEP **09**, 058, arXiv:1505.04794 [hep-ph].
Gavin, Ryan, Ye Li, Frank Petriello, and Seth Quackenbush (2011), "FEWZ 2.0: A code for hadronic Z production at next-to-next-to-leading order," Comput. Phys. Commun. **182**, 2388–2403, arXiv:1011.3540 [hep-ph].
Gehrmann, Thomas, Stefan Höche, Frank Krauss, Marek Schönherr, and Frank Siegert (2013), "NLO QCD matrix elements + parton showers in $e^+e^- \to$ hadrons," JHEP **01**, 144, arXiv:1207.5031 [hep-ph].
Gehrmann-De Ridder, A, T. Gehrmann, E. W. N. Glover, A. Huss, and T. A. Morgan (2016a), "NNLO QCD corrections for Drell-Yan p_T^Z and ϕ^* observables at the LHC," JHEP **11**, 094, [Erratum: JHEP10,126(2018)], arXiv:1610.01843 [hep-ph].
Gehrmann-De Ridder, A, T. Gehrmann, E. W. N. Glover, A. Huss, and T. A. Morgan (2016b), "Precise QCD predictions for the production of a Z boson in association with a hadronic jet," Phys. Rev. Lett. **117** (2), 022001, arXiv:1507.02850 [hep-ph].
Gehrmann-De Ridder, A, T. Gehrmann, E. W. N. Glover, A. Huss, and D. M. Walker (2018), "Next-to-Next-to-Leading-Order QCD Corrections to the Transverse Momentum Distribution of Weak Gauge Bosons," Phys. Rev. Lett. **120** (12), 122001, arXiv:1712.07543 [hep-ph].
Gehrmann-De Ridder, A, T. Gehrmann, and E. W. Nigel Glover (2005), "Antenna subtraction at NNLO," JHEP **09**, 056, arXiv:hep-ph/0505111 [hep-ph].
Gehrmann-De Ridder, A, T. Gehrmann, E.W.N. Glover, A. Huss, and D.M. Walker (2019), "Vector Boson Production in Association with a Jet at Forward Rapidities," Eur. Phys. J. C **79** (6), 526, arXiv:1901.11041 [hep-ph].
Gehrmann-De Ridder, Aude, T. Gehrmann, E. W. N. Glover, A. Huss, and T. A. Morgan (2016c), "The NNLO QCD corrections to Z boson production at large transverse momentum," JHEP **07**, 133, arXiv:1605.04295 [hep-ph].
Gerwick, Erik, Tilman Plehn, Steffen Schumann, and Peter Schichtel (2012), "Scaling Patterns for QCD Jets," JHEP **10**, 162, arXiv:1208.3676 [hep-ph].
Gieseke, Stefan, Frasher Loshaj, and Patrick Kirchgäßer (2017), "Soft and diffractive scattering with the cluster model in Herwig," Eur. Phys. J. C **77** (3), 156, arXiv:1612.04701 [hep-ph].
Glück, M, L. E. Gordon, E. Reya, and W. Vogel-

sang (1994), "High p_T photon production at $p\bar{p}$ collider," Phys. Rev. Lett. **73**, 388–391.
Goncharov, M, *et al.* (NuTeV) (2001), "Precise Measurement of Dimuon Production Cross-Sections in ν_μ Fe and $\bar{\nu}_\mu$ Fe Deep Inelastic Scattering at the Tevatron." Phys. Rev. D **64**, 112006, arXiv:hep-ex/0102049.
Hagiwara, Kaoru, S. Ishihara, R. Szalapski, and D. Zeppenfeld (1993), "Low-energy effects of new interactions in the electroweak boson sector," Phys. Rev. D **48**, 2182–2203.
Hagiwara, Kaoru, T. Kuruma, and Y. Yamada (1992), "Probing the one loop Zgg vertex at hadron colliders," Nucl. Phys. B **369**, 171–188.
Hagiwara, Kaoru, R. D. Peccei, D. Zeppenfeld, and K. Hikasa (1987), "Probing the Weak Boson Sector in e+ e- —> $W+$ W-," Nucl. Phys. B **282**, 253–307.
Hamberg, R, W.L. van Neerven, and T. Matsuura (1991), "A complete calculation of the order α_s^2 correction to the Drell-Yan K factor," Nucl. Phys. B **359**, 343–405, [Erratum: Nucl.Phys.B 644, 403–404 (2002)].
Hamilton, Keith, and Paolo Nason (2010), "Improving NLO-parton shower matched simulations with higher order matrix elements," JHEP **06**, 039, arXiv:1004.1764 [hep-ph].
Hamilton, Keith, Paolo Nason, Carlo Oleari, and Giulia Zanderighi (2013), "Merging $H/W/Z$ + 0 and 1 jet at NLO with no merging scale: a path to parton shower + NNLO matching," JHEP **05**, 082, arXiv:1212.4504 [hep-ph].
Hamilton, Keith, Paolo Nason, and Giulia Zanderighi (2012), "MINLO: Multi-Scale Improved NLO," JHEP **10**, 155, arXiv:1206.3572 [hep-ph].
Hamilton, Keith, and Peter Richardson (2006), "Simulation of QED radiation in particle decays using the YFS formalism," JHEP **07**, 010, arXiv:hep-ph/0603034 [hep-ph].
Hamilton, Keith, Peter Richardson, and Jon Tully (2008), "A Positive-Weight Next-to-Leading Order Monte Carlo Simulation of Drell-Yan Vector Boson Production," JHEP **10**, 015, arXiv:0806.0290 [hep-ph].
Hamilton, Keith, Peter Richardson, and Jon Tully (2009), "A Modified CKKW matrix element merging approach to angular-ordered parton showers," JHEP **11**, 038, arXiv:0905.3072 [hep-ph].
Hartanto, H B, and L. Reina (2014), "Hard-photon production with b jets at hadron colliders," Phys. Rev. D **89** (7), 074001, arXiv:1312.2384 [hep-ph].
Höche, S, F. Krauss, S. Pozzorini, M. Schönherr, J. M. Thompson, and K. C. Zapp (2014), "Triple vector boson production through Higgs-Strahlung with NLO multijet merging," Phys. Rev. D **89** (9), 093015, arXiv:1403.7516 [hep-ph].
Höche, Stefan, Johannes Krause, and Frank Siegert (2019a), "Multijet Merging in a Variable Flavor Number Scheme," Phys. Rev. D **100** (1), 014011, arXiv:1904.09382 [hep-ph].
Höche, Stefan, Frank Krauss, Marek Schönherr, and Frank Siegert (2011a), "Automating the POWHEG method in Sherpa," JHEP **04**, 024, arXiv:1008.5399 [hep-ph].
Höche, Stefan, Frank Krauss, Marek Schönherr, and Frank Siegert (2011b), "NLO matrix elements and truncated showers," JHEP **08**, 123, arXiv:1009.1127 [hep-ph].
Höche, Stefan, Frank Krauss, Marek Schönherr, and Frank Siegert (2012), "A critical appraisal of NLO+PS matching methods," JHEP **09**, 049, arXiv:1111.1220 [hep-ph].
Höche, Stefan, Frank Krauss, Marek Schönherr, and Frank Siegert (2013a), "QCD matrix elements + parton showers: The NLO case," JHEP **04**, 027, arXiv:1207.5030 [hep-ph].
Höche, Stefan, Frank Krauss, Marek Schönherr, and Frank Siegert (2013b), "$W+$ n-Jet predictions at the Large Hadron Collider at next-to-leading order matched with a parton shower," Phys. Rev. Lett. **110** (5), 052001, arXiv:1201.5882 [hep-ph].
Höche, Stefan, Frank Krauss, Steffen Schumann, and Frank Siegert (2009), "QCD matrix elements and truncated showers," JHEP **05**, 053, arXiv:0903.1219 [hep-ph].
Höche, Stefan, Ye Li, and Stefan Prestel (2015), "Drell-Yan lepton pair production at NNLO QCD with parton showers," Phys. Rev. D **91** (7), 074015, arXiv:1405.3607 [hep-ph].
Höche, Stefan, Stefan Prestel, and Holger Schulz (2019b), "Simulation of Vector Boson Plus Many Jet Final States at the High Luminosity LHC," Phys. Rev. D **100** (1), 014024, arXiv:1905.05120 [hep-ph].
Hollik, W, B. A. Kniehl, E. S. Scherbakova, and O. L. Veretin (2015), "Electroweak corrections to Z-boson hadroproduction at finite transverse momentum," Nucl. Phys. B **900**, 576–602, arXiv:1504.07574 [hep-ph].
Ita, H, Z. Bern, L. J. Dixon, Fernando Febres Cordero, D. A. Kosower, and D. Maître (2012), "Precise Predictions for Z + 4 Jets at Hadron Colliders," Phys. Rev. D **85**, 031501, arXiv:1108.2229 [hep-ph].
Jäger, B (2010), "Next-to-leading order QCD corrections to photon production via weak-boson fusion," Phys. Rev. D **81**, 114016, arXiv:1004.0825 [hep-ph].
Jäger, Barbara, Steven Schneider, and Giulia Zanderighi (2012), "Next-to-leading order QCD corrections to electroweak Zjj production in the POWHEG BOX," JHEP **09**, 083, arXiv:1207.2626 [hep-ph].
Ježo, Tomas, Michael Klasen, and Florian König (2016), "Prompt photon production and photon-hadron jet correlations with POWHEG," JHEP **11**, 033, arXiv:1610.02275 [hep-ph].
Johnson, Mark, and Daniel Maître (2018), "Strong coupling constant extraction from high-multiplicity Z+jets observables," Phys. Rev. D **97** (5), 054013, arXiv:1711.01408 [hep-ph].
Kallweit, Stefan, Jonas M. Lindert, Philipp Maierhöfer, Stefano Pozzorini, and Marek Schönherr (2015a), "NLO electroweak automation and precise predictions for W+multijet production at the LHC," JHEP **04**, 012, arXiv:1412.5157 [hep-ph].
Kallweit, Stefan, Jonas M. Lindert, Philipp Maierhöfer, Stefano Pozzorini, and Marek Schönherr (2016), "NLO QCD+EW predictions for V + jets

including off-shell vector-boson decays and multijet merging," JHEP **04**, 021, arXiv:1511.08692 [hep-ph].

Kallweit, Stefan, Jonas M. Lindert, Stefano Pozzorini, Marek Schönherr, and Philipp Maierhöfer (2015b), "NLO QCD+EW automation and precise predictions for V+multijet production," in *Proceedings, 50th Rencontres de Moriond, QCD and high energy interactions: La Thuile, Italy, March 21-28, 2015*, pp. 121–124, arXiv:1505.05704 [hep-ph].

Karlberg, Alexander, Emanuele Re, and Giulia Zanderighi (2014), "NNLOPS accurate Drell-Yan production," JHEP **09**, 134, arXiv:1407.2940 [hep-ph].

Kom, Chun-Hay, and W.James Stirling (2010), "Charge asymmetry in W + jets production at the LHC," Eur. Phys. J. C **69**, 67–73, arXiv:1004.3404 [hep-ph].

Kosower, David A (1998), "Antenna factorization of gauge theory amplitudes," Phys. Rev. D **57**, 5410–5416, arXiv:hep-ph/9710213 [hep-ph].

Krauss, Frank, Petar Petrov, Marek Schönherr, and Michael Spannowsky (2014), "Measuring collinear W emissions inside jets," Phys. Rev. D **89** (11), 114006, arXiv:1403.4788 [hep-ph].

Kühn, Johann H, A. Kulesza, S. Pozzorini, and M. Schulze (2005a), "Logarithmic electroweak corrections to hadronic Z+1 jet production at large transverse momentum," Phys. Lett. B **609**, 277–285, arXiv:hep-ph/0408308 [hep-ph].

Kühn, Johann H, A. Kulesza, S. Pozzorini, and M. Schulze (2005b), "One-loop weak corrections to hadronic production of Z bosons at large transverse momenta," Nucl. Phys. B **727**, 368–394, arXiv:hep-ph/0507178 [hep-ph].

Kühn, Johann H, A. Kulesza, S. Pozzorini, and M. Schulze (2006), "Electroweak corrections to hadronic photon production at large transverse momenta," JHEP **03**, 059, arXiv:hep-ph/0508253 [hep-ph].

Kühn, Johann H, A. Kulesza, S. Pozzorini, and M. Schulze (2007), "Electroweak corrections to large transverse momentum production of W bosons at the LHC," Phys. Lett. B **651**, 160–165, arXiv:hep-ph/0703283 [HEP-PH].

Kühn, Johann H, A. Kulesza, S. Pozzorini, and M. Schulze (2008), "Electroweak corrections to hadronic production of W bosons at large transverse momenta," Nucl. Phys. B **797**, 27–77, arXiv:0708.0476 [hep-ph].

Ladinsky, G A, and C. P. Yuan (1994), "The Nonperturbative regime in QCD resummation for gauge boson production at hadron colliders," Phys. Rev. D **50**, R4239, arXiv:hep-ph/9311341 [hep-ph].

Lam, C S, and Wu-Ki Tung (1978), "A Systematic Approach to Inclusive Lepton Pair Production in Hadronic Collisions," Phys. Rev. D **18**, 2447.

Lam, C S, and Wu-Ki Tung (1980), "A Parton Model Relation Sans QCD Modifications in Lepton Pair Productions," Phys. Rev. D **21**, 2712.

Lavesson, Nils, and Leif Lönnblad (2008a), "Extending CKKW-merging to One-Loop Matrix Elements," JHEP **12**, 070, arXiv:0811.2912 [hep-ph].

Lavesson, Nils, and Leif Lönnblad (2008b), "Merging parton showers and matrix elements: Back to basics," JHEP **04**, 085, arXiv:0712.2966 [hep-ph].

LHCb Collaboration, (2014a), "Observation of associated production of a Z boson with a D meson in the forward region," JHEP **04**, 091, arXiv:1401.3245 [hep-ex].

LHCb Collaboration, (2014b), "Study of forward Z + jet production in pp collisions at $\sqrt{s} = 7$ TeV," JHEP **01**, 033, arXiv:1310.8197 [hep-ex].

LHCb Collaboration, (2015a), "LHCb Detector Performance," Int. J. Mod. Phys. A **30** (07), 1530022, arXiv:1412.6352 [hep-ex].

LHCb Collaboration, (2015b), "Measurement of the forward-backward asymmetry in $Z/\gamma^* \to \mu^+\mu^-$ decays and determination of the effective weak mixing angle," JHEP **11**, 190, arXiv:1509.07645 [hep-ex].

LHCb Collaboration, (2015c), "Measurement of the Z+b-jet cross-section in pp collisions at $\sqrt{s} =$ 7 TeV in the forward region," JHEP **01**, 064, arXiv:1411.1264 [hep-ex].

LHCb Collaboration, (2015d), "Study of W boson production in association with beauty and charm," Phys. Rev. D **92**, 052001, arXiv:1505.04051 [hep-ex].

LHCb Collaboration, (2016), "Measurement of forward W and Z boson production in association with jets in proton-proton collisions at $\sqrt{s} = 8$ TeV," JHEP **05**, 131, arXiv:1605.00951 [hep-ex].

LHCb Collaboration, (2019a), "Design and performance of the LHCb trigger and full real-time reconstruction in Run 2 of the LHC," JINST **14** (04), P04013, arXiv:1812.10790 [hep-ex].

LHCb Collaboration, (2019b), "Measurement of charged hadron production in Z-tagged jets in proton-proton collisions at $\sqrt{s} = 8$ TeV," Phys. Rev. Lett. **123**, 232001, arXiv:1904.08878 [hep-ex].

LHCb Collaboration, (2019c), "Measurement of the electron reconstruction efficiency at LHCb," JINST **14** (11), P11023–P11023, arXiv:1909.02957 [hep-ex].

Li, Ye, and Frank Petriello (2012), "Combining QCD and electroweak corrections to dilepton production in FEWZ," Phys. Rev. D **86**, 094034, arXiv:1208.5967 [hep-ph].

Lindert, J M, *et al.* (2017), "Precise predictions for V+ jets dark matter backgrounds," Eur. Phys. J. C **77** (12), 829, arXiv:1705.04664 [hep-ph].

Lönnblad, Leif (2002), "Correcting the color dipole cascade model with fixed order matrix elements," JHEP **05**, 046, arXiv:hep-ph/0112284 [hep-ph].

Lönnblad, Leif, and Stefan Prestel (2012), "Matching Tree-Level Matrix Elements with Interleaved Showers," JHEP **03**, 019, arXiv:1109.4829 [hep-ph].

Lönnblad, Leif, and Stefan Prestel (2013a), "Merging Multi-leg NLO Matrix Elements with Parton Showers," JHEP **03**, 166, arXiv:1211.7278 [hep-ph].

Lönnblad, Leif, and Stefan Prestel (2013b), "Unitarising Matrix Element + Parton Shower merging," JHEP **02**, 094, arXiv:1211.4827 [hep-ph].

Maguire, Eamonn, Lukas Heinrich, and Graeme

Watt (2017), "HEPData: a repository for high energy physics data," *Proceedings, 22nd International Conference on Computing in High Energy and Nuclear Physics (CHEP2016): San Francisco, CA, October 14-16, 2016*, J. Phys. Conf. Ser. **898** (10), 102006, arXiv:1704.05473 [hep-ex].

Maître, Daniel, and Sebastian Sapeta (2013), "Simulated NNLO for high-p_T observables in vector boson + jets production at the LHC," Eur. Phys. J. C **73** (12), 2663, arXiv:1307.2252 [hep-ph].

Mangano, Michelangelo L, Mauro Moretti, and Roberto Pittau (2002), "Multijet matrix elements and shower evolution in hadronic collisions: $Wb\bar{b}$ + n jets as a case study," *Workshop on Monte Carlo Generator Physics for Run II at the Tevatron Batavia, Illinois, April 18-20, 2001*, Nucl. Phys. B **632**, 343–362, arXiv:hep-ph/0108069 [hep-ph].

Mantry, Sonny, and Frank Petriello (2011), "Transverse Momentum Distributions in the Non-Perturbative Region," Phys. Rev. D **84**, 014030, arXiv:1011.0757 [hep-ph].

Melnikov, Kirill, and Frank Petriello (2006a), "Electroweak gauge boson production at hadron colliders through $O(\alpha_s^2)$," Phys. Rev. D **74**, 114017, arXiv:hep-ph/0609070 [hep-ph].

Melnikov, Kirill, and Frank Petriello (2006b), "The W boson production cross section at the LHC through $O(\alpha_s^2)$," Phys. Rev. Lett. **96**, 231803, arXiv:hep-ph/0603182 [hep-ph].

Mirkes, E (1992), "Angular decay distribution of leptons from W bosons at NLO in hadronic collisions," Nucl. Phys. B **387**, 3–85.

Mirkes, E, and J. Ohnemus (1994), "W and Z polarization effects in hadronic collisions," Phys. Rev. D **50**, 5692–5703, arXiv:hep-ph/9406381 [hep-ph].

Moch, Sven, Peter Uwer, and Stefan Weinzierl (2002), "Two loop amplitudes with nested sums: Fermionic contributions to $e^+e^- \to q\bar{q}g$," Phys. Rev. D **66**, 114001, arXiv:hep-ph/0207043 [hep-ph].

Monni, Pier Francesco, Paolo Nason, Emanuele Re, Marius Wiesemann, and Giulia Zanderighi (2020), "MiNNLO$_{PS}$: a new method to match NNLO QCD to parton showers," JHEP **05**, 143, arXiv:1908.06987 [hep-ph].

Monni, Pier Francesco, Emanuele Re, and Paolo Torrielli (2016), "Higgs Transverse-Momentum Resummation in Direct Space," Phys. Rev. Lett. **116** (24), 242001, arXiv:1604.02191 [hep-ph].

Mück, Alexander, and Lennart Oymanns (2017), "Resonace-improved parton-shower matching for the Drell-Yan process including electroweak corrections," JHEP **05**, 090, arXiv:1612.04292 [hep-ph].

Nason, Paolo (2004), "A New method for combining NLO QCD with shower Monte Carlo algorithms," JHEP **11**, 040, arXiv:hep-ph/0409146 [hep-ph].

Oleari, Carlo, and Laura Reina (2011), "$W^{\pm}\, b\bar{b}$ production in POWHEG," JHEP **08**, 061, [Erratum: JHEP11,040(2011)], arXiv:1105.4488 [hep-ph].

Oleari, Carlo, and Dieter Zeppenfeld (2004), "QCD corrections to electroweak $l\nu_l jj$ and $l^+l^- jj$ production," Phys. Rev. D **69**, 093004, arXiv:hep-ph/0310156 [hep-ph].

Plätzer, Simon (2013), "Controlling inclusive cross sections in parton shower + matrix element merging," JHEP **08**, 114, arXiv:1211.5467 [hep-ph].

Re, Emanuele (2012), "NLO corrections merged with parton showers for Z+2 jets production using the POWHEG method," JHEP **10**, 031, arXiv:1204.5433 [hep-ph].

Rubin, Mathieu, Gavin P. Salam, and Sebastian Sapeta (2010), "Giant QCD K-factors beyond NLO," JHEP **09**, 084, arXiv:1006.2144 [hep-ph].

Schissler, Franziska, and Dieter Zeppenfeld (2013), "Parton shower effects on W and Z production via vector boson fusion at NLO QCD," JHEP **04**, 057, arXiv:1302.2884.

Schönherr, Marek, and Frank Krauss (2008), "Soft Photon Radiation in Particle Decays in SHERPA," JHEP **12**, 018, arXiv:0810.5071 [hep-ph].

Seymour, Michael H (1992), "Photon radiation in final state parton showering," Z. Phys. C **56**, 161–170.

Siegert, Frank (2017), "A practical guide to event generation for prompt photon production with Sherpa," J. Phys. G **44** (4), 044007, arXiv:1611.07226 [hep-ph].

Sjöstrand, T, and Peter Z. Skands (2004), "Multiple interactions and the structure of beam remnants," JHEP **03**, 053, arXiv:hep-ph/0402078 [hep-ph].

Sjöstrand, Torbjörn, Stefan Ask, Jesper R. Christiansen, Richard Corke, Nishita Desai, Philip Ilten, Stephen Mrenna, Stefan Prestel, Christine O. Rasmussen, and Peter Z. Skands (2015), "An introduction to PYTHIA 8.2," Comput. Phys. Commun. **191**, 159, arXiv:1410.3012 [hep-ph].

Sjöstrand, Torbjörn, and Maria van Zijl (1987), "A Multiple Interaction Model for the Event Structure in Hadron Collisions," Phys. Rev. D **36**, 2019.

Stavreva, T P, and J. F. Owens (2009), "Direct Photon Production in Association With A Heavy Quark At Hadron Colliders," Phys. Rev. D **79**, 054017, arXiv:0901.3791 [hep-ph].

Stewart, Iain W, Frank J. Tackmann, and Wouter J. Waalewijn (2011), "The Beam Thrust Cross Section for Drell-Yan at NNLL Order," Phys. Rev. Lett. **106**, 032001, arXiv:1005.4060 [hep-ph].

Tackmann, Frank J, Jonathan R. Walsh, and Saba Zuberi (2012), "Resummation Properties of Jet Vetoes at the LHC," Phys. Rev. D **86**, 053011, arXiv:1206.4312 [hep-ph].

Vesterinen, M, and T. R. Wyatt (2009), "A Novel Technique for Studying the Z Boson Transverse Momentum Distribution at Hadron Colliders," Nucl. Instrum. Meth. A **602**, 432–437, arXiv:0807.4956 [hep-ex].

Webber, B R (1984), "A QCD Model for Jet Fragmentation Including Soft Gluon Interference," Nucl. Phys. B **238**, 492–528.

Winter, Jan-Christopher, Frank Krauss, and Gerhard Soff (2004), "A Modified cluster hadroniza-

tion model," Eur. Phys. J. C **36**, 381–395, arXiv:hep-ph/0311085 [hep-ph].
Yennie, D R, Steven C. Frautschi, and H. Suura (1961), "The infrared divergence phenomena and high-energy processes," Annals Phys. **13**, 379–452.